The growth and contamination mechanism of the Cana Brava layered mafic-ultramafic complex: new field and geochemical evidences

Tommaso Giovanardi[1] · Vicente A.V. Girardi[1] · Ciro T. Correia[1] · Silvano Sinigoi[2] · Colombo C.G. Tassinari[1] · Maurizio Mazzucchelli[3]

✉ Tommaso Giovanardi
tommaso.giovanardi@gmail.com

[1] Instituto de Geociências, Universidade de São Paulo, Rua do Lago, 562, Cidade Universitária, 05508-900 São Paulo, Brazil

[2] Dipartimento di Geoscienze, Università degli Studi di Trieste, Via E.Weiss 8, I-34128 Trieste, Italy

[3] Dipartimento di Scienze Chimiche e Geologiche, Università di Modena e Reggio Emilia, Via Campi, 103, I-41125 Modena, Italy

Abstract The Cana Brava complex is the northernmost of three layered complexes outcropping in the Goiás state (central Brasil). New field and geochemical evidences suggest that Cana Brava underwent hyper- to subsolidus deformation during its growth, acquiring a high-temperature foliation that is generally interpreted as the result of a granulite-facies metamorphic event. The increase along the stratigraphy of the incompatible elements abundances (LREE, Rb, Ba) and of the

Sr isotopic composition, coupled with a decrease in $\varepsilon Nd_{(790)}$, indicate that the complex was contaminated by the embedded xenoliths from the Palmeirópolis Sequence. The geochemical data suggest that the contamination occurred along the entire magma column during the crystallization of the Upper Mafic Zone, with in situ variations determined by the abundance and composition of the xenoliths. These features of the Cana Brava complex point to an extremely similarity with the Lower Sequence of the most known Niquelândia intrusion (the central of the three complexes). This, together with the evidences that the two complexes have the same age (c.a. 790 Ma) and their thickness and units decrease northwards suggests that Cana Brava and Niquelândia are part of a single giant Brasilia body grown through several melt impulses.

Keywords Mafic complex · Goiás · Cana Brava · Niquelândia · Geochemistry

Introduction

The Cana Brava mafic-ultramafic complex is the northernmost of three large layered complexes that form a discontinuous, 300 km long, North-trending belt within the Brasilia Belt (Goiás state, central Brasil) (Girardi et al. 1978; Correia et al. 1997; Correia and Girardi 1998; Ferreira Filho et al. 2010). The three complexes (from South to North: Barro Alto, Niquelândia and Cana Brava) are elongated parallel to the Maranhão thrust belt, a major tectonic boundary formed during the Brazilian (Panafrican, ~600 Ma) collision of the Amazonian and São Francisco cratons. A large positive gravimetric anomaly overlaps the alignment of the complexes suggesting that the three complexes may be tectonically separated fragments of a single body, tilted and uplifted during the Brazilian event (Feininger et al. 1991; Marangoni et al. 1995; Ferreira Filho et al. 2010; Correia et al. 2012). Among the three layered complexes, Niquelândia is the best studied (Rivalenti et al.

1982, 2008; Girardi et al. 1986; Pimentel et al. 2004a, 2006; Correia et al. 2007, 2012), whereas Barro Alto and Cana Brava are less known (Matsui et al. 1976; Girardi et al. 1978; Fugi 1989; Suita et al. 1994; Correia et al. 1997, 1999; Correia and Girardi 1998; Moraes and Fuck 2000; Ferreira Filho et al. 2010; Della Giustina et al. 2011; Giovanardi et al. 2015).

The magmatic textures of the rocks of the three complexes are obliterated by a super-imposed foliation parallel to their alignment and direction. This foliation is intepreted as metamorphic, according to the observation that the complexes were re-crystallized in granulite- to amphibolite-facies (Ferreira Filho et al. 2010; and references therein). Conversely, Correia et al. (2012) re-interpreted structural, textural and chemical features of the Niquelândia complex, providing evidences that its intrusion occurred through significant shear under hyper- to sub-solidus conditions during the growth and cooling of a crystal mush. Their U-Pb SHRIMP zircons data constrain the Niquelândia intrusion at ~790 Ma (Rivalenti et al. 2008; Correia et al. 2012), an age similar to those reported by Ferreira Filho et al. (2010) and Giovanardi et al. (2015) for the Cana Brava intrusion. Correia et al. (2012) report also a detailed study of the contamination of the Niquelândia complex, due to the assimilation of xenoliths from the upper metavolcanic-metasedimentary sequence (the Indaianopólis Sequence). In a previous study, Correia et al. (1997) suggest that also the Cana Brava complex was affected by crustal contamination; however, no details about the contamination are reported.

In this paper, we present new geochemical data of the Cana Brava complex and a comparison with literature data, as well as structural observations, of Niquelândia. The data are discussed in order to: i) constrain the occurrence of the contamination process during the growth of the Cana Brava complex, ii) evaluate the style of the contamination process, iii) discuss the evidences of metamorphism versus syn-magmatic deformation, and iv) discuss the possibility that Cana Brava and Niquelândia are separated fragments of one giant layered complex.

Geological setting

The Cana Brava layered complex

The Cana Brava layered complex is about 40 km long with a 10°-20° NNE main strike and 30°-50° dip (Fig. 1; Correia and Girardi 1998). Its estimated thickness decreases progressively from about 12 km in the southern side, vanishing to the North. To the East, the Cana Brava complex overthrusts the Rio Maranhão Thrust Zone (formed by thrust of rocks of different regional units such as the Serra da Mesa Group, the Araí Group and the Araxá Group). The western contact of the complex is intrusive in the metasediments and metavolcanics of the Palmeirópolis Sequence (Ribeiro Filho and Teixeira 1981; Girardi and Kurat 1982; Correia et al. 1997; Correia and Girardi 1998). The igneous nature of the western contact is consistent with the absence of mylonites near the contact (Correia and Girardi 1998) and with the occurrence of xenoliths from the Palmeirópolis Sequence (SP) within the upper levels of the Cana Brava complex (Correia et al. 1997; Correia and Girardi 1998; Giovanardi et al. 2015). To the South and North the complex is bounded by normal and strike-slip faults (Fig. 1).

Correia et al. (1997) and Correia and Girardi (1998) divided the Cana Brava complex in five units, however, in this study, we will use the simpler subdivision in three units based on the lithological criteria proposed by Ferreira Filho et al. (2010). From the lower unit (East) to the top (West), the complex consists of:

i) a Lower Mafic Zone (LMZ) mainly formed by epidote-bearing amphibolites and interlayered gabbros commonly with mylonitic texture. Rare porphyroclastic textures and pyroxenes partially substituted by amphibole (Tremolite-Actinolite) are recognized (Correia and Girardi 1998). Correia and Girardi (1998) suggest that the mylonitic texture and the pyroxenes and

plagioclase substitution are a consequence of pervasive fluid percolation within this unit during the tectonic emplacement of the Cana Brava complex.

ii) an Ultramafic Zone (UZ) mainly of meta-peridotites with locally interlayered meta-pyroxenites. Serpentinites and amphibolites are the result of fluid-assisted low-grade metamorphism and hydrothermal processes, which affected dunites, peridotites and pyroxenite layers (Dreher et al. 1989; Correia et al. 1997; Correia and Girardi 1998; see Biondi 2014, for a detailed study). Locally, it is possible to recognize the primary cumulus texture. The top of the unit consists mainly of cumulate websterite (orthopyroxene between 15-25%, clinopyroxene between 75-85%). Approaching the top of the websterite layer, a gradational modal increase of orthopyroxene and plagioclase and a decrease of clinopyroxene are observed (Correia and Girardi 1998). Plagioclase is generally interstitial. Pyroxenes are sometimes replaced by amphibole and biotite (Correia and Girardi 1998). The transition to the Upper Mafic Zone is gradational with an increase of gabbro layers approaching the boundary. The thickness of the UZ is around 1.9 km in the southern part of the body and decreases progressively northwards. In the northern part, the UZ locally disappears, in a sort of boudinage. The websterite layer at the roof of the UZ has a thickness of ~500 m in the southern part of the complex and tends to disappear northward (Fig. 1).

iii) an Upper Mafic Zone (UMZ) mainly consisting of gabbros, gabbronorites and norites, with subordinate diorites, quartz-rich gabbros, quartz-rich diorites and, locally, tonalites mostly near the complex roof (Correia and Girardi 1998). The rocks commonly show igneous textures overprinted locally by a high temperature foliation, defined by the orientation of orthopyroxene, clinopyroxene and plagioclase (Correia and Girardi 1998). Minor/accessories phases are quartz, biotite, amphibole, spinel, apatite, titanite, rutile and zircon. Epidote and calcite are secondary phases. Approaching the roof of the complex, the rocks of the UMZ show an increase in biotite, amphibole and quartz and a decrease in orthopyroxene and clinopyroxene.

The contact with the stratigraphic upper Palmeirópolis Sequence is magmatic (Girardi and Kurat 1982; Correia and Girardi 1998). Xenoliths of the rocks of the Palmeirópolis Sequence are common in this unit, especially in the proximity of the roof, and may occur as both isolated fragments or layers parallel to the foliation. In the southern and central part of the Cana Brava complex, the majority of the crustal xenoliths are amphibolites, whereas quartzite levels have been observed in the northern part (Correia et al. 1997; Correia and Girardi 1998).

The Palmeirópolis Sequence is the most extended (c.a. 80 km long and up to 35 km wide) among the metavolcanic-metasedimentary sequences in contact with the Goiás layered complexes (the others are the Juscelândia Sequence at Barro Alto and the Indaianopólis at Niquelândia). The Palmeirópolis, Indaianopólis and Juscelândia sequences share similar stratigraphy and lithologies (Ferreira Filho et al. 2010 and references therein). These sequences mainly consist of metasediments (i.e. metacherts, metapelites and calc-silicate rocks) with interbedded amphibolites, gneisses and intrusive and sub-volcanic granites with typical MORB-like affinity (Brod and Jost 1991; Araújo et al. 1995; Araújo 1996; Moraes and Fuck 1994, 1999; Moraes et al. 2003, 2006; Ferreira Filho et al. 2010). The metavolcanics have both E-MORB and N-MORB affinities and this bi-modal volcanism has been ascribed to a transitional setting from a continental rift to an oceanic basin (Araújo 1996; Moraes et al. 2003, 2006). The rocks show metamorphic recrystallization, from amphibolite-facies, near the contacts with the complexes, to greenschist-facies (Araújo 1996; Moraes et al. 2003, 2006; Ferreira Filho et al. 2010 and references therein). Local granulite-facies conditions were also reported (Ferreira Filho et al. 2010 and references therein).

Comparison of Cana Brava and Niquelândia stratigraphy

The Niquelândia layered complex is the best known among the three Goiás layered complexes. It is about 40 km long and 20 km wide and lies in tectonic contact with the rocks of the Rio Maranhão

Thrust Zone to the E and in magmatic contact with the highest stratigraphic portion of the metavolcanic-metasedimentary sequence of Indaianopólis to the W (Correia et al. 2012 and references therein). The stratigraphy of the Niquelândia complex has been defined in various ways (see Ferreira Filho et al. 2010 and Correia et al. 2012). According to Correia et al. (2012), we divide the Niquelândia complex in two main sequences: the Lower Sequence (LS) and the Upper Sequence (US).

The LS is similar to the Cana Brava complex. From the E to the W it is formed by:

1) the Basal Gabbro Zone (BGZ), formed by gabbros interlayered with pyroxenites and peridotites. These rocks are commonly recrystallized by tectonic deformation, and correspond to the LMZ of the Cana Brava complex.

2) the Basal Peridotite Zone (BPZ) formed by massive cumulus dunites and harzburgites.

3) the Lower Ultramafic Zone (LUZ) formed by interlayered pyroxenites and peridotites with subordinate gabbros. The entire unit of BPZ and LUZ corresponds to the UZ of Cana Brava.

4) the Layered Gabbro Zone (LGZ) mainly formed by gabbros, gabbronorites and norites with subordinate biotite- and amphibole-gabbros, quartz-diorites and, locally, tonalites near the roof (the so-called 'Hydrous Zone', HZ). In this unit, bands and swarms of xenoliths of the same lithotypes from the upper portion of the Indaianopólis Sequence also occur. This unit corresponds to the UMZ of Cana Brava.

The US is divided in two units: the Upper Gabbro-Anorthosite Zone (UGAZ) and the Upper Amphibolite (UA):

5) the UGAZ is formed by olivine-gabbros, gabbros and anorthosites.

6) the UA mainly represents the magmatic, gradational contact between the Niquelândia complex and the Indaianopólis Sequence. This unit is formed by the alternation of amphibole-gabbro (considered as part of the complex) and garnet-bearing amphibolite (considered as part of the metavolcanic-metasedimentary sequence, which is similar to the Palmeirópolis Sequence).

A comparison of the Niquelândia and Cana Brava stratigraphy reveals that the US rocks are missing in the Cana Brava complex. The estimated thickness of the whole Niquelândia complex is c.a. 18 km. The estimated thicknesses, considering direction and dip, of the Niquelândia LS and the Cana Brava complex in its southern part (c.a. 12 km) are similar.

Age of the intrusion

Several intrusion ages of the Cana Brava complex have been published in the literature. Matsui et al. (1976) provided two Ar-Ar whole-rock isochrones on gabbros, norites and amphibolites of 1935 ± 110 Ma and 475 ± 15 Ma and several K-Ar ages distributed over a wide time span from 3950 Ma to 480 Ma. Girardi et al. (1978) dated two gneisses from the Palmeirópolis Sequence and the Serra da Mesa Group with Rb-Sr whole-rock isochrones at 1157 ± 150 Ma and 644 ± 27 Ma, respectively. They interpreted these ages as two distinct metamorphic events, which recrystallized the gneisses under amphibolite facies.

Fugi (1989) provided a Sm-Nd whole-rock isochron for the Cana Brava complex at 1970 ± 69 Ma, interpreted as the intrusion age. Correia et al. (1997) reported a Rb-Sr whole-rock isochron and an internal Sm-Nd isochron (plagioclase + biotite + pyroxene), which yielded ages of 1350 ± 35 Ma and 770 ± 43 Ma, respectively. They calculated the regression of the Sr isotopes evolution curve of the Cana Brava complex, obtaining a minimum age for mantle differentiation at 2250 Ma, interpreted as the time of the Cana Brava intrusion, whereas the younger isochron ages (i.e. 1350 ± 35 Ma and 770 ± 43 Ma) were attributed to two different metamorphic events.

The large age range given by whole rock “isochrones” is likely an artefact of the variability of the initial isotopic ratios of these largely contaminated rocks, as proposed by Ferreira Filho et al. (2010). Contamination processes are well known for the Niquelândia complex (Correia et al. 2007, 2012; Rivalenti et al. 2008) and have also affected the Cana Brava complex, as shown in this paper.

In such circumstances, the best methodology to obtain reliable ages is by U-Pb zircon geochronology. Ferreira Filho et al. (2010) determined U-Pb TIMS zircon ages at 782 ± 3 Ma and 779 ± 1 Ma on two samples from the UMZ and UZ (four and three analyses, respectively) and interpreted them as the intrusion age of the Cana Brava complex. U-Pb SHRIMP-II analyses on zircons from 4 samples of the Cana Brava complex (from the UMZ) reported by Giovanardi et al. (2015) provided concordia ages between 791.9 ± 9.0 Ma and 778.0 ± 6.7 Ma, consistent with those obtained by Ferreira Filho et al. (2010).

Post igneous evolution of the Cana Brava complex

Girardi and Kurat (1982), Correia et al. (1997), Correia and Girardi (1998), Ferreira Filho et al. (2010) and Biondi (2014) recognized that several metamorphic episodes have affected the Cana Brava complex. According to Correia et al. (1997), a first metamorphic event was responsible for the re-equilibration of pyroxenes and plagioclase under granulite-facies conditions at about 900° C and 6-7 kbar. However, Girardi and Kurat (1982) and Correia and Girardi (1998) suggested that this recrystallization "event" could be the consequence of the slow cooling of the Cana Brava complex. In contrast, Ferreira Filho et al. (2010) and Biondi (2014) documented a later granulite-facies event, which would have occurred around 770-760 Ma. According to all, the first metamorphic event caused the penetrative, high-temperature foliation and lineation of the rocks, a re-orientation of the igneous layering and the formation of mylonites and shear zones. Moreover, Correia et al. (1997) proposed that the tectonic transport of the Cana Brava complex occurred during this phase. The second metamorphic event proposed by Girardi and Kurat (1982) and Correia et al. (1997) occurred in upper-amphibolite facies as the retrograde event related to the first metamorphic peak (i.e. the granulite-facies metamorphism). During a late reactivation of faults and shear zones, hydrous fluids

migrated from the deformed area through the complex and produced the substitution of pyroxenes by amphibole (Girardi and Kurat 1982; Correia et al. 1997).

The last metamorphic event occurred as a low-grade episode under hydrothermal conditions, with fluids introduction in the lower units of the Cana Brava complex (i.e. the LMZ and UZ) and the formation of serpentinites, low-grade amphibolites and rodingites (Girardi and Kurat 1982; Dreher et al. 1989; Girardi et al. 1991; Correia and Girardi 1998; Ferreira Filho et al. 2010; Biondi 2014). According to Correia and Girardi (1998), Ferreira Filho et al. (2010) and Biondi (2014), this event was concurrent to the exhumation and the overthrust of the Cana Brava complex above the Serra da Mesa Group at 630 Ma, during the continental collision between the São Francisco and Amazonian cratons.

Field observations

A recent study of the Niquelândia complex re-interpreted the structural features and provided new evidences suggesting that the deformation of the complex occurred during its growth under hyper- to sub-solidus conditions (Correia et al. 2012). New field studies were conducted in the Cana Brava area to provide new constraints on the dispute about metamorphic vs syn-magmatic deformation. These field works were also performed in order to better define the nature of the western contact of the complex and the relationship between the Cana Brava complex and the Palmeirópolis Sequence.

The websterite layer at the roof of the UZ is about 500 m thick in the southern sector of the Cana Brava complex (Correia and Girardi 1998). In the central sector, it grades in a <10 m thick swarm of thin layers (mm-to-cm, Fig. 2a) of pyroxenite interfingered with gabbro. This layered package is locally anastomosed and vanishes to the north. The layering is parallel to the foliation, and both are locally cut by undeformed gabbro or pyroxenite dykes (Fig. 2a). Some of these

undeformed dykes crosscut a boulder at the base of UMZ in the central sector of the complex formed by foliated gabbro in contact with a major felsic domain (Fig. 2b) and late swarms of felsic veins and layers in the UMZ gabbros (Fig. 2c).

Most igneous rocks of both Cana Brava and Niquelândia are affected by granoblastic re-crystallization and high-T foliation parallel to the modal banding. These features were interpreted by various authors as evidences of a granulite-facies metamorphic event (Ferreira Filho et al. 1992, 1998; Ferreira Filho and Pimentel 2000). However, Correia et al. (2012) observed that, in Niquelândia, the high-T foliation is locally cut by undeformed veins of leuco-gabbro (Fig. 3), as commonly found in other large mafic intrusions (e.g., Ivrea-Verbano, Quick et al. 1992, 1994).

Similar structures are also present in Cana Brava (Fig. 2), providing evidences for melt percolation after the development of the foliation. This leads to conclude that, rather than evidence of a later granulite-facies metamorphic event, the high-T foliation is the result of hyper-solidus shear, which affected a largely crystallized crystal mush during the growth of the igneous body. The stretching that caused the high-T foliation may also be responsible, at least in part, for the progressive thinning northwards of the entire igneous complex.

In general, the abundance of hydrous phases increases approaching the top of the Cana Brava complex; however, it is not constant along the roof, showing a heterogeneous distribution. Their maximum amount is recognized in patches of amphibole- and biotite-rich, locally garnet-bearing diorites, which in general contain abundant xenoliths (amphibolites) from the Palmeirópolis Sequence (Fig. 4a). The xenoliths are rimmed by a micro-gabbro chilled margin (Fig. 4b). Banding is parallel to a high-T foliation defined by iso-orientation of plagioclase, biotite ± amphibole (Fig. 4b).

The dimension of the Palmeirópolis Sequence xenoliths seems to decrease from the base to the top of the UMZ. At the deepest levels of the UMZ, crustal inclusions are mainly quartzite layers of big size (cm-to-m thick and hundreds of meters long, elongated parallel to the foliation), which

are predominant in the northern sector of the complex. At higher levels, in the central UMZ, the xenoliths are mainly separated fragments (rarely longer than 1 m). Locally, crustal xenoliths from the Palmeirópolis Sequence are surrounded by undeformed leucosome, which may eventually fill the pressure shadow of pseudo-boudinage structures, suggesting that the xenoliths were partially molten during the shear that caused the foliation (Figs. 4c, d). Frequently, the xenoliths are elongated parallel to the foliation, as observed in the "Hydrous Zone" in Niquelândia (Figs. 3 and 4).

In the central and upper parts of UMZ, the xenoliths are mainly garnet-bearing amphibolite and amphibolite. Subordinate xenoliths of quartzites and garnet-bearing schists rich in biotite occur approaching the complex roof. Similar rocks are common in the lower Palmeirópolis Sequence near and at the contact with the Cana Brava complex (Figueiredo et al. 1981). Minor quartzite, metachert and iron banded layers are intercalated within the amphibolites (Figueiredo et al. 1981), and are similar to the quartzite septa included in the lower UMZ (Correia and Girardi 1998; this study). The similarities between xenoliths and rocks of the complex suggest that, if not from the Palmeirópolis Sequence, the xenoliths derived from an extremely similar metavolcanic-metasedimentary sequence.

Analytical methods

A total of 34 new samples from the Cana Brava complex were analysed for bulk rock major and trace elements to integrate the dataset of Correia and Girardi (1998) and to compare the geochemical variations of Cana Brava and Niquelândia. Ten of these samples were selected for mineral chemistry (for both major and trace elements) and their petrography is reported in Online Resource A.

Major element bulk rock analyses were performed by X-ray fluorescence, using a wavelength dispersive Philips PW 2400 spectrometry, using fused glass disks according to procedures described by Mori et al. (1999). Accuracy was greater than 2%. Trace element analyses in selected samples were performed by Inductively Coupled Plasma-Mass Spectrometry (ICP-MS) using the procedure described by Navarro et al. (2008). Accuracy, determined with respect to the reference standards BHVO-2 and BR, was 0.5–2%. Data are reported in Online Resource B.

On selected samples, Sm-Nd and Rb-Sr isotopic determination were carried out by Isotope Dilution Thermal Ionization Mass Spectrometry (ID-TIMS), following the procedure described in Sato et al. (1995). The isotopic ratios of the studied samples were measured on a VG Iso-mass 354 automated mass spectrometer using five Faraday collectors in static mode. Data are reported in Table 1. The $^{143}Nd/^{144}Nd$ ratio was corrected to standard JNdi-1 (Tanaka et al. 2000) with a reference value $^{143}Nd/^{144}Nd = 0.512097$ (± 0.000009, n=23). The $^{87}Sr/^{86}Sr$ ratio was corrected to standard NBS-987 (Moore et al. 1982) with a reference value $^{87}Sr/^{86}Sr = 0.710235$ (± 0.000025 between March and April 2015).

Major element in mineral were analysed by Electron Probe Micro Analyses (EMPA) with a JEOL 8200 Super Probe (data are reported in Online Resource C) after thin section carbon coating. Analytical conditions were 15 kV of acceleration voltage, 15 nA of primary current beam, 10 s counting time for each element and 5 s counting time for the background. Data were checked and corrected using cation mass balance with different O normalization for each phases (Amphibole and Biotite: 23 O; pyroxenes: 6 O and 4 cations p.f.u.; Titanite: 5 O and 3 cations p.f.u.; Ilmenite: 3 O and 2 cations p.f.u.; Garnet: 12 O and 8 cations p.f.u.; Plagioclase: 8 O and 5 cations p.f.u.; Fe_T as Fe^{2+}). Average analyses of the mineral phases are reported in Table 2 and full analyses are reported in Online Resource C.

Trace elements spot analyses on the same samples were determined by Laser ablation-inductively coupled plasma-mass spectrometry (LA-ICP-MS), using a ThermoFisher Scientific

Mass Spectrometer coupled to a laser ablation New Wave UP 213. Data reduction was achieved with the Thermo Fisher Scientific PlasmaLab® software using NIST610, NIST612 and NIST614 as external standards. The isotope ^{44}Ca was used as internal standard for Amphibole, Clinopyroxene, Plagioclase and Garnet and ^{29}Si for Biotite and Quartz. Laser spot size was calibrated at 80 μm and laser beam fluency at 20 microJoule for cm^2. Data are reported in Online Resource C.

Quartz internal structures of the quartzite sample CB1425 were observed by CathodoLuminescence (CL) images obtained during EMPA analytical sessions by JEOL 8200 Super Probe and a CL-C detector (JEOL). Analytical conditions were: high voltage = 15 kV, work distance = 11 mm, detector = PMT, filament emission = 15 nA, and magnification range = 40 to 65 ×.

Results

Chemical variations vs stratigraphy

In figures 5, 6 and 7 we present plots of the chemical variations vs. stratigraphy of the most significant trace elements for Cana Brava (this paper and Correia and Girardi 1998) and the lower Niquelândia (Correia et al. 2012). Given that the upper Niquelândia sector has a different stratigraphy when compared to Cana Brava, we disregard it in this comparison.

The most prominent feature is a sudden increase in incompatible elements abundances (K, Rb, Ba, and others) in the uppermost 2 km of the section approaching the roof of Cana Brava. Similar features are also observed in the "Hydrous Zone" of Niquelândia (Rivalenti et al. 2008; Correia et al. 2012; Fig. 7). In addition, an increase in the scattering of $(La/Yb)_N$ up section is observed. This

ratio, which is roughly indicative of the REE pattern, reaches the highest values at levels where xenoliths are particularly abundant, especially in the proximity of the roof and on a specific level at about 8 km from the bottom of the sequence.

The K_2O, Ba, Rb and La abundances are constant throughout the UMZ, with local enrichments between 6-8 km and a strong enrichment at the roof of the complex. The K_2O content ranges between 0.03-0.44 wt% in the UMZ and between 0.09-2.62 wt% at the roof (Figs. 5 and 6). The Ba content varies between 8-142 ppm in the UMZ and between 11-1760 ppm in the uppermost 2 km. The Rb content varies between 0.4-74 ppm in the UMZ and between 1.3-105 ppm at the roof of the complex. The La content varies between 1-24 ppm in the UMZ and between 6-40 ppm in the uppermost 2 km.

Moderately incompatible elements such as Sr, Nd and Y show two distinct enrichment peaks, the first in the central UMZ (corresponding to the 6-8 km level) and the second at the roof of the complex (Fig. 5). The Nb and Zr content shows a similar behaviour. In the central UMZ, Sr = 20-1124 ppm, Nd = 4-31.5 ppm, Y = 5-57 ppm, Nb = 2-91 ppm and Zr = 6-224 ppm, whereas at the roof of the complex Sr = 95-327 ppm, Nd = 7-47.4 ppm, Y = 7-91.3 ppm, Nb = 5-26 ppm and Zr = 23-605 ppm. The enrichment in incompatible elements approaching the roof of the complex is also shown by the REE patterns (Fig. 8). Samples from LMZ are slightly enriched in LREE and show flat trends for MREE and HREE (Fig. 8). Samples from UZ show depleted and flat trends consistent with cumulus of pyroxenes. Samples from UMZ show flat to slightly enriched LREE patterns (Fig. 8). Samples from the uppermost 2 km of the complex are enriched in LREE. Eu anomalies range from negative to positive (Fig. 8).

The $(La/Sm)_N$ ratio increases along the stratigraphy similarly to the $(La/Yb)_N$ ratio (Fig. 6). The highest variations occur between 6-8 km ($(La/Sm)_N$ = 1.19-2.74; $(La/Yb)_N$ = 1.25-4.90) and at the roof of the complex ($(La/Sm)_N$ = 2.38-4.03; $(La/Yb)_N$ = 2.53-17.98).

The spread and increase of incompatible and moderately incompatible elements approaching the complex roof is concomitant with the increase of hydrous phases and the maximum abundance of xenoliths within the complex. However, local enrichments are also present throughout the entire UMZ, in particular between 6-8 km (Figs. 5 and 6). These local enrichments occur in gabbros in contact/near xenoliths (sometimes clustered in levels).

Several amphibolites from the Palmeirópolis Sequence were analysed by Correia and Girardi (1998). Amphibolites show heterogeneous compositions, with some samples enriched in incompatible elements (e.g. Ba, Rb, Sr and Nd; Figs. 5 and 6): K_2O = 0.12-2.81 wt%, Ba = 12-1711 ppm, Rb = 2-101 ppm, Sr = 9-1150 ppm, Nd = 9-38 ppm, Y = 12-54 ppm. Amphibolite compositional ranges are similar to those of xenoliths within the complex (Figs. 5 and 6) and only few xenoliths from the complex roof, which are representative of the subordinate quartzites and garnet-bearing schists, show higher values for K_2O, Nd and Y. The similar compositions of amphibolites from the Palmeirópolis Sequence and from xenoliths within the complex, suggest that the latter were rocks of the Palmeirópolis Sequence incorporated during the growth of the complex.

Sr and Nd isotopes

Table 1 reports Sr and Nd isotopic compositions determined on 10 new samples and 3 samples analysed by Correia et al. (1997). All isotopic ratios are recalculated at 790 Ma. Pyroxenite sample CB1133 has a $^{87}Sr/^{86}Sr_{(790)}$ ratio of 0.708243 (which is the lowest value within the Cana Brava sample collection) and an $\varepsilon Nd_{(790)}$ of -0.78 (Table 1; Fig. 9). Across the stratigraphy, the $^{87}Sr/^{86}Sr_{(790)}$ ratio shows a continuous increase approaching the roof of the complex (Table 1; Fig. 9), reaching a maximum value of 0.730470 in the Garnet-diorite sample (CB1482) and of 0.736590 in an Amphibole-bearing gabbro (sample CB1490). These values are higher than the two samples reported by Correia et al. (1997) at the roof of the complex ($^{87}Sr/^{86}Sr_{(790)}$ =0.724609 and 0.725265),

resulting in a large spread in $^{87}Sr/^{86}Sr_{(790)}$ in the uppermost 2 Km, similar to what is observed in LIL elements (Table 1; Figs. 5 and 9). Conversely, the $\varepsilon Nd_{(790)}$ trend decreases only moderately approaching the top, where it reaches values of -8.42 in the diorite sample and of -8.47 in the gabbro sample (Table 1; Fig. 9). Comparing $^{87}Sr/^{86}Sr_{(790)}$ and $\varepsilon Nd_{(790)}$ an inverse correlation between the two values is evident (Fig. 10). Only sample CB1434 deviates from this trend showing an $\varepsilon Nd_{(790)}$ value of 1.70, with a $^{87}Sr/^{86}Sr_{(790)}$ ratio (0.711978) (Table 1; Figs. 9 and 10).

The xenolith shows $^{87}Sr/^{86}Sr_{(790)}$ ratio and $\varepsilon Nd_{(790)}$ comparable with the gabbroic rocks (0.728076 and -8.01 respectively; Fig. 9). Conversely, the Palmeirópolis Sequence sample has a clear mantle signature, with $^{87}Sr/^{86}Sr_{(790)} = 0.703278$ and $\varepsilon Nd_{(790)} = 12.81$.

Mineral chemistry

Mafic phases in igneous rocks of Cana Brava are generally in equilibrium as shown by the good correlation trends for Mg# (R^2 between 0.95-0.98; Fig. 11). Mineral compositions along the stratigraphy vary according to bulk-rock variation (Online Resource D). Amphibole (classified as Pargasite, Pargasite-Edenite and Mg-Hornblende in the rocks of the complex) cores are enriched in TiO_2 and FeO relative to the rims, but are depleted in Al_2O_3 (Tab. 2). In amphibole, the CaO content is higher in the cores than in the rims in the rocks of the lowest statigraphic levels (between 0 and 6 km), whereas the opposite zoning is observed at the highest levels (Tab. 2). Along the UMZ stratigraphy, amphibole shows enrichments in TiO_2, FeO and CaO and depletion in Al_2O_3. The Na_2O and K_2O content shows depletion trend up to 8 km and enrichments approaching the complex roof. Similar trends are recognizable for clinopyroxene and orthopyroxene (except for K_2O, Tab. 2). Clinopyroxene cores are enriched in FeO and depleted in CaO (Tab. 2). Conversely, the orthopyroxene cores are enriched in CaO in rocks at stratigraphic levels underneath 8 km and became depleted afterwards (Tab. 2). Plagioclase crystals show a reverse zoning, with rims enriched

in anorthite (An) relative to cores (with the exception of sample CB1482; Tab. 2). Minerals from the garnet-amphibolite xenolith (sample CB1060) within the complex show no or poor zoning.

Amphibole and clinopyroxene, when co-existing, show similar REE patterns and equilibrium in the partition of trace elements (Fig. 12). When only clinopyroxene occurs, it shows higher trace element abundance compared to samples containing also amphibole (Fig. 12).

In the UZ pyroxenite sample CB1042, amphibole and clinopyroxene show similar patterns depleted in LREE (Fig. 12; $(La/Sm)_N$ = 0.41 and between 0.29-0.35 respectively; $(La/Yb)_N$ = 0.22 and between 0.15-0.19; values normalized to the Primitive Mantle, PM, Hofmann, 1988). Both amphibole and clinopyroxene show a slightly negative Eu anomaly ($(Eu/Eu^*)_N$ = 0.86 and between 0.88-1.00), very low U, Th, Nb and Ta contents (<1) and similar Zr and Hf contents (Fig. 13; Zr = 12.06 ppm in amphibole and between 10.63-13.71 ppm in clinopyroxene; Hf = 0.59 ppm in amphibole and between 0.54-0.64 ppm in clinopyroxene).

Amphibole and clinopyroxene from UMZ gabbroic samples (samples CB1414, CB1464 and CB1475) have REE patterns depleted in LREE similar to the UZ sample (Fig. 12; $(La/Sm)_N$ = 0.58-0.62 in amphibole and between 0.25-0.61 in clinopyroxene; $(La/Yb)_N$ = 0.78-0.89 and 0.31-0.84, respectively). All the gabbroic samples cited above have a negative Eu anomaly (Fig. 12; $(Eu/Eu^*)_N$ = 0.35-0.47 for amphibole and 0.22-0.61 for clinopyroxene) related to plagioclase fractionation. Clinopyroxenes have similar $(Th/U)_N$, $(Zr/Hf)_N$ and $(Nb/Ta)_N$ ratios (Fig. 13; higher than 1 for $(Th/U)_N$ and lower for others respectively).

The two diorite samples (CB1424 and CB1482) show REE patterns enriched in LREE (Fig. 12; $(La/Sm)_N$ = 1.03-2.63 for amphibole and between 1.36-1.53 for clinopyroxene; $(La/Yb)_N$ = 1.28-186.58 and 1.56-1.65 respectively). Whereas amphiboles from sample CB1424 show t MREE-HREE trends almost flat and those from sample CB1482 show a strong depletion in MREE and HREE (Fig. 12). This may be an artefact of the co-existence of amphibole with garnet. Compared to gabbroic samples, clinopyroxenes from diorite CB1424 have a positive Eu anomaly ($(Eu/Eu^*)_N$ =

1.57-1.68 and 1.98-2.29 respectively). This feature was also observed in other layered complexes (e.g. the Val Sesia complex; Mazzucchelli et al. 1992) and was interpreted as the evidence of mixing between a mantle-derived melt and a crustal component derived from anatexis of granulite-facies metasediments. Amphibole and clinopyroxene from diorites have $(Th/U)_N$, $(Zr/Hf)_N$ and $(Nb/Ta)_N$ ratios similar to gabbros (Fig. 13).

Amphibole from the garnet-amphibolite xenolith (classified as Tschermakite, sample CB1060) is depleted in HREE, suggesting equilibrium with Garnet (Fig. 12; $(Sm/Yb)_N$ = 5.61-19.48), and in LREE, suggesting depletion during the incorporation within the complex (Fig. 12; $(La/Sm)_N$ = 0.08-0.13). Conversely, amphibole (classified as Hornblende) and clinopyroxene from the amphibolite of the Palmeirópolis Sequence show almost flat REE patterns, with a slight enrichment in LREE of clinopyroxene compared to amphibole (Fig. 12; $(La/Sm)_N$ = 0.74-0.98 and 1.32-1.94 respectively; $(La/Yb)_N$ = 0.58-0.87 and 0.89-1.37). Amphibole from garnet-bearing amphibolite (sample CB1060) has negative $(Th/U)_N$, $(Zr/Hf)_N$ and $(Nb/Ta)_N$ ratios (Fig. 13), while amphibole from Palmeirópolis Sequence sample (SP0003) has positive $(Zr/Hf)_N$ and $(Nb/Ta)_N$ ratios (Fig. 13). Differently from the amphibole, clinopyroxene from sample SP0003 has negative $(Zr/Hf)_N$ ratio (Fig. 13).

Discussion

Metamorphic overprint versus syn-magmatic deformation

The widespread high-T foliation and common hypersolidus deformation structures (see the *field evidences* chapter) indicate that the Cana Brava complex underwent hyper-to-sub solidus deformation during its intrusion, in the same way of the Niquelândia complex (Correia et al. 2012).

The close similarity of the metamorphic age (770-760 Ma of Ferreira Filho et al. 2010) and the crystallization ages (800-770 Ma of Ferreira Filho et al. 2010 and Giovanardi et al. 2015) reported in the literature, reinforce the interpretation that the granulite facies foliation and re-crystallization are not related to a later metamorphic event but a consequence of stretching during the intrusion growth. The 770-760 Ma recrystallization age of Niquelândia, inferred as metamorphic by Pimentel et al. (2004a), was later reinterpreted by Ferreira Filho et al. (2010) as indicative of the regional metamorphism that affected also Cana Brava and Barro Alto. This age is based on a concordant U-Pb SHRIMP analysis on low Th/U zircon rims from sample CF-04 (765 ± 8 Ma) (Pimentel et al. 2004a) and on a Sm-Nd garnet age of a metasediment sample (MR-137A) from the Mara Rosa Arc at 760 ± 75 Ma (Junges et al. 2002). As pointed out by Correia et al. (2012), sample CF-04 is likely a xenolith incorporated within Niquelândia (Pimentel et al. 2004a describe the sample as a 'quartz-rich mylonitic rock from a shear zone cutting through gabbros of the Upper Complex' and containing garnet and quartz with accessory plagioclase, kyanite ilmenite and zircon). Sample MR-137A, instead, belongs to a unit outcropping more than 100 km away from the Niquelândia complex and seems unrelated to the complexes intrusion. We infer that the rims of several zircons from sample CF-04 record the incorporation of the xenoliths in the mafic magma rather than a separate metamorphic overprint. Moreover, the Sm-Nd garnet age from the metasediment of the Mara Rosa Arc, if related to the studied area, records an age indistinguishable, within error, from the crystallization age of the complexes. Therefore, we conclude that, like in Niquelândia, the Cana Brava complex did not experience a later metamorphic event (Correia et al. 1997) or granulite-facies metamorphism (Ferreira Filho et al. 2010; Biondi 2014), and that the high-T “metamorphic” features are a consequence of shear of a crystallizing crystal mush during the growth of the complex. This hypothesis is also supported by mineral geochemistry. Minerals from the complex show igneous zoning (Table 2). The reverse zoning of plagioclase is common in several magmatic contexts and is generally interpreted as the evidence of i) diminishing P conditions, ii) mixing with

a new input of mafic melt or iii) increase of the H_2O in the residual melt (Sisson and Grove 1993; Singer et al. 1995 and references therein). The increase of CaO content in all phases along the stratigraphy (Table 2) rules out that the reverse zoning is an effect of subsolidus recrystallization because it should have depleted the other phases in Ca. However, the present data does not allow discriminating the process responsible for the inverse plagioclase zonation. Mg# correlation between the main mafic phases (i.e. clinopyroxene, orthopyroxene and amphibole) shows excellent linear trends (Fig. 11; R^2 = 0.95-0.98). Trace elements distribution between coexisting amphibole and clinopyroxene shows equilibrium patterns (e.g. samples CB1042, CB1414 and CB1424, Fig. 13). Magmatic zonations and the trace elements equilibrium between amphibole and clinopyroxene are consistent with crystallization of these phases from the same melt and not with metamorphic recrystallization. Amphibole absence results in higher trace elements abundance in clinopyroxene (Fig. 13), possibly because this is the only phase that can incorporate them.

In contrast, phase composition and textural evidences of the amphibolite sample from the Palmeirópolis Sequences (SP0003) suggest that amphibole and clinopyroxene are not in equilibrium in this rock. In particular, clinopyroxene occurs as relict often partially substituted by amphibole in small-grain bands. The trace element distribution show that clinopyroxene is slightly enriched in LREE ($(La/Sm)_N$ 1.32-1.94) whereas amphibole is slightly depleted ($(La/Sm)_N$ 0.74-0.98; Fig. 12). Clinopyroxene major element composition is similar to that one reported by Ferreira Filho et al. (1999) for the metamorphic clinopyroxene of the Juscelândia Sequence metabasalt (i.e SiO_2 > 52 wt%, Al_2O_3 < 2 wt% and CaO > 22 wt%; Table 2), whereas the plagioclase composition is similar to the igneous plagioclase in the metabasalt (i.e. An = 78.5-85.0 %, Ferreira Filho et al. 1999; Table 2). These observations suggest that sample SP0003 is only partially recrystallized by the metamorphic event that affected the metavolcanic-metasedimentary sequences (Ferreira Filho et al. 2010 and references therein). Conversely, amphibole from the garnet-amphibolite within the complex (CB1060) does not show crystal zonation and the plagioclase zonation is minor compared

to the Palmeirópolis amphibolite (Fig. 13). The amphibole has trace elements patterns in equilibrium with the garnet (Figs. 12 and 13). The absence of phase zonation and the amphibole/garnet trace elements equilibrium and LREE depletion suggest that sample CB1060 was more re-equilibrated than the amphibolite of Palmeirópolis (sample SP0003). The more evolved re-equilibration of the xenoliths in comparison to the partial re-equilibration of the Palmeirópolis amphibolite, is consistent with the protracted entrapment (or sinking) of the xenolith within a substantial amount of magma.

Geothermometry

We used four different geothermometers to evaluate the temperature of the Cana Brava parent melt and the temperature reached by the xenoliths. Data are reported in °C in Table 3. For gabbroic rocks of the complex, we used the Fe-Mg exchange between clinopyroxene and orthopyroxene (Wells 1977), the Ca and Al in orthopyroxene and clinopyroxene (Mercier 1980) and the amphibole-plagioclase equilibrium (Holland and Blundy 1994). Two xenolith samples were investigated: the garnet-amphibolite CB1060, using the Holland and Blundy (1994) geothermometer, and the quartzite CB1425. Quartz crystals from the latter were studied in cathodoluminescence (Fig. 14) and analysed for Ti by LA-ICP-MS to estimate the "Ti in quartz temperature" according to Thomas et al. (2010). The temperature of an amphibolite of the Palmeirópolis Sequence was estimated using the Holland and Blundy (1994) geothermometer.

Temperatures of the gabbroic rocks obtained with the geothermometers of Wells (1977) and Mercier (1980) range between 819-993°C and 879-1144°C, respectively, and differ by about 150°C. Temperatures obtained with the Holland and Blundy (1994) geothermometer show intermediate values in the range of 879-995°C, but closer to those calculated according to Wells (1977) (Table 3; Fig. 15). Notwithstanding the differences, all temperatures are high and we

interpret them as closure temperatures of the different systems during the crystallization of the complex.

The temperatures estimated for the garnet-amphibolite xenolith according to the thermometer of Holland and Blundy (1994) range from 866° to 956°C and are comparable to those obtained for the gabbroic rocks (Table 3; Fig. 15). This suggests that the xenolith attained granulite-facies conditions after its incorporation into the complex.

We used the Ti in quartz geothermometer of Thomas et al. (2010) to estimate temperatures along two cm-large crystal transects (Fig. 14). Due to the absence of other Ti-rich phases, the α TiO_2 was fixed at 0.1 and the pressure at 6 kbar (the minimum pressure estimated in literature for the crystallization of the complex). Temperatures estimated for the one crystal are much lower than the other, ranging between 669-886°C and 735°-1157°C, respectively (Table 3; Fig. 15). Possibly, the highest values represent the heating of the quartzite layer during its permanence in the magma batch, consistent with its location in the complex at a level deeper than the garnet-amphibolite. The high T reached by the xenoliths is consistent with their restitic composition after melt extraction.

Contamination process and comparison with the Niquelândia complex

Based on Sr isotopic ratios, Correia et al. (1997) proposed that the Cana Brava complex was affected by crustal contamination. The new isotopic data and the revision of the geochemical data support this hypothesis as explained here below (Figs. 9 and 10).

The K_2O, LILEs, Rb and Ba content in the rocks of the Cana Brava complex show constant values or a mild enrichment along stratigraphy, followed by higher values and a large spread approaching the roof (from 10 km; Figs. 5 and 6). The UZ pyroxenites show LREE depletion and flat trends (Fig. 8) consistent with cumulates from a MORB magma similar to the one estimated as the Cana Brava parental melt by Correia and Girardi (1998). The LREEs in the UMZ whole rock

show a continuous increase upwards ($(La/Sm)_N$ range from 1.18 to 4.01; Figs. 6 and 8). Similarly to the $(La/Sm)_N$, the Rb-Sr and Sm-Nd isotopes along the Cana Brava stratigraphy show a gradual increase of contamination approaching the roof (Fig. 9). These features suggest that the contamination affected the entire magma column during the UMZ crystallization and was more intense in the igneous rocks containing abundant xenoliths, particularly in the uppermost 2 km of the complex. Locally, an increase of the contamination due to xenoliths contribution is supported by the spread of $^{87}Sr/^{86}Sr_{(790)}$ ratios observed at the roof of the complex ($^{87}Sr/^{86}Sr_{(790)}$= 0.724609-0.736590), where xenoliths are more abundant, and by isotopes of the two samples at the base of the UMZ (CB1434 and CB1464, $^{87}Sr/^{86}Sr_{(790)}$ = 0.711978, 0.715871 and $\varepsilon Nd_{(790)}$ = 1.70, -5.65 respectively; Table 1; Figs. 9 and 10), which are close to a quartzite layer (sample CB1425).

These geochemical features are extremely similar to what has been observed in the Lower Sequence of the Niquelândia complex by Rivalenti et al. (2008) and Correia et al. (2012). They demonstrated that the lower units of the Niquelândia complex reached maximum contamination in the Hydrous Zone (Fig. 9; Correia et al. 2012). Conversely, the upper unit of Niquelândia (i.e. the Upper Gabbro-Anorthosite Zone, UGAZ of Girardi et al. 1986) is poorly or not contaminated (Fig. 10). In the Hydrous Zone, the contamination is shown by an anomalous increase of the most incompatible elements (e.g. K_2O, LREE, Rb and Ba) and by the Rb-Sr and Sm-Nd isotope ratios (Rivalenti et al. 2008). Based on the random variation of the contamination degree along the stratigraphy of the Niquelândia complex (Fig. 9), Rivalenti et al. (2008) and Correia et al. (2012) proposed that crustal contamination began later and locally, during the growth of the complex, when the parental melt had already fractionated the ultramafic units (i.e. the Basal Gabbro Zone, BGZ, the Basal Peridotite Zone, BPZ and the Layered Ultramafic Zone, LUZ; Girardi et al. 1986). According to them, the anorthositic crystal mush, which crystallized the upper Niquelândia sequence, was segregated during this first stage, and the buoyant crystal mush escaped the

contamination that later affected the mafic magma in the proximity of the incorporated crustal levels (Rivalenti et al. 2008; Correia et al. 2012).

Apart from the absence of anorthosites, the Cana Brava complex shares many characteristics with the Lower Sequence of Niquelândia. The parental melts estimated for the two complexes by Correia et al. (2012) and Correia and Girardi (1998) are very similar and inferred to be picritic MORB in composition. Thus, we propose that the contamination in Cana Brava has occurred as in Niquelândia, beginning after the fractionation of the ultramafic units, as proposed by Rivalenti et al. (2008) and Correia et al. (2012), and coupling an in situ effect driven by the abundance and composition of crustal xenoliths with a process at the scale of the whole complex (an AFC as proposed by Rivalenti et al. 2008).

Evidences for a single large intrusion

Ferreira Filho (1998) were the first one to propose, based on the similarity of ages and stratigraphy, that the three large layered intrusions constitute an originally continuous magmatic structure. Carminatti (2006) suggested a similar hypothesis based on gravimetric and geophysical evidences. However, Ferreira Filho et al. (2010) inferred that the three complexes might be distinct intrusions, because of the slightly younger age of the Cana Brava complex compared to the ages of Barro Alto and Niquelândia (Cana Brava c.a. 780 Ma, Niquelândia and Barro Alto c.a. 800-790 Ma).

More recently, SHRIMP ages obtained by Giovanardi et al. (2015) for Cana Brava yielded an ~800-780 Ma age, slightly older than the age obtained by Ferreira Filho et al. (2010) and close to the age of Niquelândia by Correia et al. (2012). Therefore, we conclude that the three complexes have, within errors, the same age and possibly could be part of a single body.

Not taking into account the Barro Alto complex, we will compare now the Niquelândia and Cana Brava complexes. Both Cana Brava and Niquelândia grew in a syn-magmatic stress field that

caused hypersolidus foliation and re-crystallization of the igneous textures. Attitudes of banding and foliation in both complexes are similar (10-20° NNE, 30-50°W dip). Considering the two bodies as fragments of a single mafic batolith, it is possible to notice a progressive, northwards attenuation of the banding. In particular, the thickness of the cumulus peridotite decreases from ~2 km in the southern side of Niquelândia to ~1 km in the southern Cana Brava body and vanishes towards the North (Fig. 16). Moreover, the pyroxenite band, which is about 1 km thick in southern Niquelândia, diminishes to about 500 m in southern Cana Brava, turns northwards into a swarm of thin pyroxenite bands interlayered with gabbro and disappears in the northern sector (Fig. 1). In addition, in Niquelândia the upper anorthositic sequence of the complex is thick in the south and reduced northwards, and does not exist in Cana Brava (Fig. 16).

We re-calculated the estimated thickness of Cana Brava in the southern part of the complex to about 12 km (Figs. 1 and 16) and this value matches the thickness of the Niquelândia Lower Sequence at its northern end (Correia et al. 2012). The stratigraphic, structural, geochronological and geochemical similarities between the two sequences support the hypothesis that the Cana Brava and Niquelândia complexes are part of a single large intrusion. In Cana Brava, hydrous phases increase in gabbroic and dioritic rocks approaching the roof, same as in the Hydrous Zone of Niquelândia. In both cases, the increase in hydrous phases is associated to the common presence of crustal xenoliths. Similarly, both complexes show an increase in contamination along the stratigraphy and up to the roof. The isotopic and geochemical variations are comparable (Figs. 6, 7, 9 and 10).

At the southern end of Cana Brava, the convergence of banding and foliation suggests a sort of mega-boudinage of the entire complex (Figs. 1 and 16) (Correia et al. 1997; Correia and Girardi 1998; Ferreira Filho et al. 2010), possibly caused by tectonics during the exhumation of the complexes. According to Rivalenti et al. (2008) and Correia et al. (2012), the Upper Sequence of the Niquelândia complex consists mainly of anorthosites formed by segregation of the anorthositic

crystal mush after fractionation of abundant peridotite cumulates. In Cana Brava, their absence is associated to a reduced thickness of the cumulus peridotite. Possibly, the anorthositic crystal mush formed only above the most important feeding centre(s), located somewhere in correspondence of Niquelândia. The decrease in thickness of the Upper Sequence of the Niquelândia complex to the North suggests that the anorthosite bands tend to disappear in this direction. However, the lack of outcrops between Cana Brava and Niquelândia hides this feature in the field. Therefore, based on all new and old geochemical data and field observations we conclude that Cana Brava and Niquelândia are fragments of a single body.

Conclusions

Field and geochemical evidences are consistent with an incremental growth of the Cana Brava body in a stress field that produced a sin-magmatic to high-T foliation and a granoblastic recrystallization. Structural, geochronological and mineralogical data indicate that the foliation and re-crystallization were not related to a later metamorphic event as formerly proposed, but were the consequence of stretching during the emplacement of the complex. The new chemical and isotopic data presented in this paper demonstrate that the Cana Brava complex was contaminated during its growth, similarly to what has been observed in the Lower Sequence of Niquelândia. The contamination in the Cana Brava complex shows an effect at the local scale as revealed by the spread of trace elements and isotope values near xenoliths-rich layers and a general enrichment along the stratigraphy, suggesting a progression of the contamination during the growth of the complex.

The Cana Brava complex and the Lower Sequence of Niquelandia share very similar chemical and textural characteristics and have, within error, the same age. Considered collectively, the two

complexes show a continuous northwards thinning of the entire body as well as of individual bands (e.g. the ultramafic level). All these observations lead us to conclude that, most likely, the two complexes are separate parts of a single, large mafic body.

Acknowledgments Constructive comments by an anonymous reviewer, Cesar F. Ferreira Filho, Fernando Gervilla and Lutz Nasdala helped us improve the manuscript and are gratefully acknowledged. Anna Cipriani is deeply thanked for the stimulating discussion that improved the manuscript. Tommaso Giovanardi acknowledges the financial support of the Research Support Foundation of the State of São Paulo (FAPESP) in the frame of project 2013/19519-6. We would also like to thank the following institutions for the permission to use analytical facilities: the Mineralogy and Geotectonic Departament of the Universidade de São Paulo (Brazil) for the bulk rock major and trace element analyses, the Geochronological Research Centre of the Universidade de São Paulo (Brazil, IGc-CPGeo-USP) for the Sm-Nd and Rb-Sr isotopic analyses, the University of Milano (Italy) for the electron microprobe and cathodoluminescence analyses, the Centro Interdipartimentale Grandi Strumenti (C.I.G.S.) of the University of Modena and Reggio Emilia for the LA-ICP-MS.

References

Anders E, Edibara M (1992) Solar system abundances of the elements. Geochim Cosmochim Ac 46:2363-2380

Araújo SM, Fawcett JJ, Scott SD (1995) Metamorphism of hydrothermally altered rocks in a volcanogenic massive sulfide deposit: the Palmeirópolis, brazil, example. Rev Bras Geociências 25(3):173-184

Araújo SM (1996) Geochemical and isotopic characteristics of alteration zones in highly metamorphosed volcanogenic massive sulfide deposits and their potential application to mineral exploration. Unpublished Ph.D. Thesis, Department of Geology, University of Toronto, Canada, pp 1-210

Biondi JC (2014) Neoproterozoic Cana Brava chrysotile deposit (Goiás, Brazil): Geology and geochemistry of chrysotile vein formation. Lithos 184-187:132-154

Brod JA, Jost H (1991) Características estruturais, litológicas e magmáticas da zona de cisalhamento dúctil do Rio Traíras, bloco do Complexo Niquelândia, Goiás. Rev Bras Geociências 21: 205-217.Carminatti MG (2006) Modelagem geofisica dos corpos maficos-ultramaficos de Cana Brava, Niquelandia e Barro Alto, centro de Goias. PhD Thesis for the Universidade de São Paulo (Brazili), Instituto de Geociências, pp 1-293

Correia CT, Girardi VAV (1998) Geoquimica e petrologia das rochas maficas e ultramaficas do complexo estratiforme de Cana Brava - GO, e das suas encaixantes. Bol Inst Geociências USP 29:1-37

Correia CT, Girardi VAV, Tassinari CG, Jost H (1997) Rb-Sr and Sm-Nd geochronology of the Cana Brava layered mafic-ultramafic intrusion, Brasil, and considerations regarding its tectonic evolution. Rev Bras Geociências 27(2):163-168

Correia CT, Jost H, Tassinari CCG, Girardi VAV, Kinny PD (1999) Ectasian Mesoproterozoic U–Pb ages (SHRIMP II) for themetavolcano-sedimentary sequences of Juscelandia and Indaianopolis and for the high grade metamorphosed rocks of the Barro Alto stratiform igneous complex, Goiàs State, Central Brasil. II° South Am Symp Isotopic Geology, Cordoba, Argentina, Actas, pp 31-33

Correia CT, Girardi VAV, Basei MAS, Nutman A (2007) Cryogenian U–Pb (Shrimp I) zircon ages of anorthosites from the upper sequences of Niquelandia and Barro Alto Complexes, Central Brasil. Rev Bras Geociências 37:70-75

Correia CT, Sinigoi S, Girardi VAV, Mazzucchelli M, Tassinari CCG, Giovanardi T (2012) The growth of large mafic intrusions: Comparing Niquelandia and Ivrea igneous complexes. Lithos 155: 67-182

Della Giustina MES, Pimentel MM, Ferreira Filho CF, Fuck RA, Andrade S (2011) U–Pb–Hf-trace element systematics and geochronology of zircon from a granulite-facies metamorphosed mafic–ultramafic layered complex in Central Brazil. Precambrian Res 189:172-192

Dreher AM, Girardi VAV, Comin-Chiaramonti P (1989) Petrología dos rodingitos do complexo máfico-ultramáfico de Cana Brava, Goiás. Rev Bras Geociências 19(2):224-236

Feininger T, Dantas JJ, Girardi VAV (1991) Gravity interpretation and possible regional significance of the Niquelândia layered basic–ultrabasic complex, Goiàs, Brasil. J S Am Earth Sci 4:343-350

Ferreira Filho CF (1998) Geology and petrology of the large layered intrusions of central Brazil: implications for PGE mineralization. In: Platinum Symposium, Rustemburg, South Africa, Extended Abstracts, pp 107-110

Ferreira Filho CF, Nilson AA, Naldrett AJ (1992). The Niquelândia mafic–ultramafic complex, Goiás, Brazil: a contribution to the ophiolite vs. stratiform controversy based on new geological and structural data. Precambrian Res 59:125-143

Ferreira Filho CF, Naldrett AJ, Gorton MP (1998). REE and pyroxene compositional variation across the Niquelândia layered intrusion, Brazil: petrological and metallogenetic implications. Applied Earth Science, Transactions of the Institutions of Mining and Metallurgy, Section B 107:1-21

Ferreira Filho CF, Araujo SM, Cruz HP (1999) Estruturas vulcânicas em granulitos da sequência vulcano-sedimentar Juscelândia, GO. Rev Bras Geociências 29:461-468

Ferreira Filho CF, Pimentel MM (2000). Sm–Nd isotope systematics and REE–Hf–Ta–Th data of troctolites and their amphibolitized equivalents of the Niquelândia Complex upper layered series, central Brazil: further constraints for the timing of magmatism and high-grade metamorphism. J South Am Earth Sci 13:647-659

Ferreira Filho CS, Pimentel MM, Maria de Araujo S, Laux JH (2010) Layered intrusions and volcanic sequences in Central Brazil: geological and geochronological constraints for Mesoproterozoic (1.25 Ga) and Neoproterozoic (0.79 Ga) igneous associations. Precambrian Res 183:617-634

Figueiredo JA, Leao Neto R, Valente CR (1981). Depositos de sulfetos macros de Zn, Cu e Pb da região de Palmeirópolis, GO. In: SIMP. GEOL. CENTRO-OESTE, 1. Goiania, 1981. Ata, Goiania, SBG - Nucleos Centro-Oeste and Brasilia, pp 422-441.

Fugi MY (1989) REE geochemistry and Sm/Nd geochronology of the Cana Brava Complex, Brazil. Unpublishied Master Thesis, Kobe University, Japan, pp 1-55

Giovanardi T, Girardi VAV, Correia CT, Sinigoi S, Tassinari CCG, Mazzucchelli M (2015) U-Pb zircons SHRIMP data from the Cana Brava Layered Complex: New constraints for the mafic-ultramafic intrusions of Northern Goiás, Brazil. Open Geosci 7:197-206

Girardi VAV, Kurat G (1982) Precambrian mafic and ultramafic rocks of the Cana Brava Complex, Brazil - mineral compositions and evolution. Rev Bras Geociências 12(1-3):313-323

Girardi VAV, Kawashita K, Basei MAS, Cordani U (1978) Algumas considerações sobre a evolução geológica da região de Cana Brava, a partir de dados geocronológicos. Congresso Brasileiro do Geologia, 1978, 30, Recife, Anais SBG 1:337-348

Girardi VAV, Rivalenti G, Sinigoi S (1986) The petrogenesis of Niquelandia layered basic–ultrabasic complex, central Goias, Brasil. J Petrol 27:715-744

Girardi VAV, Censi P, Comin-Chiaramonti P, Correia CT (1991) Análises isotópicas e difratométricas em dolomitas e grafitas de veios provenientes do Maciço de Cana Brava, Goiás. Anais do 3° Congresso Brasileiro de Geoquímica e 1° Congresso de Geoquímica dos Países de Língua Portuguesa. São Paulo, SP, Brasil, pp 583-585

Hofmann AW (1988) Chemical differentiation of the Earth: The relationship between mantle, continental crust and oceanic crust. Earth Planet Sc Lett 90:297-314

Holland T, Blundy J (1994) Non-ideal interactions in calcic amphiboles and their bearing on amphibole-plagioclase thermometry. Contrib Mineral Petr 116:433-447

Junges SL, Pimentel MM, Moraes R (2002) Nd isotopic study of the Neoproterozoic Mara Rosa Arc, central Brazil: implications for the evolution of the Bras´ılia Belt. Precambrian Res 117:101-118

Marangoni Y, Assumpcão M, Fernandes EP (1995) Gravimetria em Goiás, Brasil. Rev Bras Geofísica 13:205-219

Matsui K, Girardi VAV, Basei MAS, Hasui Y (1976) Geocronologia do complexo básico-ultrabásico de cana Brava, Goiás. Congresso Brasileiro do Geologia, 1976, 29, Ouro Preto, Anais SBG 4:279-288

Mazzucchelli M, Rivalenti G, Vannucci R, Bottazzi P, Ottolini L, Hofmann AW, Parenti M (1992) Primary positive Eu anomaly in clinopyroxenes of low-crust gabbroic rocks. Geochim Cosmochim Ac 56(6):2363-2370

Mercier JCC (1980) Single-pyroxene thermobarometry. Tectonophysics 70:1-37

Moore LJ, Murphy TJ, Barnes IL, Paulsen PJ (1982) Absolute Isotopic Abundance Ratios and Atomic Weight of a Reference Sample of Strontium. J of Res (NBS) 87(1):1-8

Moraes R, Fuck RA (2000) Ultra-high-metamorphism in Central Brasil: the Barro Alto complex. J Metamorph Geol 18:345-358

Moraes R, Fuck RA, Pimentel MM, Gioia SMCL, Figueiredo AMG (2003) Geochemistry and Sm–Nd isotope characteristics of bimodal volcanic rocks of Juscelândia, Goiás, Brazil: Mesoproterozoic transition from continental rift to ocean basin. Precambrian Res 125:317-336

Moraes R, Fuck RA, Pimentel MM, Gioia SMCL, Hollanda MHBM, Armstrong R (2006) The bimodal rift-related volcanosedimentary sequence in Central Brazil: Mesoproterozoic extension and Neoproterozoic metamorphism. J S Am Earth Sci 20:287-301

Mori PE, Reeves S, Correia CT, Haukka M (1999) Development of a fused glass disc XRF facility and comparison with the pressed powder pellet technique at Instituto de Geociências. Rev Bras Geociências 29:441-446

Navarro MS, Andrade S, Ulbrich HHGJ, Gomes CB, Girardi VAV (2008) The analysis of rare earth elements with ICP-MS in basaltic and related rocks: testing the efficiency of sample decomposition procedures. Geostand Geoanal Res 32(2):167-180

Pimentel MM, Fuck RA, Jost H, Ferreira Filho CF, Araujo SM (2000) The basement of the Brasília Fold Belt and the Goiás Magmatic Arc. In: Cordani UG, Milani EJ, Thomaz Filho A, Campos DA (eds) The Tectonic Evolution of South America, Rio de Janeiro. Proceedings of the 31st International Geological Congress, Rio de Janeiro, pp 195-229

Pimentel MM, Ferreira Filho CF, Amstrong RA (2004a) Shrimp U–Pb and Sm–Nd ages of the Niquelandia Layered Complex: Meso (1,25 Ga) and Neoproterozoic (0,79 Ga) extensional events in Central Brasil. Precambrian Res 132:132-135

Pimentel MM, Jost H, Fuck RA (2004b) O embasamento da Faixa Brasilia e o Arco Magmático de Goiás. In: Geologia do Continente Sul-Americano: Evolução da Obra de Fernando Flávio Marques de Almeida, pp 355-368

Pimentel MM, Ferreira Filho CF, Armele A (2006) Neoproterozoic age of the Niquelândia complex, Central Brazil: further ID-TIMS and Sm–Nd isotopic evidence. J S Am Earth Sci 21:228-238

Quick JE, Sinigoi S, Negrini L, Demarchi G, Mayer A (1992) Synmagmatic deformation in the underplated igneous complex of the IVZ. Geology 20:613-616

Quick JE, Sinigoi S, Mayer A (1994) Emplacement dynamics of a large mafic intrusion in the lower crust, Ivrea-Verbano Zone, northern Italy. J Geophys Res 99(B11):21559-21573

Ribeiro Filho W, Teixeira NA (1981) Sequencia vulcano-sedimentar da Borda Oeste dos Complexos de Niquelandia e Cana Brava. Boletim informativo 10, SBG, Nucleo Centre-Oeste, pp 157-177

Rivalenti G, Girardi VAV, Sinigoi S, Rossi A, Siena S (1982) The Niquelandia mafic-ultramafic complex of central Goias, Brasil: petrological consideration. Rev Bras Geociências 12:380-391

Rivalenti G, Correia CT, Girardi VAV, Mazzuchelli M, Tassinari CC, Bertotto GW (2008) Sr–Nd isotopic evidence for crustal contamination in the Niquelandia complex, Goiàs, Central Brasil. J S Am Earth Sci 25:298-312

Sato K, Tassinari, CCG, Kawashita K, Petronilho L (1995) O método geocronológico Sm–Nd no IG/USP e suas aplicações. Annais, Brazilian Academy of Sciences 67:313-336

Singer BS, Dungan MA, Layne GD (1995) Textures and Sr, Ba, Mg, Fe, K, and Ti compositional profiles in volcanic plagioclase: Clues to the dynamics of calc-alkaline magma chambers. Am Mineral 80:776-798

Sisson TW, Grove TL (1993) Experimental investigations of the role of H_2O in calc-alkaline differentiation and subduction zone magmatism. Contrib Mineral Petr 113:143-166

Tanaka T, Togashi S, Kamioka H, Amakawa H, Kagami H, Hamamoto T, Yuhara M, Orihashi Y, Yoneda S, Shimizu H, Kunimaru T, Takahashi K, Yanagi T, Nakano T, Fujimaki H, Shinjo R, Asahara Y, Tanimizu M, Dragusanu C (2000) JNdi-1: a neodymium isotopic reference in consistency with LaJolla neodymium. Chem Geol 168:279–281

Thomas JB, Watson EB, Spear FS, Shemella PT, Nayak SK, Lanzirotti A (2010) TitaniQ under pressure: the effect of pressure and temperature on the solubility of Ti in quartz. Contrib Mineral Petr 160:743-759

Wells PR (1977) Pyroxene thermometry in simple and complex systems. Contrib Mineral Petr 62:129-140

Williams IS (1998) U-Th-Pb geochronology by ion microprobe. In: McKibben, M.A., Shanks, W.C.P., Ridley, W.I. (eds) Applications of Microanalytical Techniques to Understanding Mineralizing Processes, Rev Econ Geol vol 7. Soc Econ Geol, Littleton, pp 1-35

Workman, R.K., Hart, S.R., 2005. Major and trace element composition of the depleted MORB mantle (DMM). Earth Planet Sc Lett 231:53-72

Figure Captions

Fig 1 Geological map of the Cana Brava complex, modified from Correia et al. (1997) and Ferreira Filho et al. (2010)

Fig 2 Selected images of the field relationships from the Cana Brava complex: a) deformed websterite layers in the northern part of the Cana Brava complex crosscutted by late undeformed vein; b) gabbro of the lower UMZ in contact with a felsic domain crosscutted by pyroxenites and anorthositic veins; c) late felsic veins parallel to the gabbro foliation. A schematic sketch of the major features of each picture is also presented

Fig 3 Selected images of field textures from the Niquelândia complex: a) late undeformed pyroxenite vein crosscutting the superimposed foliation; b) undeformed gabbroic layers crosscutting the foliation and a deformed pyroxenite layer; c) deformed xenoliths parallel to the gabbro foliation in the LGZ; d) xenolith aligned to the gabbro foliation in the LGZ

Fig 4 Selected images of field relationships from the Cana Brava complex: a) amphibolite xenolith in a garnet-bearing diorite of the roof complex; b) section of the 4a xenolith and host diorite with highlighted areas of different composition; c) deformed mafic enclaves and felsic 'pressure shadow' domain; d) undeformed xenoliths aligned with the gabbro foliation and occurrence of late felsic domains along the deformation at the top of the complex

Fig 5 Plot of bulk-rock trace element concentrations (in ppm) along the stratigraphy of the Cana Brava complex

Fig 6 Plot of bulk-rock K_2O and trace elements ratios normalized to the Primitive Mantle (PM; Hoffman 1988) along the stratigraphy of the Cana Brava complex

Fig 7 Plot of bulk-rock K_2O and trace elements ratios normalized to the Primitive Mantle (PM; Hoffman 1988) along the stratigraphy of the Niquelândia complex

Fig 8 Plot of bulk-rock REE patterns normalized to the Chondrite I composition (CI; Anders and Edibara 1992)

Fig 9 Plot of $^{87}Sr/^{86}Sr$ ratio and εNd recalculated to 790 Ma of samples from the Niquelândia (Correia et al. 2012) and Cana Brava complexes along the stratigraphy

Fig 10 Plot of εNd and $^{87}Sr/^{86}Sr$ ratio recalculated to 790 Ma of samples from the Niquelândia (Correia et al. 2012) and Cana Brava complexes. DMM is the Depleted Mantle MORB from Workmann and Hart (2005)

Fig 11 Plot of Mg/(Mg+Fe) (Mg#, as molar ratio) of coexisting minerals in UZ and UMZ Cana Brava rocks

Fig 12 Plot of amphibole, clinopyroxene and garnet REE (and Y) compositions of analysed samples from the different units, normalized to the Chondrite I (CI; values from Anders and Ebihara 1982)

Fig 13 Plot of amphibole, clinopyroxene and garnet trace element compositions of analysed samples from the different units, normalized to the Primitive Mantle (PM; values from Hoffman 1988)

Fig 14 Selected CL images of quartz grains in sample CB1425. Circles are LA-ICP-MS analysis points.

Fig 15 Plot of temperatures (maximum, average and minimum) calculated using the geothermometers of Wells (1977), Mercier (1980) and Holland and Blundy (1994). Temperatures from all analyses on quartzite based on the Ti in quartz geothermometer (Thomas et al. 2010) calculated at 6 kbar and assuming $\alpha\ TiO_2 = 0.1$ due to the absence of other phases except for quartz

Fig 16 Comparison of the Niquelândia and Cana Brava complexes. The Niquelândia map is modified from Correia et al. (2012) and the Cana Brava map is from this work

Colour Figure 1

Click here to download Colour Figure Fig. 1_rev2.png

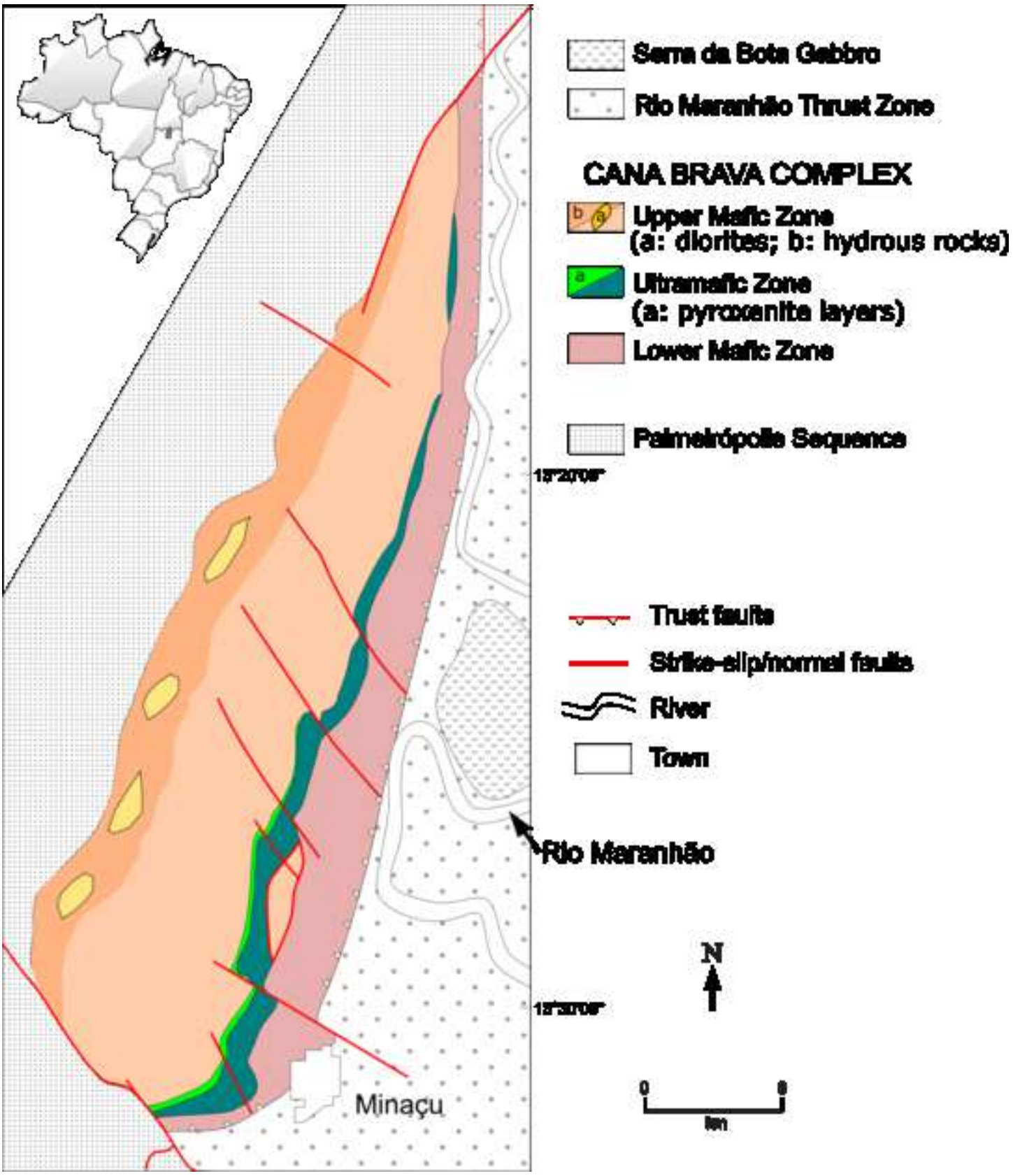

Colour Figure 2

Click here to download Colour Figure Fig. 2.png

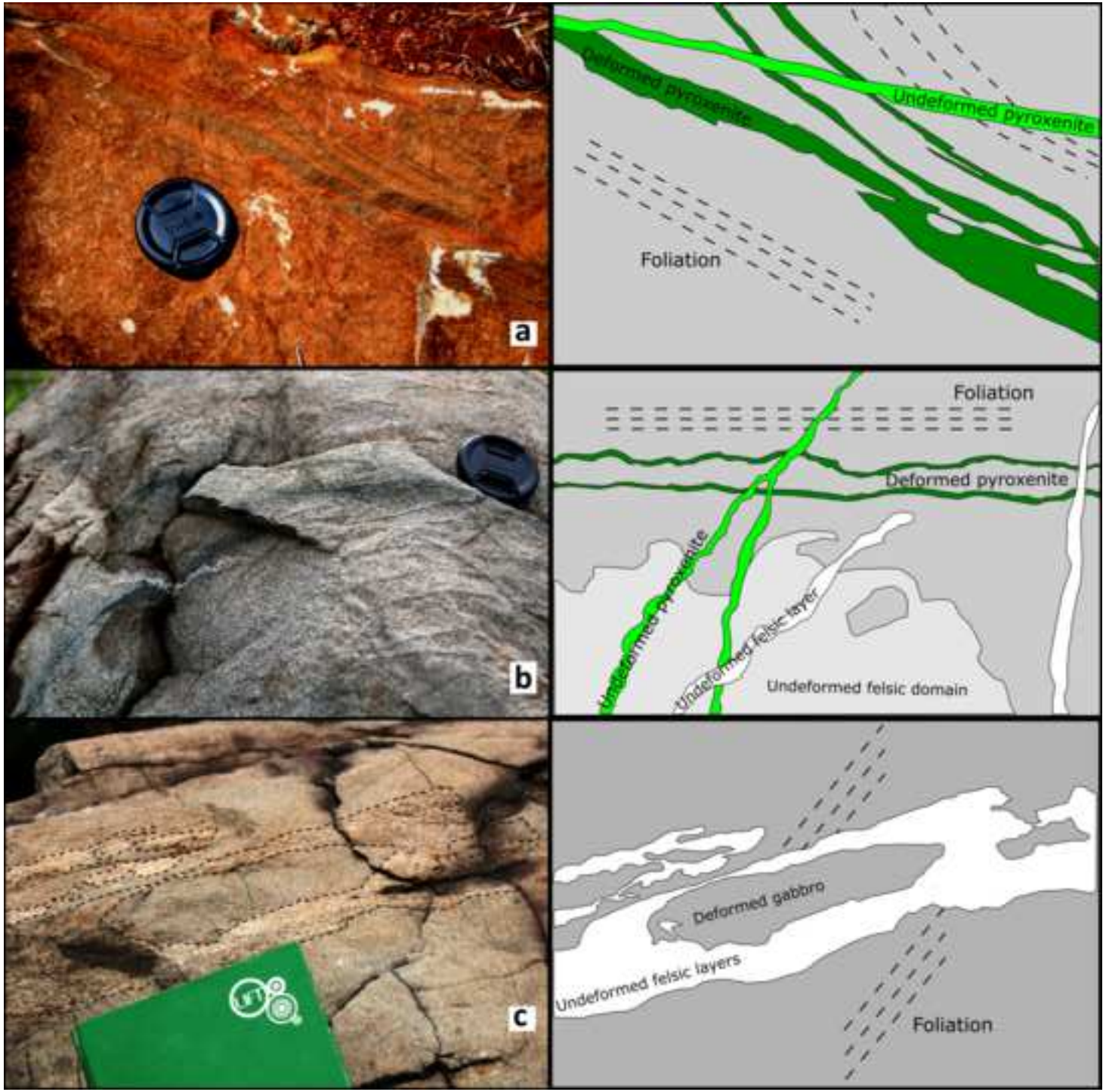

Colour Figure 3

Click here to download Colour Figure Fig. 3.png

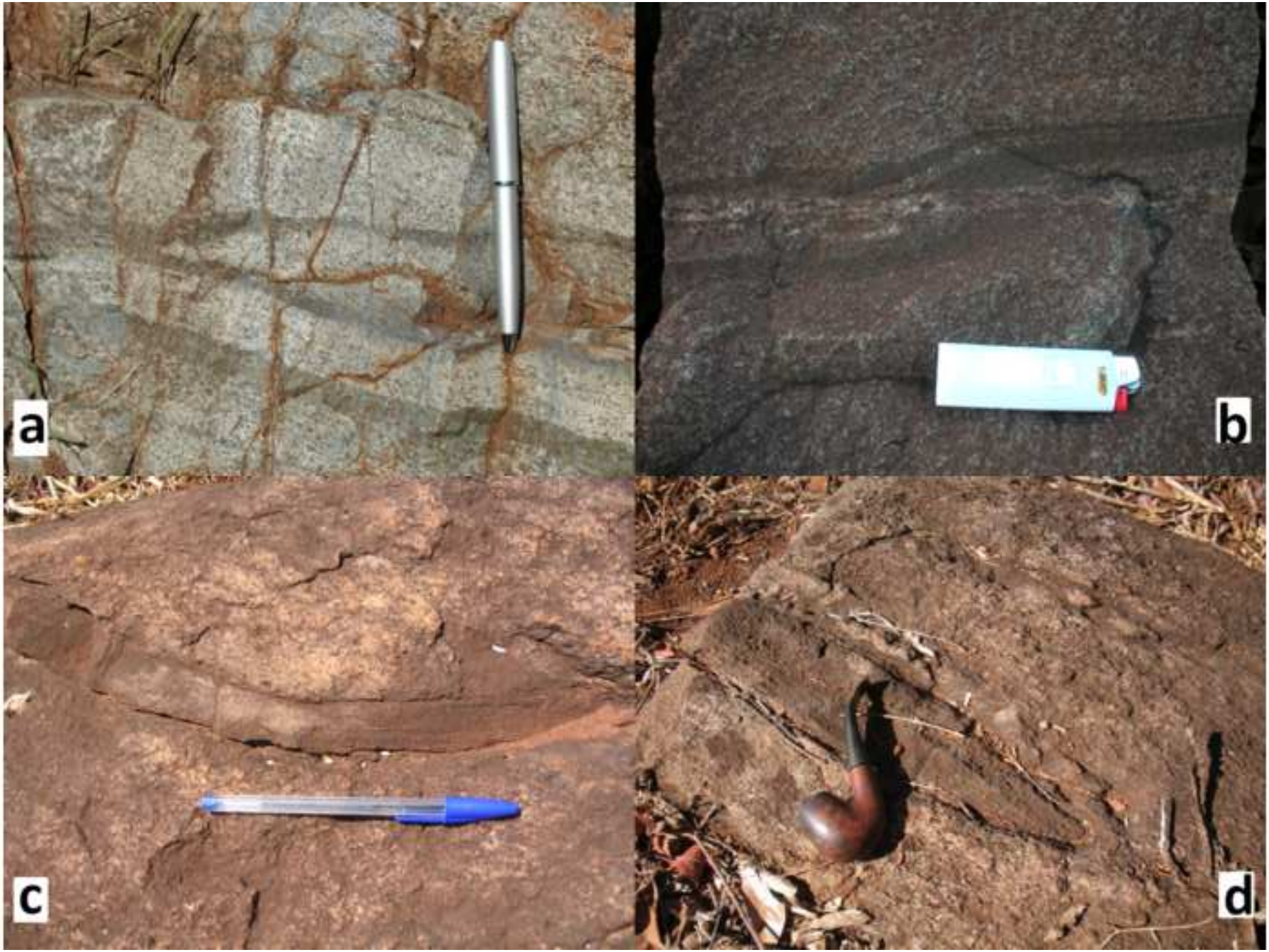

Colour Figure 4

Click here to download Colour Figure Fig. 4.png

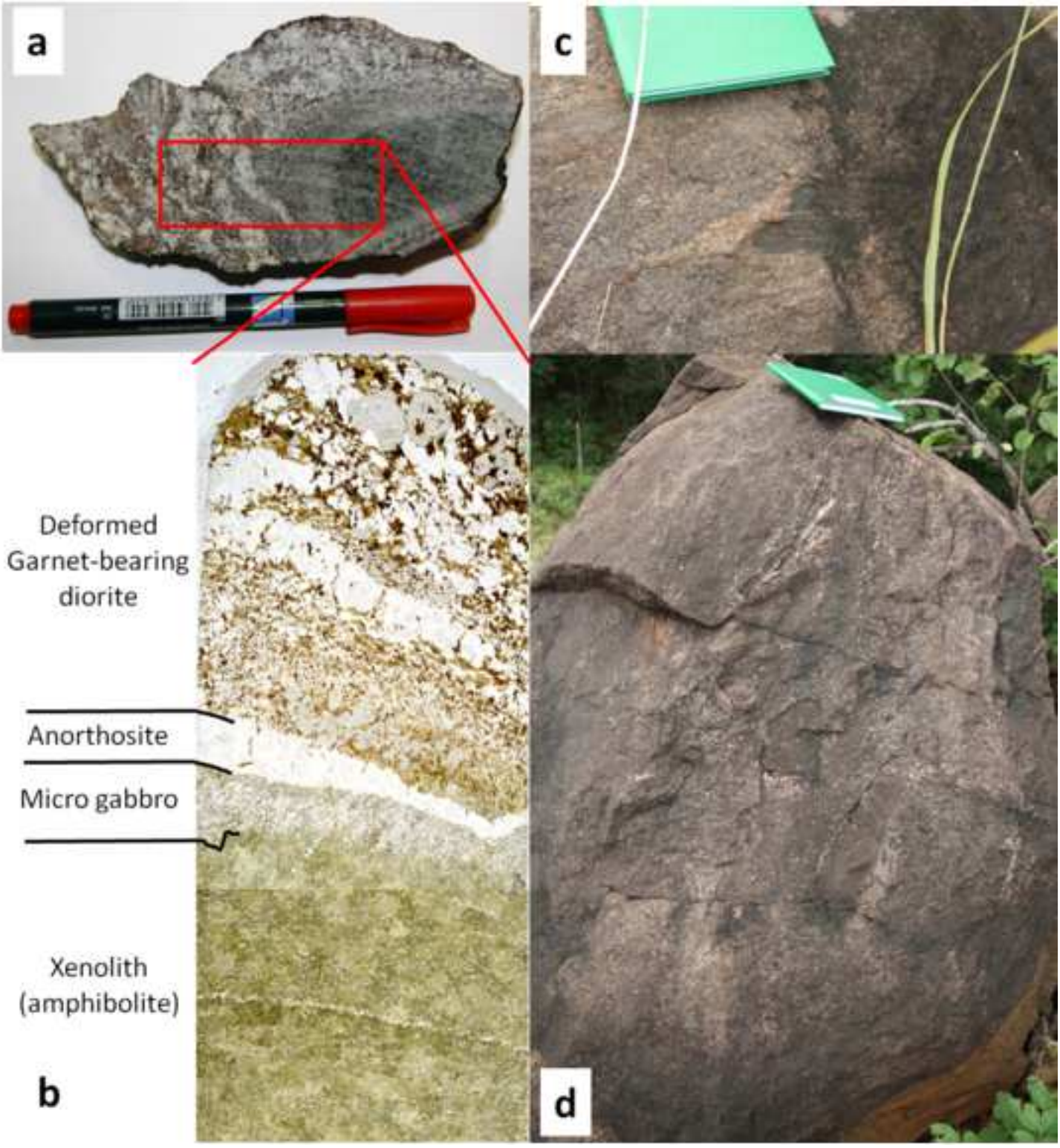

Line Figure 5

Click here to download Line Figure Fig. 5_rev2.tif

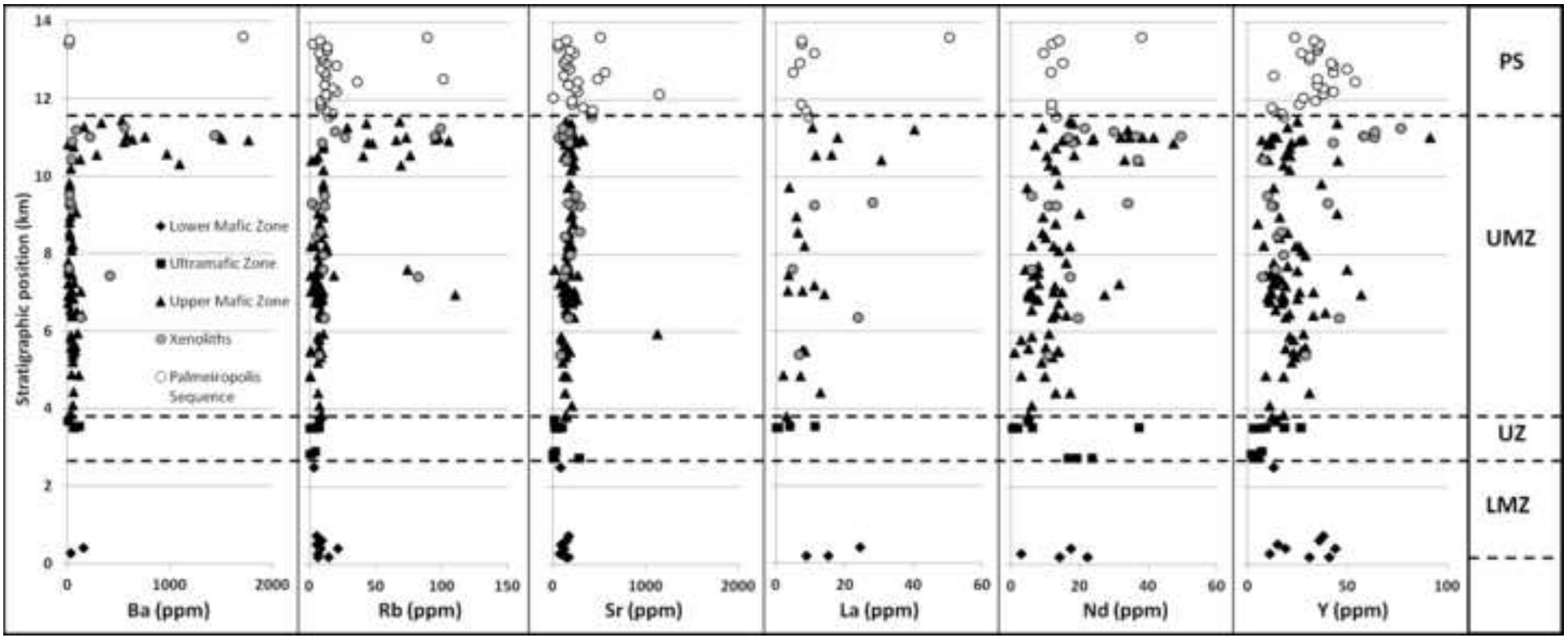

Line Figure 6

Click here to download Line Figure Fig. 6_2.tif

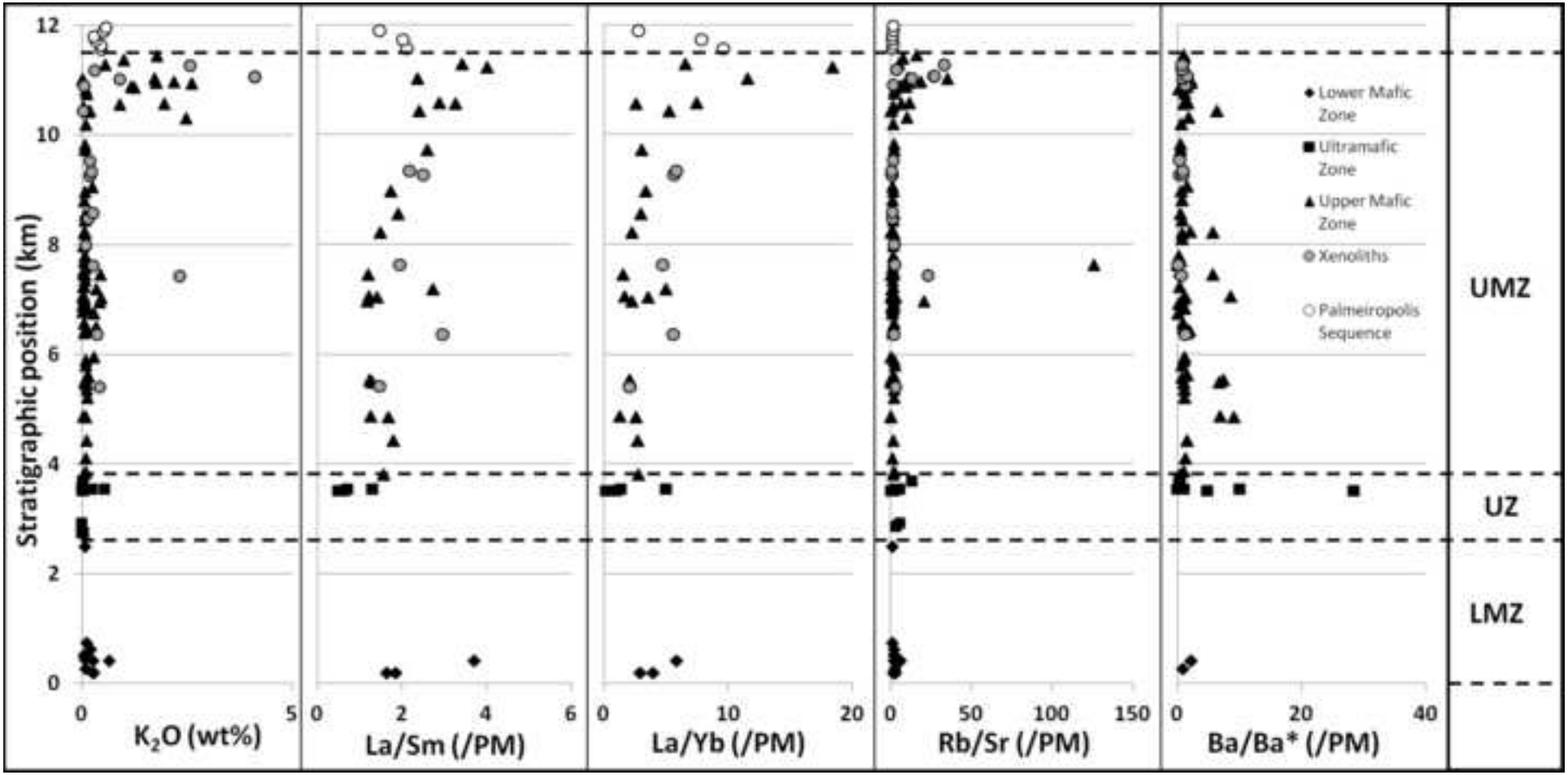

Line Figure 7

Click here to download Line Figure Fig. 7_2.tif

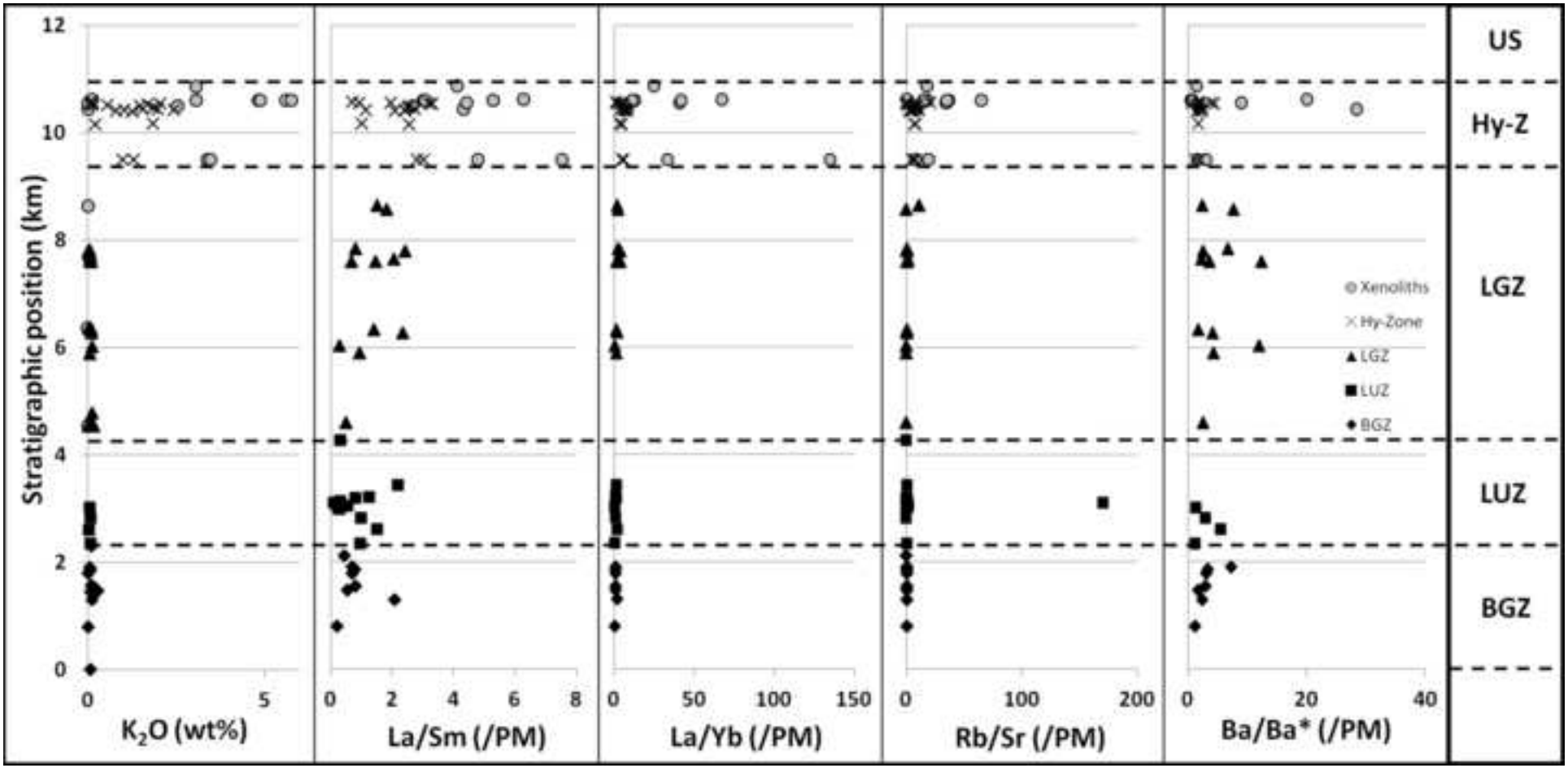

Line Figure 8

Click here to download Line Figure Fig. 8_rev2.tif

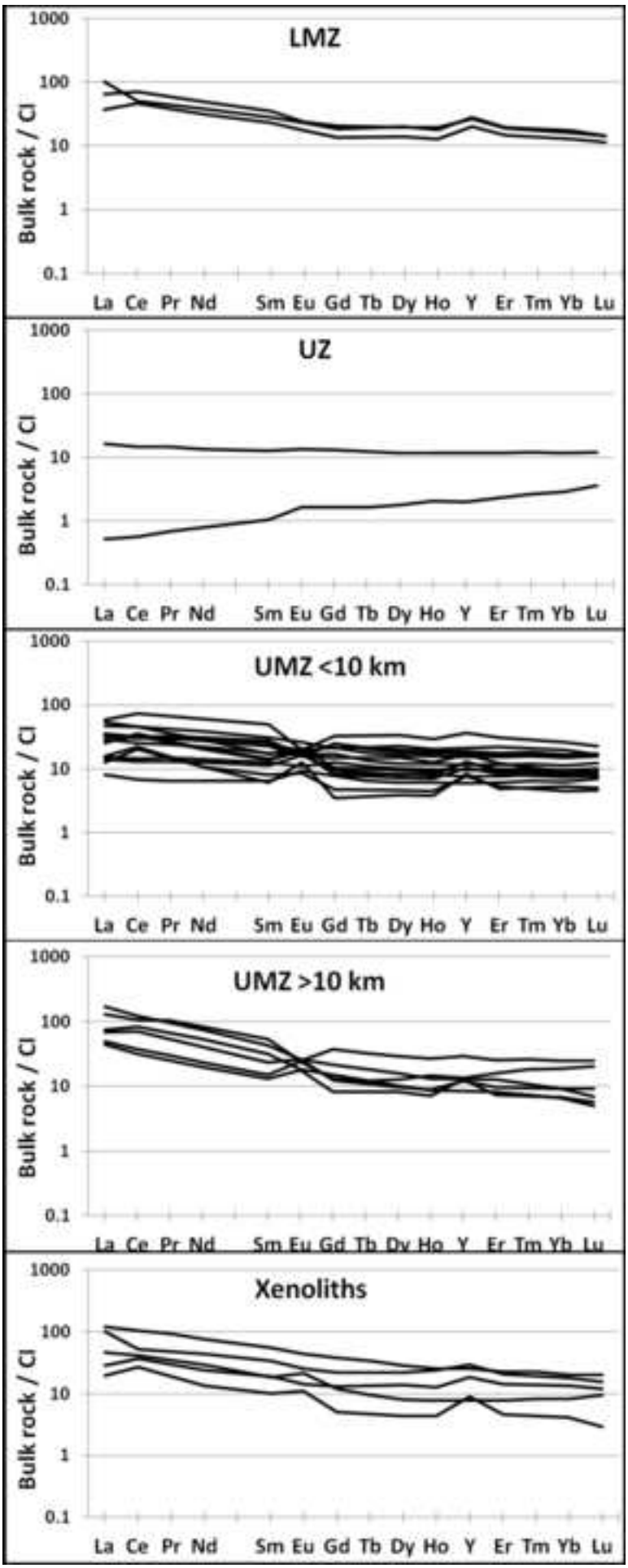

Line Figure 9

Click here to download Line Figure Fig. 9_rev2.tif

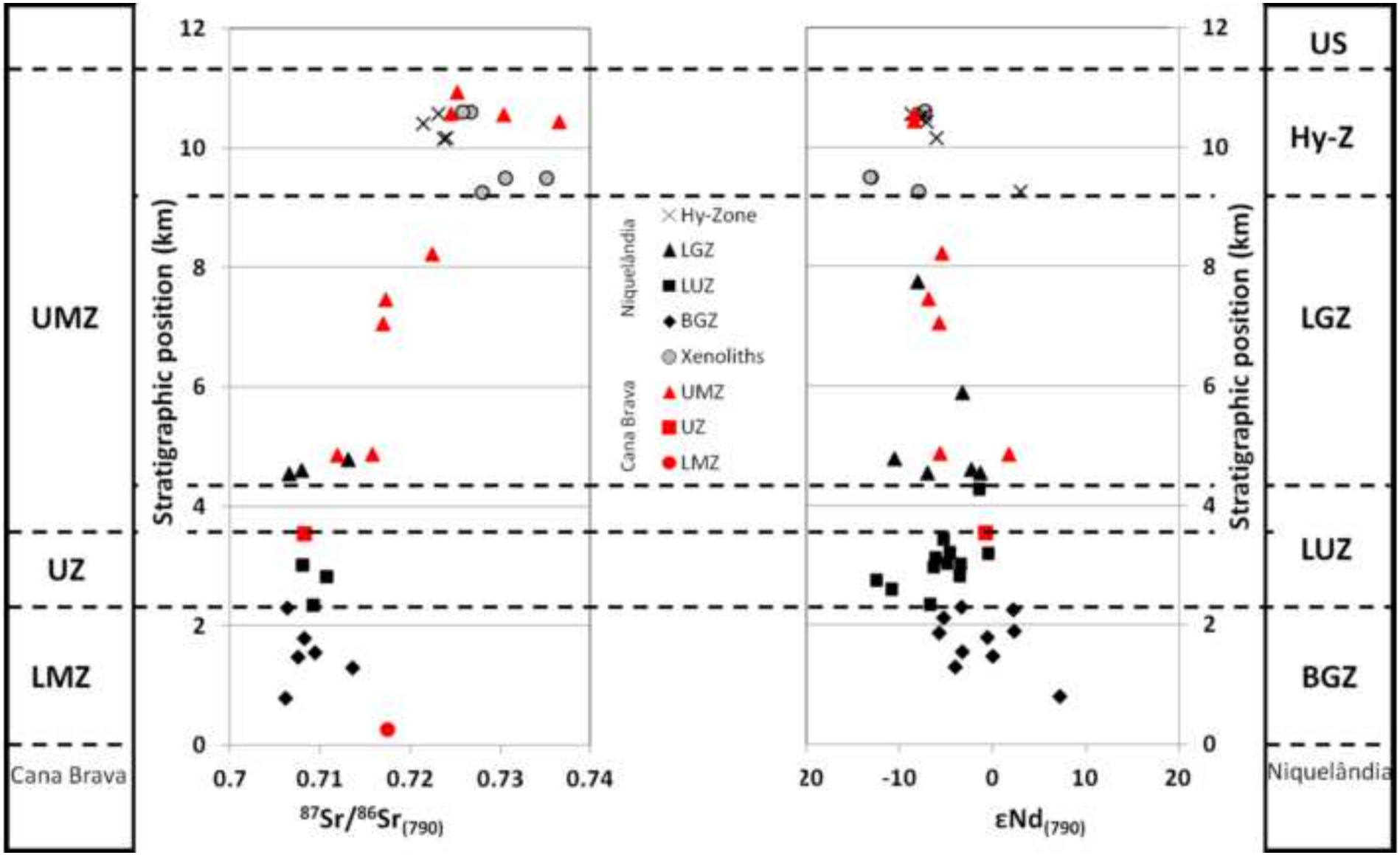

Line Figure 10

Click here to download Line Figure Fig. 10_rev2.tif

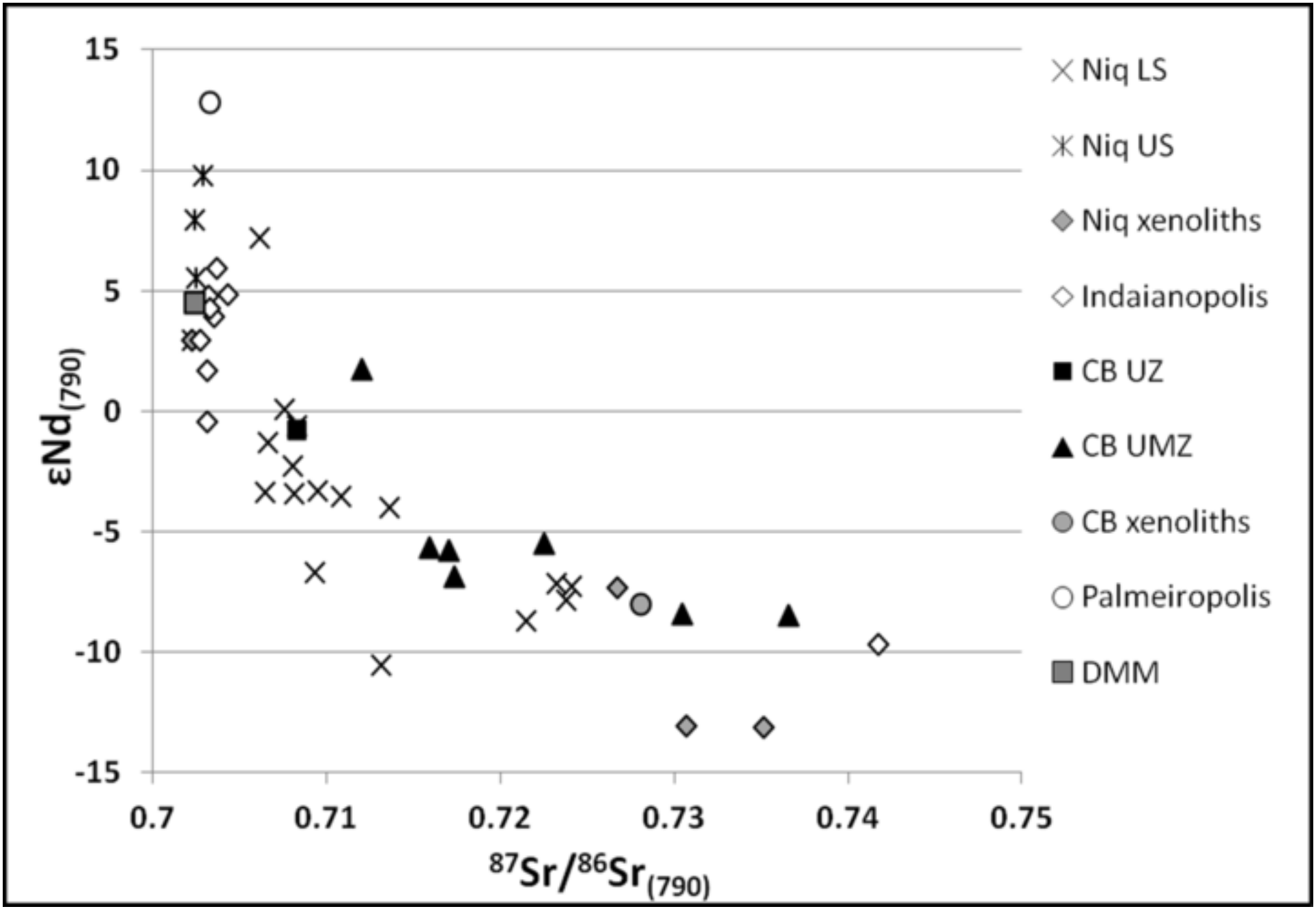

Line Figure 11

Click here to download Line Figure Fig. 11_rev2.tif

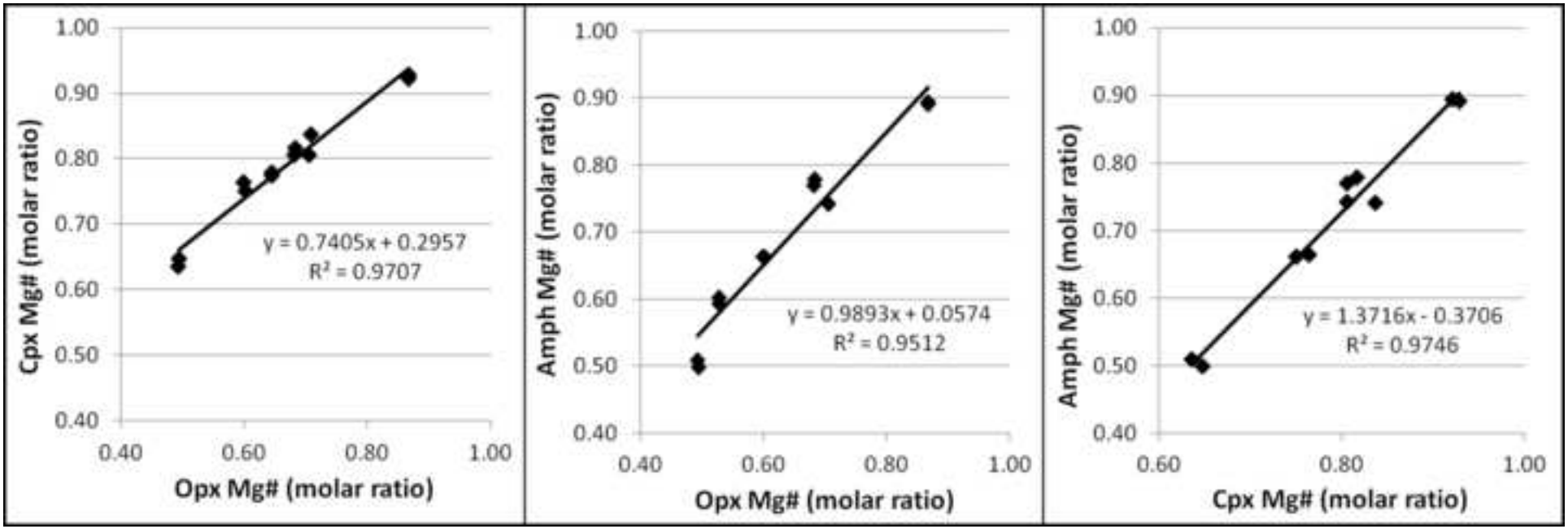

Line Figure 12

Click here to download Line Figure Fig. 12_rev2.tif

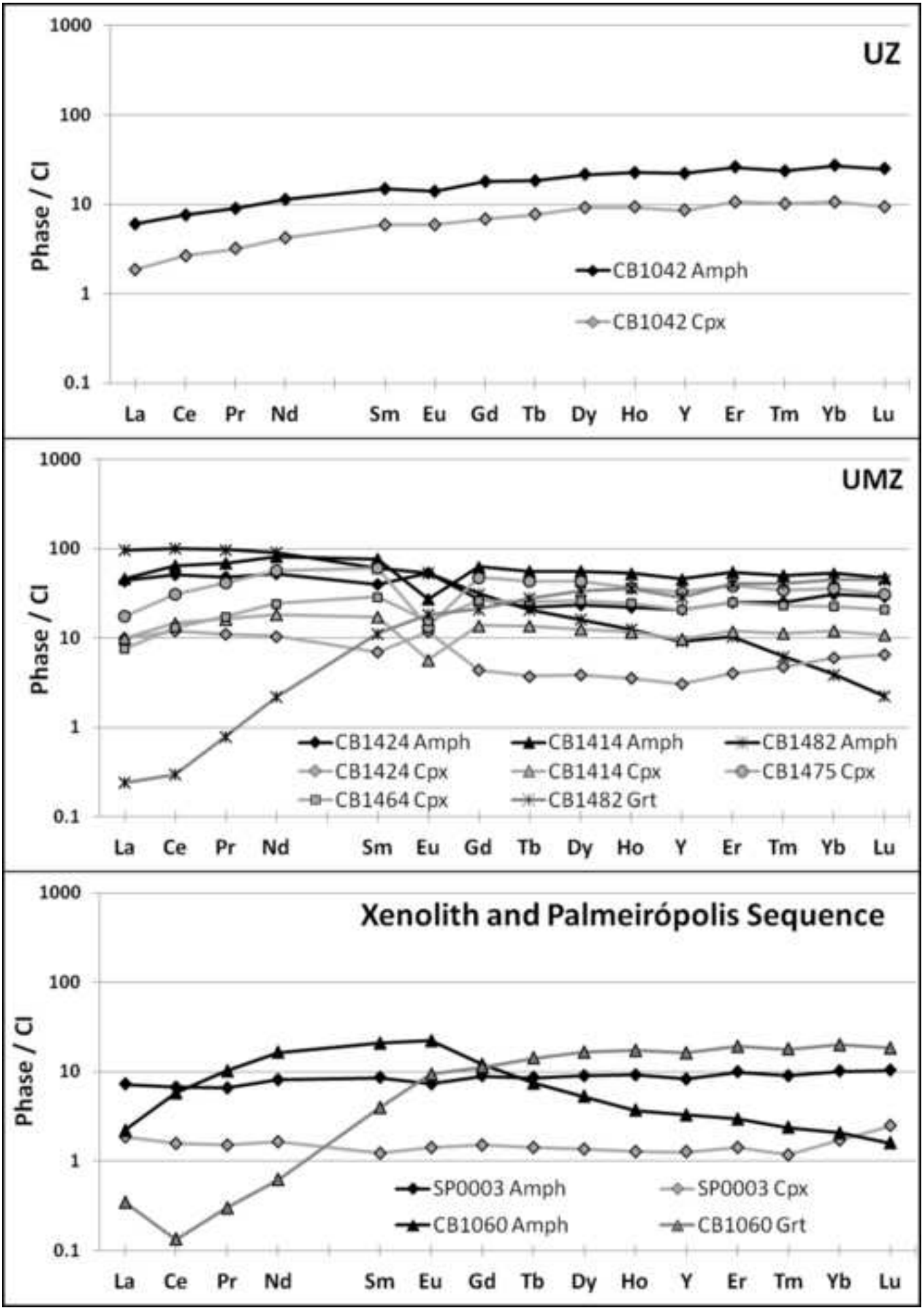

Line Figure 13

Click here to download Line Figure Fig. 13_rev2.tif

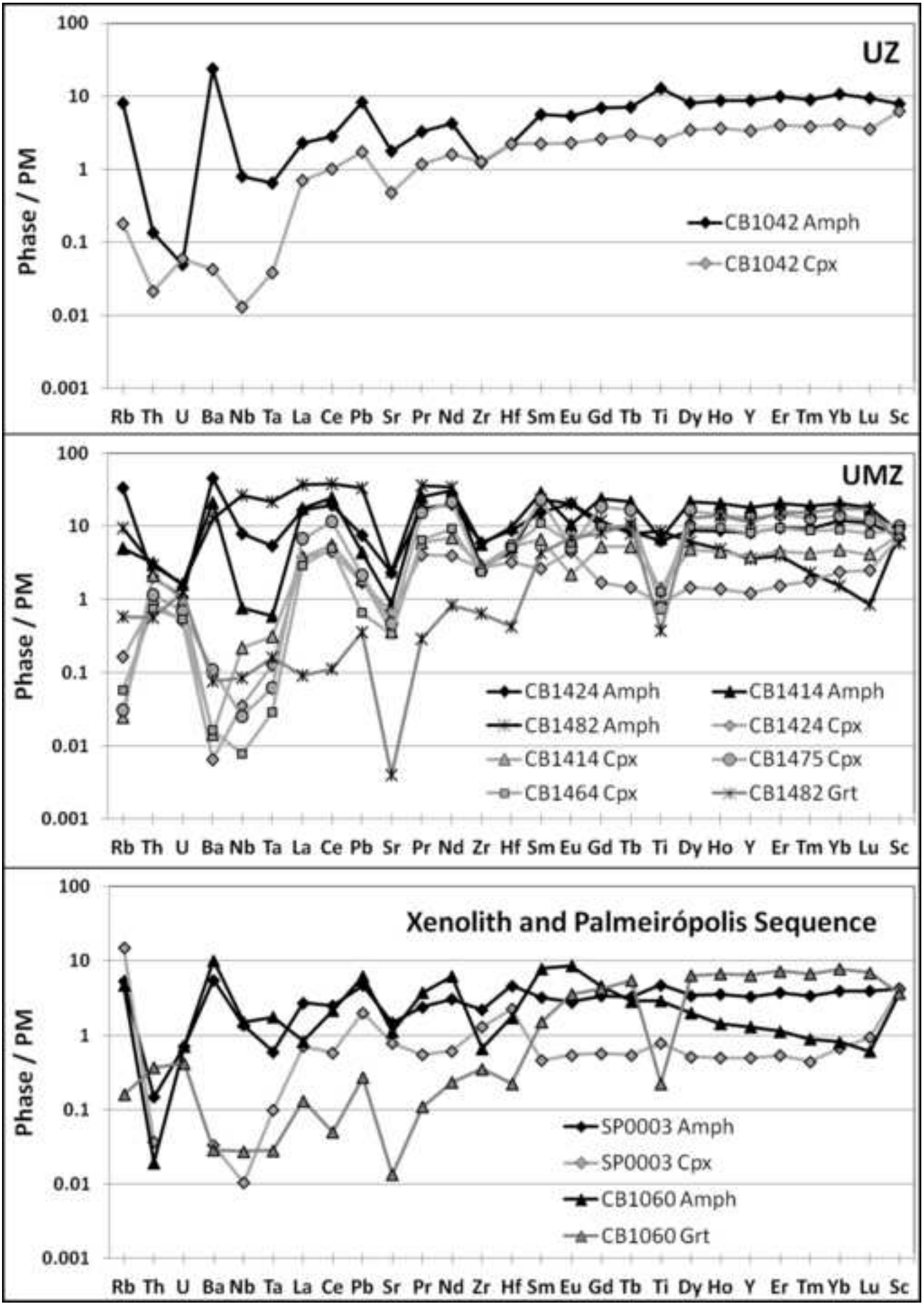

Colour Figure 14

Click here to download Colour Figure Fig. 14_rev2.jpg

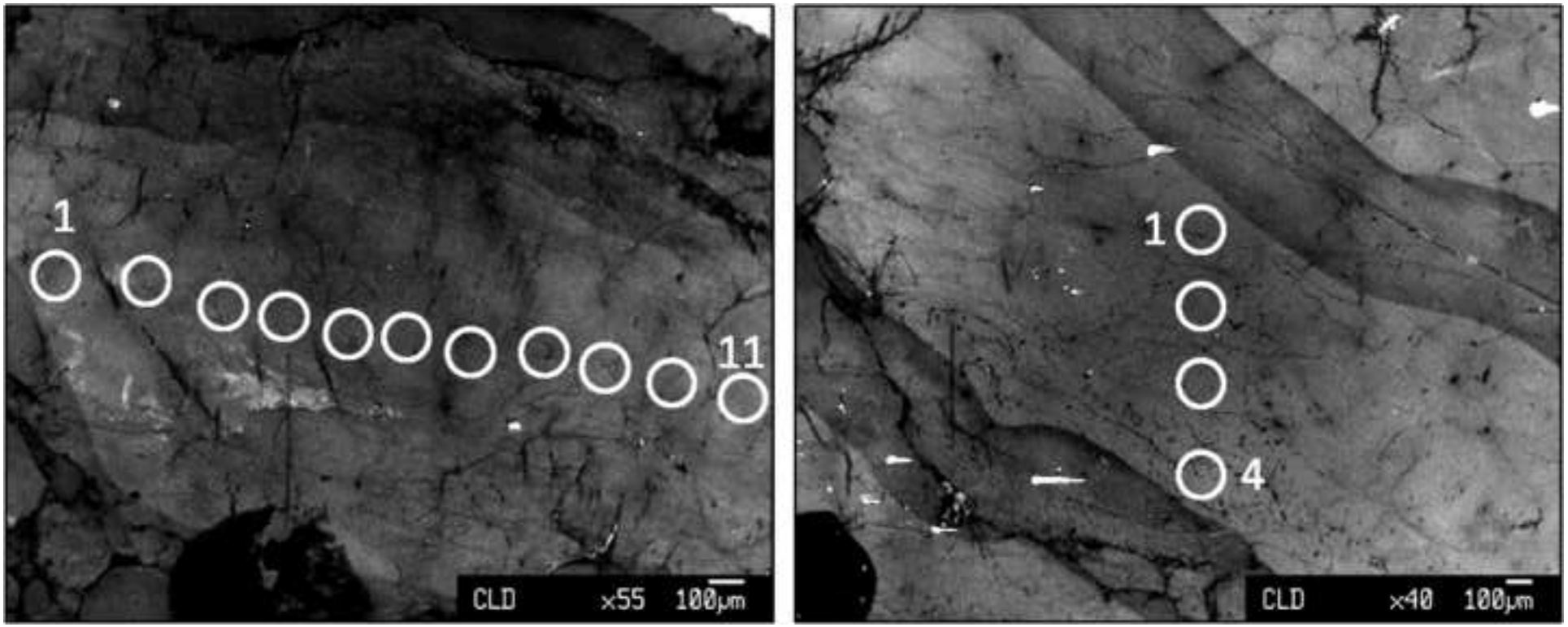

Line Figure 15

Click here to download Line Figure Fig. 15_rev2.tif

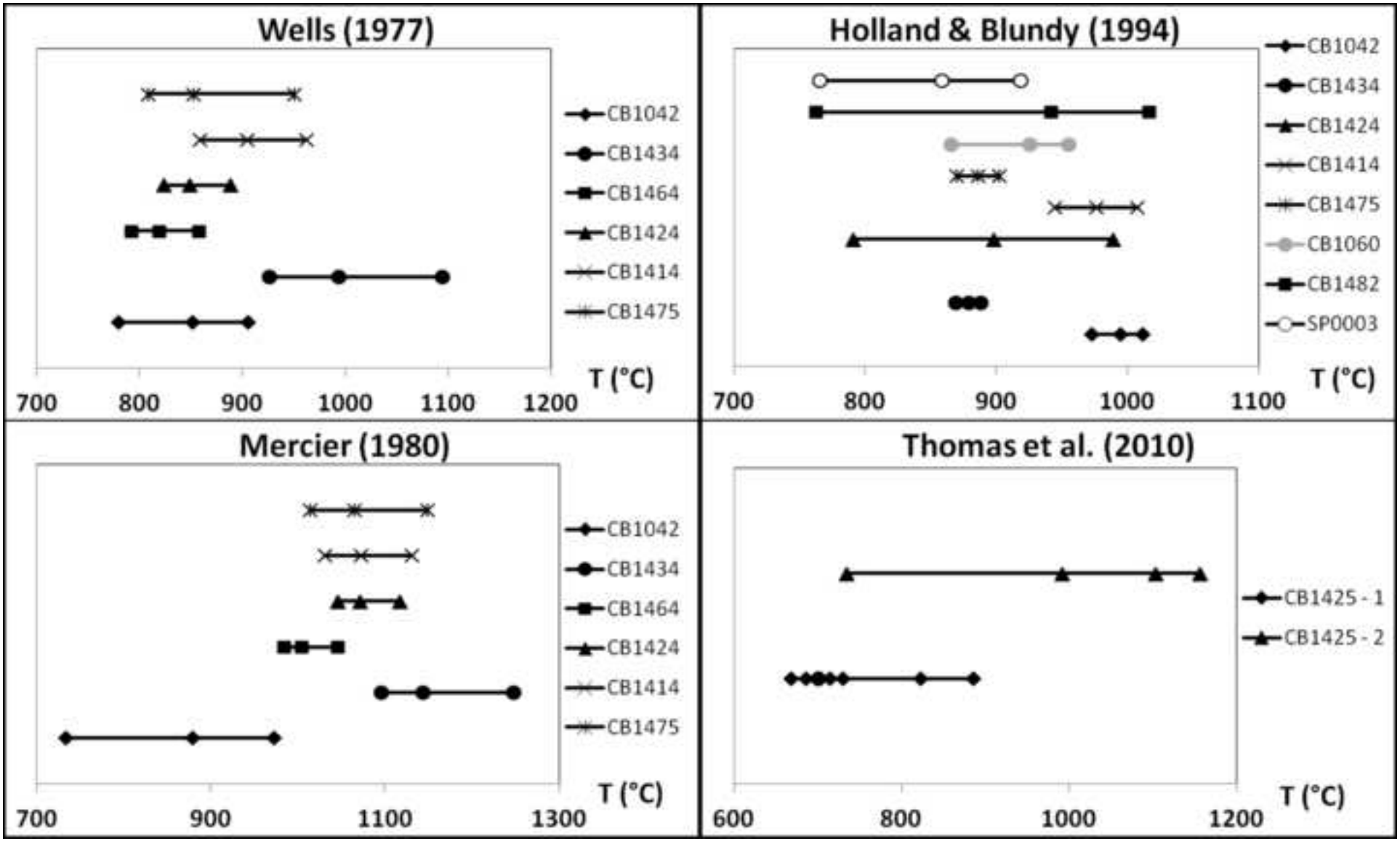

Colour Figure 16

Click here to download Colour Figure Fig. 16_rev2.png

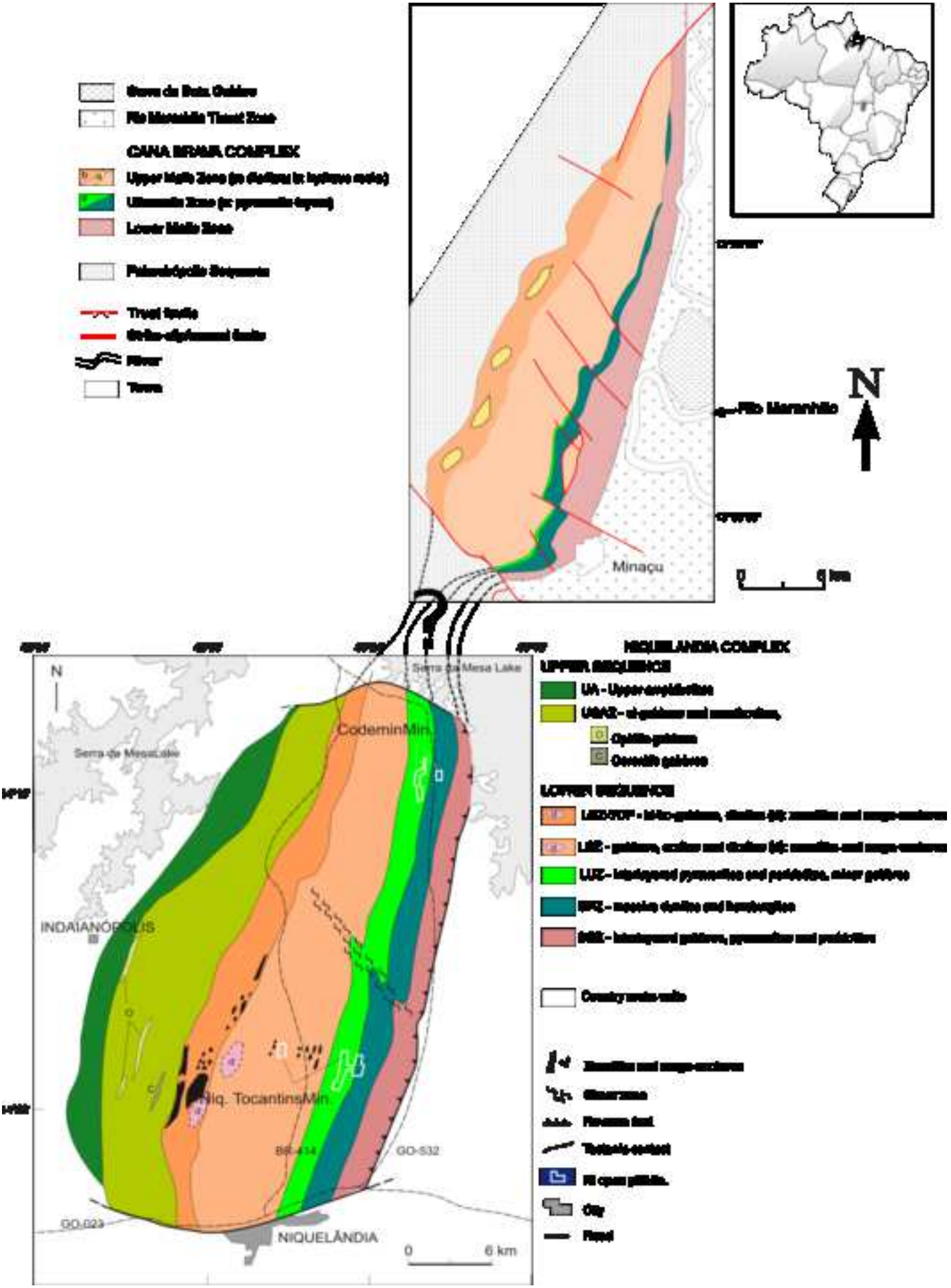

Table 1 Rb-Sr and Sm-Nd bulk-rock isotopic compositions by Isotopic Dilution Thermal Ionization Mass Spectrometry (ID-TIMS) for selected samples

Sample	Unit	Sm (ppm)	Nd (ppm)	$^{147}Sm/^{144}Nd$	$^{143}Nd/^{144}Nd$	2σ	$\varepsilon Nd_{(790)}$	Rb (ppm)	Sr (ppm)	$^{87}Rb/^{86}Sr$	2σ	$^{87}Sr/^{86}Sr$	2σ	$^{87}Sr/^{86}Sr_{(790)}$
CB1133	UZ	1.86	6.16	0.181402	0.512519	0.000009	-0.78	7.4	100	0.212365		0.710639	0.000064	0.708243
CB1434	UMZ	2.57	9.89	0.156308	0.512516	0.000008	1.70	0.723	153	0.013688		0.712132	0.000046	0.711978
CB1464	UMZ	0.932	2.87	0.195159	0.512341	0.000007	-5.65	0.396	122	0.009405		0.715977	0.000057	0.715871
CB1424	UMZ	1.66	5.75	0.174039	0.512225	0.000007	-5.78	0.439	233	0.005453		0.717050	0.000038	0.716988
CB1414	UMZ	1.87	6.37	0.176302	0.512181	0.000008	-6.87	0.569	114	0.014495		0.717464	0.000057	0.717300
CB1475	UMZ	3.39	12.5	0.163794	0.512187	0.000007	-5.48	0.639	182	0.010154		0.722621	0.000065	0.722506
CB1490	UMZ	7.98	37	0.128606	0.511852	0.000009	-8.47	1.33	169	0.022718		0.736846	0.000063	0.736590
CB1482	UMZ	2.19	10.5	0.125985	0.511841	0.000010	-8.42	40	204	0.571063		0.736912	0.000057	0.730470
CB1060	Xen UMZ	2.76	13.1	0.126365	0.511864	0.000007	-8.01	4.59	215	0.061859		0.728774	0.000070	0.728076
SP0003	PAL	4.08	14.0	0.175417	0.513183	0.000007	12.81	7.45	149	0.144361		0.704907	0.000063	0.703278
CB1006	LMZ							0.3	59.4	0.016	0.001	0.71772	0.00061	0.717540
CB1029	UMZ							75.5	209.4	1.047	0.021	0.73642	0.00022	0.724609
CB1099	UMZ							101.8	285.6	1.034	0.017	0.73693	0.00018	0.725265

The lower three lines quote Rb-Sr data of Correia et al. (1997)

Table 2 Compositions of rock-forming minerals (EPMA results, in wt%) originating from core and rim regions of each rock sample, respectively

Phase	Clinopyroxene average													
Sample	CB1042		CB1434		CB1464		CB1424		CB1414		CB1475		SP0003	
Unit	UZ		UMZ		UMZ		UMZ		UMZ		UMZ		SP	
Rock Type	websterite		gabbro		gabbro		diorite		gabbro		gabbro		amphibolite	
Strat Pos (m)	3514		4858		4874		7053		7456		8221		12000	
Position	core	rim	core	rim	core	rim	core	rim	core	rim	core	rim	core	rim
SiO_2	52.29	52.42	53.37	53.87	53.10	53.06	51.87	51.95	53.54	53.48	53.04	53.29	52.12	52.19
TiO_2	0.48	0.49	0.24	0.17	0.23	0.21	0.19	0.14	0.15	0.16	0.13	0.13	0.17	0.11
Al_2O_3	4.57	4.22	2.40	2.08	2.18	2.14	1.95	2.23	1.58	1.61	1.31	1.32	1.58	1.34
Cr_2O_3	1.05	1.07	0.12	0.08	0.16	0.22	0.01	0.03	0.35	0.30	0.03	0.03	0.01	0.02
FeO_T	2.36	2.15	6.81	5.55	7.06	7.16	11.80	11.32	6.54	6.07	8.29	7.74	12.00	11.61
MnO	0.07	0.10	0.15	0.14	0.21	0.21	0.35	0.29	0.20	0.17	0.25	0.22	0.37	0.40
NiO	0.04	0.03	0.03	0.02	0.03	0.01	0.01	0.01	0.01	0.02	0.03	0.01	0.03	0.01
MgO	15.64	15.67	15.73	16.06	13.91	13.80	11.55	11.68	15.24	15.16	13.96	14.03	10.82	11.03
CaO	22.74	23.05	20.45	21.53	22.83	22.81	21.74	21.95	22.19	22.69	22.44	22.94	22.80	23.02
Na_2O	0.75	0.73	0.60	0.56	0.50	0.52	0.39	0.44	0.38	0.37	0.34	0.35	0.34	0.30
K_2O	0.00	0.00	0.01	0.01	0.00	0.01	0.00	0.00	0.00	0.00	0.00	0.00	0.00	0.00
Mg#	0.92	0.93	0.81	0.84	0.78	0.77	0.64	0.65	0.81	0.82	0.75	0.76	0.62	0.63

Table 2 Continued

Phase	Orthopyroxene average													
Sample	CB1042		CB1434		CB1464		CB1424		CB1414		CB1475		CB1482	
Unit	UZ		UMZ		UMZ		UMZ		UMZ		UMZ		UMZ	
Rock Type	websterite		gabbro		gabbro		diorite		gabbro		gabbro		Grt-diorite	
Strat Pos (m)	3514		4858		4874		7053		7456		8221		10557	
Position	core	rim	core	rim	core	rim	core	rim	core	rim	core	rim	core	rim
SiO_2	55.11	55.14	53.69	53.62	52.90	52.74	50.71	50.74	53.57	53.56	52.33	52.46	51.46	51.56
TiO_2	0.07	0.04	0.06	0.03	0.08	0.08	0.06	0.06	0.05	0.04	0.07	0.04	0.10	0.08
Al_2O_3	3.20	3.03	1.59	1.72	1.45	1.45	1.27	1.40	1.11	1.22	1.00	0.96	0.90	0.93
Cr_2O_3	0.54	0.53	0.02	0.05	0.09	0.06	0.02	0.02	0.16	0.12	0.03	0.02	0.01	0.01
FeO_T	8.67	8.74	18.68	18.41	22.08	22.20	30.18	30.07	20.01	20.05	24.60	24.80	28.64	28.61
MnO	0.18	0.18	0.40	0.41	0.46	0.47	0.84	0.80	0.45	0.45	0.54	0.54	0.31	0.28
NiO	0.06	0.07	0.06	0.01	0.01	0.01	0.02	0.03	0.02	0.01	0.01	0.01	0.01	0.02
MgO	31.72	31.83	25.05	25.17	22.59	22.56	16.50	16.46	24.11	24.18	20.96	20.79	17.94	17.90
CaO	0.34	0.22	0.36	0.32	0.52	0.37	0.46	0.42	0.45	0.34	0.39	0.46	0.64	0.65
Na_2O	0.02	0.01	0.01	0.02	0.02	0.01	0.02	0.02	0.02	0.02	0.01	0.02	0.02	0.02
K_2O	0.01	0.00	0.01	0.01	0.01	0.01	0.00	0.00	0.00	0.00	0.00	0.00	0.01	0.00
Mg#	0.87	0.87	0.70	0.71	0.65	0.64	0.49	0.49	0.68	0.68	0.60	0.60	0.53	0.53

Table 2 Continued

Phase	Amphibole average															
Sample	CB1042		CB1434		CB1424		CB1414		CB1475		CB1060		CB1482		SP0003	
Unit	UZ		UMZ		UMZ		UMZ		UMZ		UMZ		UMZ		SP	
Rock Type	websterite		gabbro		diorite		gabbro		gabbro		xenolith		Grt-diorite		amphibolite	
Strat Pos (m)	3514		4858		7053		7456		8221		9260		10557		12000	
Position	core	rim	core	rim	core	rim	core	rim	core	rim	core	rim	core	rim	core	rim
SiO_2	44.96	45.05	43.84	46.06	43.59	42.83	48.32	48.63	45.67	44.87	43.46	43.48	43.88	44.49	44.53	44.82
TiO_2	1.80	1.89	1.40	1.23	1.27	1.28	1.32	1.25	1.54	1.64	0.59	0.54	1.80	1.64	0.95	0.69
Al_2O_3	13.66	13.38	13.30	13.09	12.20	13.53	9.75	9.58	10.83	12.07	16.74	16.77	11.63	11.91	11.28	11.89
Cr_2O_3	1.62	1.91	0.17	0.11	0.05	0.02	0.65	0.59	0.09	0.14	0.03	0.04	0.03	0.03	0.06	0.07
FeO_T	3.51	3.62	8.60	8.86	16.79	16.78	8.25	7.99	11.85	11.50	12.91	13.12	13.90	13.52	16.98	16.77
MnO	0.05	0.05	0.11	0.08	0.17	0.19	0.11	0.09	0.10	0.10	0.08	0.07	0.05	0.04	0.26	0.26
NiO	0.12	0.06	0.03	0.03	0.01	0.02	0.01	0.02	0.07	0.06	0.02	0.02	0.03	0.01	0.02	0.02
MgO	16.59	16.66	14.02	14.32	9.76	9.38	15.45	15.73	13.01	12.72	10.33	10.33	11.39	11.45	9.57	9.54
CaO	11.80	11.71	12.58	10.62	11.11	11.21	11.31	11.42	11.23	11.79	11.15	11.16	11.39	11.47	11.37	11.49
Na_2O	2.19	2.17	1.64	1.61	1.49	1.56	1.23	1.14	1.23	1.24	1.51	1.50	1.50	1.48	1.41	1.29
K_2O	0.64	0.65	1.00	0.90	0.58	0.68	0.53	0.52	0.92	1.01	0.32	0.32	1.17	1.12	0.37	0.35
Mg#	0.89	0.89	0.74	0.74	0.51	0.50	0.77	0.78	0.66	0.66	0.59	0.58	0.59	0.60	0.50	0.50

Table 2 Continued

Phase	Plagioclase average																	
Sample	CB1042		CB1434		CB1464		CB1424		CB1414		CB1475		CB1060		CB1482		SP0003	
Unit	UZ		UMZ		UMZ		UMZ		UMZ		UMZ		UMZ		UMZ		SP	
Rock Type	websterite		gabbro		gabbro		diorite		gabbro		gabbro		xenolith		Grt-diorite		amphibolite	
Strat Pos (m)	3514		4858		4874		7053		7456		8221		9260		10557		12000	
Position	core	rim	core	rim	core	rim	core	rim	core	rim	core	rim	core	rim	core	rim	core	rim
SiO_2	48.09	47.89	49.83	49.38	48.64	48.09	45.90	45.65	47.83	47.42	48.69	48.45	47.55	47.06	47.75	49.06	47.90	46.66
TiO_2	0.02	0.00	0.02	0.02	0.01	0.02	0.00	0.03	0.01	0.02	0.02	0.01	0.00	0.01	0.01	0.02	0.01	0.02
Al_2O_3	33.50	34.00	33.50	33.75	33.30	33.54	35.20	35.36	34.14	34.32	33.08	33.22	33.88	34.22	33.79	32.84	33.87	34.57
Cr_2O_3	0.01	0.03	0.00	0.01	0.00	0.00	0.00	0.00	0.01	0.00	0.02	0.01	0.01	0.00	0.01	0.01	0.00	0.01
FeO_T	0.03	0.06	0.04	0.10	0.04	0.11	0.07	0.17	0.02	0.04	0.04	0.09	0.01	0.08	0.02	0.12	0.10	0.16
MnO	0.01	0.01	0.01	0.04	0.00	0.00	0.00	0.00	0.00	0.00	0.01	0.01	0.00	0.02	0.01	0.01	0.00	0.00
NiO	0.03	0.01	0.02	0.02	0.00	0.00	0.00	0.00	0.00	0.00	0.04	0.02	0.01	0.03	0.01	0.01	0.00	0.00
MgO	0.00	0.01	0.00	0.01	0.00	0.00	0.00	0.00	0.00	0.00	0.00	0.01	0.01	0.01	0.00	0.00	0.00	0.00
CaO	15.54	15.79	12.99	13.35	15.32	15.73	17.36	17.48	15.86	16.10	15.56	15.61	16.37	16.78	16.18	15.19	15.89	16.60
Na_2O	2.45	2.31	3.51	3.29	2.61	2.36	1.40	1.30	2.28	2.12	2.55	2.49	2.10	1.83	2.18	2.75	2.29	1.79
K_2O	0.03	0.03	0.07	0.06	0.07	0.06	0.02	0.01	0.03	0.02	0.06	0.05	0.02	0.02	0.04	0.03	0.01	0.01
An	77.69	78.95	66.86	68.88	76.10	78.40	87.19	88.08	79.22	80.64	76.89	77.41	81.11	83.44	80.26	75.24	79.27	83.61
Ab	22.12	20.88	32.74	30.77	23.46	21.26	12.70	11.85	20.62	19.23	22.78	22.31	18.79	16.46	19.54	24.57	20.65	16.34
Or	0.19	0.16	0.41	0.36	0.44	0.34	0.11	0.07	0.16	0.13	0.33	0.28	0.10	0.10	0.21	0.19	0.08	0.05

Strat Pos (m) is the stratigraphic position in meters: i.e. the recalculated stratigraphic height from the base of the complex, taking into account the attitude of the layers.

Mg# was calculated as $Mg^{2+}/(Mg^{2+}+Fe^{2+})$ molar ratio

An, Ab, and Or = anorthite, albite, and orthoclase molar fractions are reported for plagioclase analyses

For abbreviations of rock units (Unit) see the geological setting chapter

Table 3 Minimum, maximum, average and median temperature values (in °C) for selected samples, calculated based on the Fe-Mg exchange between clinopyroxene and orthopyroxene (Wells 1977), the Ca and Al in orthopyroxene and clinopyroxene (Mercier 1980), the amphibole-plagioclase equilibrium (Holland and Blundy 1994) and the Ti-in quartz (Thomas et al. 2010)

			Wells (1977)				Mercier (1980)				Holland and Blundy (1994)				Thomas et al. (2010)			
Sample	Unit	Strat Pos (m)	min	max	mean	median	min	max	mean	median	min	max	mean	median	min	max	mean	median
CB1042	UZ	3514	780	905	851	853	733	972	879	896	973	1012	995	998				
CB1434	UMZ	4858	926	1094	993	996	1096	1248	1144	1133	870	889	879	880				
CB1425	Xen	4865													669	1157	801	715
CB1464	UMZ	4874	792	858	819	815	985	1046	1005	999								
CB1424	UMZ	7053	823	888	848	844	1045	1117	1071	1071	791	989	898	906				
CB1414	UMZ	7456	859	962	905	899	1031	1131	1072	1069	945	1008	977	972				
CB1060	Xen	9260									866	956	926	930				
CB1475	UMZ	8221	808	950	852	834	1014	1149	1065	1048	870	903	886	886				
CB1482	UMZ	10557									763	1017	942	953				
SP0003	SP	13530									766	919	859	873				

Strat Pos (m) is the stratigraphic position in meters: i.e. the recalculated stratigraphic height from the base of the complex, taking into account the attitude of the layers.

For abbreviations of rock units (Unit) see the geological setting chapter

Online Resource A: selected samples for mineral analyses

Petrography

Sample SP0003 is an amphibolite of the Palmeirópolis Sequence, with foliated, granoblastic texture. The sample shows bands with different grain sizes and gradual transitions between large-grain bands and fine-grain bands. Amphibole has a green-brown pleochroism and is classified as Hornblende. In the fine-grain bands, relicts of Clinopyroxene are recognizable. Titanite occurs commonly as aggregate.

Sample CB1425 is a granoblastic quartzite included in the lower UMZ (Fig. 2c, d) while sample CB1060 is an amphibolite included in the upper UMZ. Sample CB1060 shows a granoblastic texture with centimetric pecilitic Garnets including Amphibole (Fig. 2b; Tschermakite) and Plagioclase. Amphibole and Plagioclase are recrystallized as fine-grain porphyroblast while some larger millimetric residual crystals of Plagioclase sometimes occur. Rutile, Apatite, Quartz and Ilmenite occur as accessory phases.

Sample CB1042 is a Plagioclase-bearing pyroxenite of the UZ. Orthopyroxene is the most abundant phase and shows often exolution in Clinopyroxene, while Amphibole (Pargasite) is an accessory phase which occurs in interstitial positions. Plagioclase and Clinopyroxene are often associated.

Samples CB1414, CB1434, CB1464 and CB1475 are foliated gabbros with granoblastic texture. In general, there is an increase in modal amphibole in UMZ. Amphibole occurs in interstitial positions and rarely overgrowths pyroxenes. Orthopyroxene in gabbro samples shows exolution in Clinopyroxene, whereas Clinopyroxene does not. Quartz, Rutile, Ilmenite occurs as accessory phases.

Samples CB1424 and CB1482 are diorites from different stratigraphic positions. Sample CB1424 is a diorite stratigraphically upper a quartzite layer in the lower UMZ and shows a higher

grain size and Plagioclase abundance with respect to others gabbro samples. In this rock, pargasitic to edenitic Amphibole occurs as large-grain crystals. Ilmenite occurs as accessory phase. Sample CB1482 is a Garnet-rich diorite from the top of the complex. In outcrop scale, this rock contains numerous xenoliths of amphibolite from the Palmeirópolis Sequence. The contact with the xenoliths is marked by a fine-grained gabbro. The diorite presents a granoblastic texture and abundant Garnet and Biotite. Amphibole from sample CB1482 is classified as Pargasite-Edenite. Orthopyroxenes presents exolution in Clinopyroxene. Quartz is more abundant than other lithologies. Ilmenite occurs as accessory phase.

Major element data

Phases from pyroxenite sample CB1042, from the UZ, have compositions different from UMZ minerals (Table A). They show higher Mg# with respect UMZ rocks (Amphibole Mg# = 0.89-0.90; Clinopyroxene Mg# = 0.92-0.94; Orthopyroxene Mg# = 0.86-0.87). Amphibole from this sample have commonly higher TiO_2 (1.49-2.28 wt%), Al_2O_3 (12.88-14.76 wt%), CaO (11.41-12.01 wt%) and Na_2O (2.09-2.41 wt%) contents among complex samples. Similarly, Clinopyroxene have higher contents for Al_2O_3 and Na_2O (3.58-4.86 wt% and 0.65-0.79 wt% respectively) and Orthopyroxene have higher SiO_2 and Al_2O_3 (54.78-55.56 wt% and 2.64-3.50 wt%) while commonly lower CaO (0.14-0.93 wt%). Plagioclase has an Anortite (An) content between 76.80-80.25%.

Amphibole from the UMZ, along the stratigraphy, shows enrichments for TiO_2, FeO and K_2O (Table A). The Al_2O_3 content shows a depletion trend, while Na_2O and K_2O have depletion trends till to the 8 km and are successively increased up to the complex top (Table A).

Clinopyroxene variations through the stratigraphy show depletion trends for Mg#, TiO_2, Al_2O_3 and Na_2O (Table B). Conversely, the FeO and CaO contents increase (Table B). Orthopyroxene shows depletion trends for SiO_2, Al_2O_3 and MgO and enrichment trends for TiO_2, FeO and CaO (Table C).

Plagioclase shows an enrichment for Al_2O_3 till the 7 km and a successively depletion up to the top of the complex (Table D). Conversely, the SiO_2 shows first depletion and successive enrichment (Table D). The An content increase up to the 7 km and successively remains constant but lower (Table D).

Plagioclase from xenoliths from Palmeirópolis Sequence (sample CB1060) has composition and An content similar to Palmeirópolis Sequence amphibolite (sample SP0003), but with less span composition between cores and rims of the crystals (Table D). Similarly, the compositional variations between crystal cores and rims are more evident for the Amphiboles from the Palmeirópolis Sequence amphibolite (Table A). Amphibole from the xenoliths is enriched in Al_2O_3, MgO and Na_2O with respect to the amphibolite. This latter results instead enriched in SiO_2, TiO_2, FeO, CaO and K_2O (Table A).

Online Resource B Bulk rock major (X-ray fluorescence analysis in wt%) and trace (ICP-MS analysis in ppm) element compositions

Sample	CB1420	CB1399C	CB1400	CB1401	CB1401	CB1462	CB1042
Unit	LMZ	UZ	UZ	UZ	UZ	UZ	UZ
Strat Pos (m	447	2740	2740	2740	2740	3537	3514
SiO_2	48.89	46.26	38.86	49.39	49.25	45.10	54.58
TiO_2	1.14	0.18	0.09	0.17	0.17	1.64	0.17
Al_2O_3	16.30	18.07	3.60	3.99	4.00	11.19	5.38
Fe_2O_3	11.77		9.25	7.88	7.88	14.54	8.79
MnO	0.17	0.07	0.14	0.15	0.15	0.18	0.16
MgO	7.51	8.76	37.73	24.12	24.06	12.25	26.37
CaO	9.47	18.93	2.38	9.43	9.37	11.30	4.32
Na_2O	1.62		0.00	0.06	0.05	1.82	0.09
K_2O	0.08		0.00	0.03	0.02	0.53	0.01
P_2O_5	0.17	0.00	0.00	0.00	0.00	0.11	0.01
LOI	2.47	2.04	8.56	4.42	4.53	0.90	0.18
Tot	99.58	94.31	100.60	99.64	99.48	99.54	100.07
Mg#	0.56	0.75	0.89	0.86	0.86	0.63	0.86
FeO_t	10.59	5.25	8.32	7.09	7.09	13.08	7.91
Sc		45		42	37		
Ti	6841	1067	510	1001	1007	9802	1017
V		151	47	191	210		
Cr		154	646	3396	3411		
Co		598	104	70	70		
Ni		112.9	2004	775	778		
Zn		16	43	37	36		
Rb						6.7	0.213
Sr		281		14	14	68	33
Y		5.60	3.00	5.00	4.90	27	3.1
Zr		8.0	6.6	11	11	51	2.34
Nb						5.1	2.00
Cs						2.45	0.040
Ba						77	61
La						11	0.123
Ce				41	38	40	0.337
Pr						7.3	0.062
Nd		18	17	24	19	37	0.359
Sm						9.9	0.153
Eu						2.26	0.093
Gd						9.1	0.431
Tb						1.15	0.060
Dy						5.7	0.433
Ho						1.01	0.115
Er						2.31	0.365
Tm						0.292	0.064
Yb						1.56	0.468
Lu						0.218	0.088
Hf						2.38	0.108
Ta						0.224	3.2
Pb		9				1.35	0.463
Th		9.9				0.164	0.006
U		8.8		7.8	5.6	0.031	<0.010

Strat Pos (m) is the recalculated stratigraphic height from the base of the complex
Mg# was calculated as Mg2+/(Mg2++Fe2+) molar ratio. FeOt is the total iron as Fe2+
For abbreviations of rock units (Unit) see the geological setting chapter

Online Resource B Bulk rock major (X-ray fluorescence analysis in wt%) and trace (ICP-MS analysis in ppm) element compositions

Sample	CB1133	CB1434	CB1464	CB1426	CB1430	CB1424	CB1391
Unit	UZ	UMZ	UMZ	UMZ	UMZ	UMZ	UMZ
Strat Pos (m	3538	4858	4874	5486	5528	7053	7245
SiO_2	50.37	49.45	50.19	49.59	49.82	45.79	50.47
TiO_2	0.76	0.81	0.31	0.55	0.57	1.75	0.45
Al_2O_3	15.33	16.35	15.61	16.21	15.22	16.08	6.66
Fe_2O_3	8.97	10.11	9.71	11.32	10.67	14.69	9.73
MnO	0.15	0.16	0.17	0.18	0.17	0.26	0.22
MgO	8.66	8.39	9.76	7.98	9.10	6.87	15.91
CaO	11.82	12.72	12.55	12.60	12.62	12.95	15.28
Na_2O	1.72	1.42	1.13	1.14	1.28	0.65	0.29
K_2O	0.25	0.09	0.04	0.07	0.07	0.02	0.05
P_2O_5	0.07	0.08	0.02	0.08	0.06	0.09	0.02
LOI	1.44	0.12	0.33	0.03	0.09	0.36	0.36
Tot	99.54	99.70	99.80	99.75	99.66	99.50	99.44
Mg#	0.66	0.62	0.67	0.58	0.63	0.48	0.76
FeO_t	8.07	9.10	8.74	10.18	9.60	13.22	8.76
Sc							62
Ti	4550	4850	1852	3296	3414	10514	2692
V							338
Cr							1976
Co							56
Ni							175
Zn							64
Rb	7.4	0.723	0.396	0.690	0.531	0.439	
Sr	101	153	122	181	145	233	68
Y	18	18	9.2	29	27	12	12
Zr	20	18	6.4	18	17	22	28
Nb	3.5	8.2	2.46	2.79	2.04	7.9	
Cs	0.292	0.020	0.016	0.029	0.014	0.012	
Ba	63	109	41	70	67	38	68
La	3.8	6.9	1.87	8.3	7.6	3.3	
Ce	8.9	15	4.1	19	18	7.8	52
Pr	1.29	2.16	0.575	2.90	2.86	1.17	
Nd	6.2	9.9	2.87	14	14	5.7	32
Sm	1.86	2.57	0.931	4.0	3.9	1.66	
Eu	0.749	0.925	0.516	0.938	0.892	0.913	
Gd	2.54	3.4	1.77	4.8	4.8	1.87	
Tb	0.451	0.483	0.232	0.771	0.728	0.314	
Dy	2.87	2.91	1.45	4.7	4.4	1.94	
Ho	0.656	0.661	0.340	1.03	0.976	0.441	
Er	1.85	1.82	0.959	2.78	2.64	1.20	
Tm	0.292	0.284	0.153	0.437	0.414	0.197	
Yb	1.89	1.83	1.01	2.71	2.53	1.31	
Lu	0.295	0.296	0.169	0.415	0.394	0.216	
Hf	0.804	0.724	0.325	0.798	0.754	0.715	
Ta	0.882	2.51	5.6	0.331	0.247	0.626	
Pb	4.0	2.97	0.841	3.8	3.5	1.60	10
Th	0.644	0.087	0.056	0.087	0.080	0.109	8.5
U	0.154	0.043	0.008	0.027	0.018	0.034	10

Strat Pos (m) is the recalculated stratigraphic height from the base of the complex
Mg# was calculated as Mg2+/(Mg2++Fe2+) molar ratio. FeOt is the total iron as Fe2+
For abbreviations of rock units (Unit) see the geological setting chapter

Online Resource B Bulk rock major (X-ray fluorescence analysis in wt%) and trace (ICP-MS analysis in ppm) element compositions

Sample	CB1414	CB1475	CB1490	CB1389	CB1482	CB1394	CB1395	CB1397
Unit	UMZ	UMZ	UMZ	UMZ	UMZ	UMZ	UMZ	UMZ
Strat Pos (m	7456	8221	10432	10443	10557	10877	10954	11024
SiO_2	50.41	48.92	59.96	45.66	47.45	50.62	60.42	45.86
TiO_2	0.42	0.68	0.78	2.11	2.55	1.88	1.02	3.00
Al_2O_3	12.05	16.64	12.98	17.94	18.18	18.76	14.94	12.97
Fe_2O_3	10.74	11.17	7.65	13.16	14.76	11.52	8.94	
MnO	0.21	0.20	0.34	0.12	0.21	0.21	0.14	0.60
MgO	12.66	8.62	7.36	7.29	4.85	5.65	4.68	10.77
CaO	12.30	11.97	9.29	10.86	9.39	7.97	5.85	6.86
Na_2O	0.67	1.11	0.80	0.99	0.86	1.07	0.87	0.53
K_2O	0.05	0.07	0.13	0.18	0.90	1.24	1.76	0.01
P_2O_5	0.04	0.11	0.29	0.16	0.15	0.12	0.05	0.19
LOI	0.19	0.23	0.34	0.95	0.35	0.10	0.22	< 0.01
Tot	99.73	99.72	99.92	99.43	99.64	99.14	98.89	80.80
Mg#	0.70	0.60	0.66	0.52	0.39	0.49	0.51	0.50
FeO_t	9.66	10.05	6.89	11.84	13.28	10.37	8.04	19.18
Sc				47		27	23	37
Ti	2513	4067	4660	12674	15294	11247	6133	17991
V				263		171	141	287
Cr				172		167	236	125
Co				62		33	27	47
Ni				58		60	54	80
Zn				138		132	99	185
Rb	0.569	0.639	1.33	4	40	47	65	
Sr	114	182	169	183	204	170	119	111
Y	15	24	45	11	21	12	7.0	12
Zr	18	8.2	94	67	62	302	154	153
Nb	91	3.2	12	15	19	19	9.5	26
Cs	0.021	0.020	0.042		0.932			
Ba	46	56	124		288	550	631	
La	3.6	8.1	31		11	34		
Ce	8.8	19	64	60	23	66	60	60
Pr	1.31	2.65	9.3		2.64			
Nd	6.4	12	37	33	10	47	24	38
Sm	1.87	3.4	8.0		2.19			
Eu	0.620	1.11	1.40		1.36			
Gd	2.49	4.2	7.3		2.57			
Tb	0.394	0.641	1.19		0.444			
Dy	2.44	3.9	7.0		3.1			
Ho	0.550	0.875	1.50		0.806			
Er	1.53	2.41	4.1		2.54			
Tm	0.243	0.382	0.641		0.437			
Yb	1.54	2.43	4.0		3.1			
Lu	0.244	0.379	0.609		0.490			
Hf	0.653	0.456	2.84		1.56			
Ta	8.4	0.313	0.925		1.45			
Pb	1.64	2.79	5.3	19	9.7	19	11	22
Th	0.258	0.248	8.5	10	0.496	9.9		9.9
U	0.049	0.039	1.99	8.6	0.144	7.3	6.4	11

Strat Pos (m) is the recalculated stratigraphic height from the base of the complex
Mg# was calculated as Mg2+/(Mg2++Fe2+) molar ratio. FeOt is the total iron as Fe2+
For abbreviations of rock units (Unit) see the geological setting chapter

Online Resource B Bulk rock major (X-ray fluorescence analysis in wt%) and trace (ICP-MS analysis in ppm) element compositions

Sample	CB1397	CB1398	CB1393	CB1403	CB1060	CB1480	CB1390
Unit	UMZ	UMZ	UMZ	Xen	Xen	Xen	Xen
Strat Pos (m	11024	11024	11032	7431	9260	9338	10443
SiO_2	45.90		52.89	71.60	47.36	46.22	45.67
TiO_2	2.99		0.78	0.42	1.83	1.01	2.06
Al_2O_3	13.04		15.39	11.80	18.24	13.06	17.79
Fe_2O_3			8.08	4.32	14.52	14.80	15.57
MnO	0.60		0.15	0.04	0.26	0.46	0.33
MgO	10.84		8.93	3.05	6.09	10.67	7.73
CaO	6.86		9.96	2.88	10.07	11.78	10.02
Na_2O	0.54		0.78	1.56	0.97	0.85	0.54
K_2O	0.01		1.73	2.32	0.18	0.22	0.04
P_2O_5	0.20		0.12	0.05	0.25	0.21	0.10
LOI	< 0.01		0.64	1.05	0.28	0.86	0.01
Tot	80.98		99.45	99.08	100.05	100.13	99.86
Mg#	0.50		0.69	0.58	0.45	0.59	0.50
FeO_t	19.17		7.27	3.89	13.06	13.32	14.01
Sc	37	32	32				45
Ti	17931	b.d.l.	4670	2512	11000	6063	12332
V	271	147	259	59			265
Cr	129	148	421	123			175
Co	48	35	39	17			49
Ni	81	59	55	34			46
Zn	186	102	70	64			120
Rb		97	73	82	4.6	1.87	
Sr	113	95	241	121	214	173	148
Y	14	91	15	7.6	12	40	8.2
Zr	153	536	48	71	32	152	36
Nb	26	15		9.7	9.6	14	11
Cs					0.027	0.007	
Ba		755	576	412	41	27	39
La					11	28	
Ce	73	70	52	60	25	63	42
Pr					3.2	8.2	
Nd	42	32	35	17	13	34	37
Sm					2.76	8.1	
Eu					1.21	2.44	
Gd					2.35	7.5	
Tb					0.346	1.24	
Dy					1.96	7.0	
Ho					0.430	1.40	
Er					1.23	3.6	
Tm					0.200	0.551	
Yb					1.34	3.3	
Lu					0.234	0.493	
Hf					0.993	4.0	
Ta					1.01	1.15	
Pb	21	18	12	7.5	2.97	3.2	15
Th	12	10	9.1	18	0.854	6.8	8.9
U	12	8.2	6	2.90	0.375	1.26	9.6

Strat Pos (m) is the recalculated stratigraphic height from the base of the complex
Mg# was calculated as Mg2+/(Mg2++Fe2+) molar ratio. FeOt is the total iron as Fe2+
For abbreviations of rock units (Unit) see the geological setting chapter

Online Resource B Bulk rock major (X-ray fluorescence analysis in wt%) and trace (ICP-MS analysis in ppm) element compositions

Sample	CB1396	CB1392	CB1392	CB1399E	SP0002	SP0003	SP0006
Unit	Xen	Xen	Xen	Xen	SP	SP	SP
Strat Pos (m	11024	11062	11062	11268	13448	13530	13612
SiO_2	73.50	69.48	69.43	66.94	43.17	47.71	53.78
TiO_2	0.26	0.66	0.67	1.19	1.61	1.71	0.95
Al_2O_3	11.90	12.54	12.51	11.67	13.56	14.11	17.06
Fe_2O_3	5.90	6.04	6.03	9.68	16.48	13.71	6.47
MnO	0.18	0.15	0.15	0.24	0.26	0.20	0.14
MgO	1.45	1.90	1.89	3.41	8.24	6.74	2.36
CaO	2.67	1.90	1.91	1.74	14.20	13.46	11.83
Na_2O	1.60	1.10	1.12	1.06	1.57	1.39	3.99
K_2O	0.89	4.11	4.12	2.58	0.37	0.26	2.81
P_2O_5	0.02	0.06	0.06	0.01	0.13	0.18	0.10
LOI	0.51	1.07	1.06	0.74	0.31	0.35	0.24
Tot	98.89	99.01	98.95	99.25	99.90	99.82	99.74
Mg#	0.33	0.38	0.38	0.41	0.50	0.49	0.42
FeO_t	5.31	5.43	5.43	8.71	14.83	12.34	5.83
Sc	17	16	15	26			
Ti	1559	3957	3987	7110	9682	10276	5681
V	39	64.3	40.9	150.5			
Cr	56	27.6	30.1	124.1			
Co	6.5	12	10.7	30.8			
Ni	17	13.6	11.8	54.7			
Zn	38	96	95	103			
Rb	27	94	94	99	2.31	7.4	89
Sr	71	121	119	103	61	149	511
Y	64	58	59	77	36	33	24
Zr	346	290	290	381	51	22	60
Nb		13	13	14	9.5	7.5	19
Cs					0.016	0.012	1.44
Ba	219	1445	1432	554	12	22	1712
La		42	48		7.3	7.3	51
Ce	48	91	99	62	17	18	94
Pr					2.49	2.84	11
Nd	17	50	36	21	12	14	38
Sm					3.6	4.1	6.4
Eu					1.28	1.40	1.17
Gd					4.9	5.1	4.1
Tb					0.875	0.869	0.706
Dy					5.5	5.4	3.9
Ho					1.27	1.20	0.799
Er					3.5	3.2	2.09
Tm					0.550	0.505	0.320
Yb					3.5	3.2	2.01
Lu					0.530	0.483	0.305
Hf					1.63	1.23	1.84
Ta					1.37	0.817	1.17
Pb	9.4	26	26	15	0.948	1.41	6.5
Th		27	28	11	1.31	0.623	13
U	4.1	3.3	5.0	5.4	0.352	0.199	1.06

Strat Pos (m) is the recalculated stratigraphic height from the base of the complex
Mg# was calculated as Mg2+/(Mg2++Fe2+) molar ratio. FeOt is the total iron as Fe2+
For abbreviations of rock units (Unit) see the geological setting chapter

Online Resource C Compositions of Amphibole in terms of major (EPMA results, in wt%) and trace (LA-IC

Sample	CB1042	CB1042	CB1042	CB1042	CB1042	CB1042	CB1434
Phase	Amph	Amph	Amph	Amph	Amph	Amph	Amph
Site	A	A	E	E	H	P	D
Analysis #	125	126	135	136	143	157	166
Position	core	rim	core	rim	core	core	core
SiO_2	45.49	45.83	42.79	44.26	46.03	45.52	45.30
TiO_2	1.61	1.49	2.28	2.28	1.59	1.72	1.44
Al_2O_3	13.60	13.08	14.76	13.68	13.41	12.88	14.01
Cr_2O_3	1.22	1.88	2.16	1.94	1.36	1.72	0.15
FeO_T	3.62	3.80	3.53	3.43	3.38	3.51	9.30
MnO	0.09	0.05	0.03	0.04	0.03	0.04	0.13
NiO	0.19	0.00	0.08	0.12	0.15	0.07	0.06
MgO	16.56	16.88	16.07	16.43	17.01	16.72	13.50
CaO	11.97	12.01	11.45	11.41	11.76	12.00	10.93
Na_2O	2.12	2.16	2.41	2.18	2.14	2.09	1.59
K_2O	0.61	0.49	0.84	0.80	0.39	0.71	1.04
Total	97.08	97.67	96.40	96.57	97.25	96.98	97.45
C.p.f.u.							
Si	6.455	6.471	6.160	6.333	6.495	6.475	6.525
Ti	0.172	0.158	0.247	0.245	0.169	0.184	0.156
Al	2.275	2.177	2.504	2.307	2.230	2.159	2.378
Cr	0.137	0.210	0.246	0.219	0.152	0.193	0.017
Fe^{2+}	0.430	0.449	0.425	0.410	0.399	0.418	1.120
Fe^{3+}	0.000	0.000	0.000	0.000	0.000	0.000	0.000
Mn	0.011	0.006	0.004	0.005	0.004	0.005	0.016
Ni	0.022	0.000	0.009	0.014	0.017	0.008	0.007
Mg	3.500	3.550	3.445	3.501	3.575	3.542	2.896
Ca	1.820	1.817	1.766	1.749	1.778	1.829	1.687
Na	0.583	0.591	0.673	0.605	0.585	0.576	0.444
K	0.110	0.088	0.154	0.146	0.070	0.129	0.191
Cations	15.514	15.517	15.632	15.534	15.473	15.518	15.438
ppm							
Sc			117				
Ti			13890				
V			89				
Cr			16360				
Co			52				
Ni			982				
Rb			4.4				
Sr			32				
Y			34				

Zr	12
Nb	0.495
Cs	0.015
Ba	144
La	1.41
Ce	4.6
Pr	0.802
Nd	5.1
Sm	2.19
Eu	0.786
Gd	3.5
Tb	0.669
Dy	5.2
Ho	1.26
Er	4.1
Tm	0.576
Yb	4.4
Lu	0.605
Hf	0.592
Ta	0.023
Pb	1.46
Th	0.011
U	0.001

CP-MS results, in ppm) elements originating from core and rim regions of each rock sample, respectively

CB1434 Amph D 167 rim	CB1434 Amph L 178 rim	CB1434 Amph R 195 core	CB1434 Amph R 196 rim	CB1434 Amph T 201 core	CB1434 Amph T 202 rim	CB1424 Amph A 101 core	CB1424 Amph A 102 rim
46.35	46.19	42.87	47.48	43.34	44.20	44.17	41.20
0.99	1.21	1.68	1.68	1.07	1.02	1.33	1.64
12.02	13.02	11.61	13.35	14.28	13.97	12.07	15.01
0.21	0.08	0.18	0.13	0.18	0.01	0.08	0.01
8.76	9.85	8.54	9.09	7.96	7.72	16.92	16.92
0.13	0.12	0.11	0.08	0.09	0.00	0.17	0.20
0.00	0.06	0.02	0.00	0.00	0.04	0.00	0.01
14.95	12.95	12.65	13.11	15.92	16.28	9.82	8.35
10.90	10.53	15.86	10.12	10.94	10.92	11.08	11.30
1.42	1.61	1.66	1.71	1.66	1.69	1.55	1.64
0.78	0.86	1.08	1.16	0.89	0.80	0.58	0.89
96.51	96.48	96.26	97.91	96.33	96.65	97.77	97.17
6.707	6.708	6.387	6.754	6.305	6.385	6.578	6.216
0.108	0.132	0.188	0.180	0.117	0.111	0.149	0.186
2.050	2.228	2.038	2.238	2.449	2.378	2.119	2.669
0.024	0.009	0.021	0.015	0.021	0.001	0.009	0.001
1.060	1.196	1.064	1.081	0.968	0.933	2.107	2.135
0.000	0.000	0.000	0.000	0.000	0.000	0.000	0.000
0.016	0.015	0.014	0.010	0.011	0.000	0.021	0.026
0.000	0.007	0.002	0.000	0.000	0.005	0.000	0.001
3.222	2.801	2.807	2.778	3.449	3.502	2.178	1.876
1.690	1.638	2.532	1.543	1.705	1.690	1.768	1.827
0.398	0.453	0.479	0.472	0.468	0.473	0.448	0.480
0.144	0.159	0.205	0.211	0.165	0.147	0.110	0.171
15.419	15.348	15.738	15.280	15.660	15.625	15.488	15.588

CB1424 Amph C 107 core	CB1424 Amph C 108 rim	CB1424 Amph I 121 core	CB1424 Amph I 122 rim	CB1424 Amph L 123 core	CB1424 Amph L 124 rim	CB1424 Amph M 125 core	CB1424 Amph M 126 rim	CB1424 Amph R 137 core
43.34	43.88	43.86	43.80	44.08	43.14	43.91	42.15	42.74
0.98	1.04	1.24	1.12	1.17	1.25	1.45	1.36	1.36
12.29	12.11	12.02	12.66	11.72	13.38	12.35	14.47	12.61
0.03	0.07	0.06	0.01	0.06	0.00	0.06	0.00	0.04
16.64	16.93	16.77	16.52	16.69	16.71	16.49	16.83	17.37
0.21	0.22	0.18	0.16	0.15	0.19	0.14	0.20	0.18
0.02	0.00	0.00	0.01	0.05	0.08	0.01	0.00	0.00
9.66	10.02	10.21	10.04	9.97	9.69	9.80	8.79	9.30
11.20	11.17	11.13	11.22	11.10	11.07	11.07	11.31	11.05
1.40	1.46	1.41	1.51	1.44	1.53	1.56	1.66	1.56
0.54	0.56	0.58	0.59	0.56	0.60	0.61	0.75	0.59
96.31	97.46	97.46	97.64	96.99	97.64	97.45	97.52	96.80
6.553	6.561	6.553	6.522	6.612	6.436	6.550	6.317	6.462
0.111	0.117	0.139	0.125	0.132	0.140	0.163	0.153	0.155
2.190	2.134	2.116	2.222	2.072	2.353	2.171	2.556	2.247
0.004	0.008	0.007	0.001	0.007	0.000	0.007	0.000	0.005
2.104	2.117	2.095	2.057	2.094	2.085	2.057	2.109	2.196
0.000	0.000	0.000	0.000	0.000	0.000	0.000	0.000	0.000
0.027	0.028	0.023	0.020	0.019	0.024	0.018	0.025	0.023
0.002	0.000	0.000	0.001	0.006	0.010	0.001	0.000	0.000
2.175	2.231	2.272	2.227	2.227	2.153	2.177	1.962	2.094
1.814	1.789	1.782	1.790	1.784	1.769	1.769	1.816	1.790
0.410	0.423	0.408	0.436	0.419	0.443	0.451	0.482	0.457
0.104	0.107	0.111	0.112	0.107	0.114	0.116	0.143	0.114
15.496	15.516	15.506	15.515	15.479	15.526	15.481	15.565	15.543

100	108	108	112
7443	6333	6480	7115
885	1029	1007	979
151	130	149	134
65	64	62	64
20	21	20	22
17	17	19	18
42	44	43	40
32	32	30	34

57	58	58	62
4.8	4.8	4.9	4.8
0.194	0.203	0.317	0.312
260	281	273	290
9.5	11	10	11
29	33	30	32
4.0	4.4	4.1	4.5
23	24	22	25
5.8	5.9	5.7	6.2
2.93	3.1	2.80	3.1
5.1	5.4	4.9	5.8
0.782	0.800	0.759	0.883
5.7	5.7	5.0	6.3
1.21	1.26	1.11	1.36
3.9	4.0	3.6	4.3
0.603	0.582	0.567	0.654
5.0	5.2	4.7	5.0
0.694	0.750	0.654	0.743
2.28	2.30	2.23	2.60
0.190	0.195	0.190	0.177
1.38	1.34	1.25	1.34
0.104	0.107	0.230	0.223
0.018	0.019	0.028	0.022

CB1424 Amph S 144 core	CB1414 Amph A 74 core	CB1414 Amph A 75 rim	CB1414 Amph B 76 core	CB1414 Amph B 77 rim	CB1414 Amph F 92 core	CB1414 Amph G 94 core	CB1414 Amph G 95 rim
43.01	48.28	47.91	47.87	48.27	47.67	48.75	50.32
1.36	1.34	1.29	1.36	1.29	1.33	1.33	1.13
12.34	9.77	9.86	9.46	9.76	10.07	10.23	9.15
0.04	0.62	0.55	0.71	0.69	0.67	0.65	0.56
16.62	8.96	8.58	8.61	8.71	9.22	7.66	7.17
0.15	0.10	0.14	0.16	0.12	0.08	0.08	0.01
0.00	0.00	0.06	0.00	0.00	0.01	0.00	0.03
9.54	15.47	15.52	15.57	15.41	14.38	15.94	15.85
11.15	11.50	11.65	11.36	11.63	11.27	11.14	11.21
1.52	1.17	1.13	1.25	1.18	1.20	1.23	1.03
0.57	0.53	0.54	0.52	0.58	0.56	0.54	0.47
96.30	97.74	97.23	96.87	97.64	96.46	97.55	96.93
6.510	6.897	6.878	6.899	6.902	6.907	6.919	7.139
0.155	0.144	0.139	0.147	0.139	0.145	0.142	0.121
2.201	1.645	1.668	1.607	1.645	1.720	1.711	1.530
0.005	0.070	0.062	0.081	0.078	0.077	0.073	0.063
2.104	1.070	1.030	1.038	1.041	1.117	0.909	0.851
0.000	0.000	0.000	0.000	0.000	0.000	0.000	0.000
0.019	0.012	0.017	0.020	0.015	0.010	0.010	0.001
0.000	0.000	0.007	0.000	0.000	0.001	0.000	0.003
2.151	3.291	3.318	3.342	3.281	3.103	3.370	3.349
1.808	1.760	1.792	1.754	1.782	1.750	1.694	1.704
0.446	0.324	0.315	0.349	0.327	0.337	0.338	0.283
0.110	0.097	0.099	0.096	0.106	0.104	0.098	0.085
15.510	15.311	15.325	15.332	15.315	15.270	15.265	15.128
						120	116
						7131	7870
						1018	995
						4773	4759
						56	55
						135	125
						2.22	3.3
						17	17
						75	72

63	71
0.030	0.029
130	127
11	11
40	39
6.8	6.1
39	37
12	11
1.46	1.34
13	12
2.20	2.03
14	14
3.1	2.96
9.1	8.5
1.32	1.16
8.7	8.3
1.14	1.13
3.0	3.3
0.035	
0.814	0.792
0.267	0.298
0.036	0.051

CB1414 Amph H 97 core	CB1414 Amph H 98 rim	CB1414 Amph H 99 core inc Opx	CB1414 Amph H 100 rim inc Opx	CB1414 Amph R 116 core	CB1414 Amph R 117 rim	CB1414 Amph S 118 core	CB1414 Amph S 119 rim
48.76	48.25	49.78	49.43	47.95	48.41	47.49	47.83
1.14	1.21	1.17	1.14	1.39	1.37	1.52	1.29
9.50	10.01	9.33	8.85	9.73	9.46	9.92	9.94
0.63	0.56	0.50	0.40	0.81	0.73	0.57	0.61
7.56	7.48	7.19	7.37	8.29	8.43	8.49	8.18
0.10	0.05	0.13	0.09	0.11	0.06	0.12	0.13
0.00	0.00	0.05	0.00	0.02	0.06	0.02	0.00
15.72	15.95	16.44	16.59	15.24	15.63	14.81	15.15
11.05	11.05	11.14	11.11	11.59	11.69	11.45	11.60
1.36	1.19	1.15	1.16	1.15	1.24	1.29	1.02
0.50	0.51	0.53	0.46	0.54	0.52	0.55	0.54
96.32	96.26	97.41	96.60	96.82	97.60	96.23	96.29
7.006	6.934	7.048	7.063	6.903	6.918	6.886	6.911
0.123	0.131	0.125	0.123	0.151	0.147	0.166	0.140
1.609	1.695	1.557	1.490	1.651	1.593	1.695	1.693
0.072	0.064	0.056	0.045	0.092	0.082	0.065	0.070
0.908	0.899	0.851	0.881	0.998	1.007	1.029	0.988
0.000	0.000	0.000	0.000	0.000	0.000	0.000	0.000
0.012	0.006	0.016	0.011	0.013	0.007	0.015	0.016
0.000	0.000	0.006	0.000	0.002	0.007	0.002	0.000
3.364	3.414	3.467	3.530	3.267	3.326	3.198	3.260
1.701	1.701	1.690	1.701	1.788	1.790	1.779	1.796
0.379	0.332	0.316	0.321	0.321	0.344	0.363	0.286
0.092	0.093	0.096	0.084	0.099	0.095	0.102	0.100
15.266	15.269	15.226	15.249	15.285	15.317	15.300	15.260
				131	126	120	126
				7378	7097	6458	7741
				1204	1286	1013	1175
				4124	4729	3577	4953
				66	57	58	56
				158	145	140	131
				2.64	2.71	2.88	2.33
				17	13	13	17
				82	65	60	73

61	46	42	50
0.572	0.381	0.288	0.666
0.068	0.053	0.196	0.019
134	123	123	134
12	9.4	9.2	11
45	34	35	42
7.0	5.2	5.3	6.4
42	31	32	40
13	9.5	9.9	11
1.65	1.52	1.57	1.60
15	10	10	13
2.45	1.75	1.69	2.11
16	12	12	14
3.3	2.47	2.78	2.98
10	7.6	7.6	8.9
1.46	1.03	1.14	1.14
10	7.9	8.0	8.6
1.33	1.05	1.04	1.13
3.0	2.05	1.95	2.48
0.013	0.006	0.018	0.033
0.856	0.617	0.767	0.808
0.285	0.146	0.320	0.207
0.039	0.013	0.028	0.027

CB1475 Amph G 74 core	CB1475 Amph G 75 rim	CB1060 Amph A 166 core	CB1060 Amph A 167 rim	CB1060 Amph C 172 core	CB1060 Amph C 173 rim	CB1060 Amph D 174 core	CB1060 Amph D 175 rim
45.67	44.87	44.39	43.53	43.58	43.86	43.82	43.54
1.54	1.64	0.57	0.59	0.70	0.56	0.64	0.48
10.83	12.07	16.60	16.17	16.17	16.36	16.91	16.95
0.09	0.14	0.02	0.03	0.03	0.04	0.03	0.07
11.85	11.50	12.21	12.67	12.98	13.34	13.27	13.20
0.10	0.10	0.09	0.08	0.02	0.09	0.04	0.05
0.07	0.06	0.02	0.04	0.00	0.02	0.00	0.09
13.01	12.72	10.89	10.95	10.44	10.55	10.25	10.06
11.23	11.79	11.10	11.11	10.98	11.02	11.20	11.21
1.23	1.24	1.68	1.49	1.44	1.49	1.50	1.56
0.92	1.01	0.31	0.32	0.30	0.33	0.31	0.31
96.54	97.14	97.88	96.98	96.64	97.66	97.97	97.52
6.727	6.578	6.411	6.372	6.400	6.387	6.355	6.350
0.171	0.181	0.062	0.065	0.077	0.061	0.070	0.053
1.880	2.086	2.826	2.790	2.799	2.808	2.891	2.913
0.010	0.016	0.002	0.003	0.003	0.005	0.003	0.008
1.460	1.410	1.475	1.551	1.594	1.624	1.610	1.610
0.000	0.000	0.000	0.000	0.000	0.000	0.000	0.000
0.012	0.012	0.011	0.010	0.002	0.011	0.005	0.006
0.008	0.007	0.002	0.005	0.000	0.002	0.000	0.011
2.854	2.777	2.342	2.387	2.283	2.288	2.214	2.185
1.772	1.852	1.718	1.742	1.728	1.719	1.740	1.752
0.351	0.352	0.470	0.423	0.410	0.421	0.422	0.441
0.173	0.189	0.057	0.060	0.056	0.061	0.057	0.058
15.419	15.461	15.377	15.408	15.354	15.387	15.367	15.386
				55	55	57	54
				3513	3444	3474	3073
				390	370	395	383
				181	119	157	133
				59	60	59	58
				64	68	67	65
				2.28	2.40	1.98	2.38
				22	20	21	21
				3.5	4.6	5.3	6.3

8.2	7.0	7.3	6.0
2.62	0.896	0.334	0.786
0.012	0.017	0.012	0.030
59	57	58	68
0.741	0.576	0.473	0.459
4.5	3.6	3.3	3.9
1.09	0.955	0.904	0.892
8.8	8.2	7.4	7.1
3.5	3.2	3.1	2.75
1.38	1.31	1.29	1.18
2.49	2.48	2.44	2.33
0.238	0.262	0.248	0.290
1.09	1.23	1.25	1.46
0.144	0.198	0.182	0.256
0.319	0.387	0.396	0.638
0.027	0.034	0.046	0.081
0.192	0.288	0.268	0.525
0.026	0.030	0.036	0.067
0.649	0.475	0.491	0.418
0.135	0.032	0.061	0.062
1.09	1.10	1.12	1.17
0.001	0.001	0.001	0.003
0.024	0.022	0.012	0.010

CB1060 Amph D 176 core	CB1060 Amph F 180 core	CB1060 Amph F 181 rim	CB1060 Amph G 183 core	CB1060 Amph G 184 rim	CB1060 Amph G 185 core	CB1060 Amph L 190 core	CB1060 Amph L 191 rim	CB1060 Amph L 192 core
42.77	43.05	43.35	42.87	42.76	43.54	42.91	42.95	43.87
0.59	0.59	0.56	0.47	0.37	0.47	0.53	0.51	0.59
17.14	17.38	17.00	17.14	17.76	17.45	16.73	17.24	16.72
0.00	0.03	0.11	0.00	0.00	0.01	0.00	0.04	0.04
12.95	12.88	13.43	13.12	13.81	13.39	13.37	13.09	13.10
0.04	0.09	0.08	0.10	0.08	0.08	0.17	0.06	0.04
0.02	0.00	0.02	0.06	0.00	0.00	0.05	0.00	0.05
10.15	9.96	10.19	9.67	9.53	9.90	10.08	9.97	10.17
11.17	11.13	11.18	11.21	11.27	11.38	10.86	11.02	11.23
1.51	1.48	1.47	1.51	1.48	1.46	1.53	1.43	1.45
0.32	0.35	0.32	0.31	0.33	0.31	0.35	0.33	0.29
96.66	96.94	97.71	96.46	97.39	97.99	96.58	96.64	97.55
6.291	6.306	6.317	6.324	6.264	6.320	6.330	6.314	6.385
0.065	0.065	0.061	0.052	0.041	0.051	0.059	0.056	0.065
2.971	3.001	2.920	2.980	3.066	2.985	2.909	2.987	2.868
0.000	0.003	0.013	0.000	0.000	0.001	0.000	0.005	0.005
1.593	1.578	1.637	1.618	1.692	1.625	1.649	1.609	1.594
0.000	0.000	0.000	0.000	0.000	0.000	0.000	0.000	0.000
0.005	0.011	0.010	0.012	0.010	0.010	0.021	0.007	0.005
0.002	0.000	0.002	0.007	0.000	0.000	0.006	0.000	0.006
2.224	2.173	2.212	2.124	2.079	2.140	2.215	2.183	2.204
1.760	1.747	1.746	1.772	1.769	1.770	1.717	1.736	1.751
0.431	0.420	0.415	0.432	0.420	0.411	0.438	0.408	0.409
0.060	0.065	0.059	0.058	0.062	0.057	0.066	0.062	0.054
15.403	15.370	15.392	15.380	15.403	15.370	15.409	15.368	15.346
						52	53	
						2820	2785	
						346	362	
						204	159	
						52	55	
						61	62	
						2.52	3.5	
						18	19	
						4.5	6.3	

5.2	4.9
0.504	0.463
0.007	0.021
56	71
0.343	0.49
2.44	3.0
0.768	0.834
6.5	6.6
2.89	2.88
1.15	1.20
2.25	2.26
0.266	0.325
1.18	1.47
0.18	0.27
0.413	0.672
0.060	0.095
0.307	0.445
0.028	0.046
0.399	0.373
0.042	0.040
0.914	1.14
0.001	0.003
0.009	0.009

CB1060	CB1060	CB1060	CB1482	CB1482	CB1482	CB1482	CB1482
Amph	Amph	Amph	Amph	Amph	Amph	Amph	Amph
N	N	N	A	A	A	A	C
197	198	199	209	210	210	211	213
core inc Grt	rim inc Grt	core inc	core	rim	core	rim	core
43.26	44.38	43.95	44.21	44.60	43.81	44.02	43.11
0.60	0.69	0.73	1.75	1.65	1.64	1.35	1.61
15.98	15.91	15.89	10.89	11.18	12.26	12.47	12.77
0.12	0.00	0.07	0.05	0.01	0.07	0.01	0.05
12.63	12.27	12.13	13.68	13.63	13.84	13.41	13.43
0.05	0.02	0.11	0.04	0.03	0.02	0.02	0.00
0.03	0.00	0.01	0.06	0.00	0.02	0.00	0.04
10.60	11.08	11.57	11.67	11.85	11.10	11.07	11.49
11.10	11.31	11.31	11.15	11.40	11.17	11.33	11.42
1.50	1.59	1.59	1.44	1.55	1.52	1.44	1.59
0.32	0.33	0.33	1.09	1.03	1.19	1.09	1.27
96.19	97.58	97.69	96.03	96.93	96.64	96.21	96.78
6.387	6.437	6.377	6.633	6.622	6.535	6.571	6.428
0.067	0.075	0.080	0.197	0.184	0.184	0.152	0.181
2.781	2.720	2.717	1.926	1.956	2.155	2.194	2.244
0.014	0.000	0.008	0.006	0.001	0.008	0.001	0.006
1.559	1.488	1.472	1.716	1.692	1.727	1.674	1.675
0.000	0.000	0.000	0.000	0.000	0.000	0.000	0.000
0.006	0.002	0.014	0.005	0.004	0.003	0.003	0.000
0.004	0.000	0.001	0.007	0.000	0.002	0.000	0.005
2.331	2.393	2.500	2.608	2.620	2.466	2.461	2.552
1.756	1.758	1.758	1.792	1.814	1.785	1.812	1.825
0.429	0.447	0.447	0.419	0.446	0.440	0.417	0.460
0.060	0.061	0.061	0.209	0.195	0.226	0.208	0.242
15.394	15.382	15.435	15.518	15.535	15.532	15.492	15.616
			135	115	118	116	
			9395	7204	9676	9143	
			393	360	491	485	
			113	92	134	131	
			48	48	52	50	
			32	30	33	32	
			4.8	4.2	5.4	5.2	
			41	37	50	50	
			10	7.6	34	34	

27	25	31	29
15	16	18	18
0.019	0.018	0.017	0.029
73	74	88	83
24	24	22	21
62	65	55	53
7.6	8.5	7.0	6.9
32	38	37	37
5.7	7.2	9.5	9.3
3.3	3.4	2.87	2.78
3.2	3.9	9.5	9.6
0.389	0.447	1.35	1.40
2.39	2.31	8.4	8.9
0.469	0.402	1.65	1.82
1.34	0.887	4.1	4.0
0.130	0.093	0.354	0.343
0.655	0.409	1.31	1.26
0.064	0.034	0.109	0.093
1.06	1.06	1.42	1.51
0.647	0.895	0.820	0.804
6.0	5.4	6.4	6.5
0.146	0.135	0.170	0.167
0.031	0.036	0.039	0.034

CB1482	CB1482	CB1482	CB1482	CB1482	CB1482	CB1482	CB1482	CB1482
Amph	Amph	Amph	Amph	Amph	Amph	Amph	Amph	Amph
D	D	E	E	H	H	H	H	H
218	219	224	225	228	229	230	231	234
core	rim	core	rim	core	core (dark)	core (bright	core (dark)	core
43.88	44.52	44.17	44.78	40.54	47.53	50.32	45.20	44.18
1.88	1.55	1.79	1.41	1.67	0.50	0.02	0.02	2.04
12.00	12.08	11.97	12.54	10.80	4.82	0.56	0.63	11.95
0.03	0.02	0.07	0.00	0.03	0.00	0.06	0.06	0.00
14.04	13.55	13.65	13.45	15.12	12.58	24.27	30.57	14.37
0.00	0.05	0.09	0.01	0.06	0.04	0.25	0.28	0.08
0.04	0.00	0.04	0.00	0.03	0.01	0.08	0.11	0.03
11.20	11.46	11.15	10.97	12.73	17.03	19.66	19.60	11.01
11.22	11.29	11.46	11.51	12.70	12.81	1.08	0.55	11.17
1.61	1.52	1.54	1.47	1.41	0.61	0.05	0.01	1.61
1.22	0.97	1.25	1.12	1.13	0.34	0.03	0.00	1.21
97.12	97.01	97.18	97.26	96.22	96.27	96.38	97.03	97.65
6.526	6.590	6.555	6.606	6.212	7.062	7.574	7.058	6.540
0.210	0.173	0.200	0.156	0.192	0.056	0.002	0.002	0.227
2.103	2.107	2.094	2.180	1.950	0.844	0.099	0.116	2.085
0.004	0.002	0.008	0.000	0.004	0.000	0.007	0.007	0.000
1.746	1.677	1.694	1.659	1.938	1.563	3.055	3.992	1.779
0.000	0.000	0.000	0.000	0.000	0.000	0.000	0.000	0.000
0.000	0.006	0.011	0.001	0.008	0.005	0.032	0.037	0.010
0.005	0.000	0.005	0.000	0.004	0.001	0.010	0.014	0.004
2.481	2.526	2.464	2.410	2.905	3.769	4.407	4.558	2.427
1.788	1.791	1.822	1.819	2.085	2.039	0.174	0.092	1.772
0.464	0.436	0.443	0.420	0.419	0.176	0.015	0.003	0.462
0.231	0.183	0.237	0.211	0.221	0.064	0.006	0.000	0.229
15.558	15.492	15.534	15.463	15.938	15.580	15.381	15.880	15.535

102
10960
396
109
53
34
5.8
50
11

23
17

95
25
69
9.5
50
11
2.84
7.1
0.746
3.7
0.549
1.12
0.100
0.406
0.030
0.683
0.891
6.3
0.192
0.040

CB1482 Amph H 235 rim	CB1482 Amph L 237 core	CB1482 Amph L 238 rim	CB1482 Amph M 243 core	CB1482 Amph M 244 rim	CB1482 Amph M 244 core	CB1482 Amph M 245 rim	CB1482 Amph O 252 core	CB1482 Amph O 253 rim
44.73	43.53	43.61	43.88	43.77	44.76	46.18	45.23	44.71
1.25	1.98	1.51	2.10	2.15	1.77	1.47	1.75	2.01
12.42	12.03	11.83	11.91	12.48	10.81	9.91	10.62	11.16
0.02	0.00	0.07	0.05	0.02	0.05	0.05	0.07	0.00
13.52	14.36	13.55	13.57	13.86	13.97	13.66	13.37	13.43
0.06	0.06	0.05	0.06	0.06	0.06	0.11	0.04	0.07
0.00	0.01	0.06	0.05	0.00	0.00	0.00	0.08	0.04
11.18	11.05	11.69	11.24	10.97	11.22	11.97	11.84	11.83
11.63	11.16	11.18	11.36	11.47	11.21	11.74	11.36	11.49
1.51	1.56	1.37	1.46	1.59	1.54	1.26	1.42	1.53
1.14	1.30	1.12	1.31	1.35	1.06	0.88	0.96	1.19
97.46	97.04	96.04	96.99	97.72	96.45	97.23	96.74	97.46
6.596	6.496	6.541	6.527	6.473	6.686	6.815	6.711	6.606
0.139	0.222	0.170	0.235	0.239	0.199	0.163	0.195	0.223
2.158	2.116	2.091	2.088	2.175	1.903	1.724	1.857	1.943
0.002	0.000	0.008	0.006	0.002	0.006	0.006	0.008	0.000
1.667	1.792	1.700	1.688	1.714	1.745	1.686	1.659	1.659
0.000	0.000	0.000	0.000	0.000	0.000	0.000	0.000	0.000
0.007	0.008	0.006	0.008	0.008	0.008	0.014	0.005	0.009
0.000	0.001	0.007	0.006	0.000	0.000	0.000	0.010	0.005
2.455	2.456	2.611	2.490	2.416	2.496	2.631	2.616	2.603
1.837	1.784	1.797	1.810	1.817	1.794	1.856	1.806	1.819
0.432	0.451	0.398	0.421	0.456	0.446	0.361	0.408	0.438
0.214	0.247	0.214	0.249	0.255	0.202	0.166	0.182	0.224
15.508	15.574	15.545	15.526	15.555	15.485	15.420	15.457	15.530
	144	130			125	137		
	9167	8330			9875	10231		
	467	439			294	315		
	142	135			86	83		
	50	49			52	57		
	31	32			33	35		
	4.8	4.2			4.7	4.7		
	44	38			49	46		
	7.6	5.4			15	14		

29	26	26	27
18	18	16	17
0.039	0.042		0.008
71	69	67	68
24	23	21	22
63	61	52	55
8.1	8.1	6.6	7.0
37	37	34	36
6.2	6.7	8.0	8.0
3.2	3.5	2.58	2.79
3.7	3.5	6.0	5.6
0.416	0.399	0.863	0.701
2.01	1.61	3.8	3.6
0.3565	0.265	0.682	0.585
1.03	0.606	2.14	1.19
0.123	0.075	0.188	0.116
0.754	0.412	0.732	0.516
0.091	0.046	0.056	0.041
1.61	1.46	0.892	0.755
0.918	0.975	0.597	0.657
6.7	6.4	5.1	5.0
0.230	0.192	0.103	0.094
0.048	0.035	0.030	0.027

CB1482 Amph P 255 core	CB1482 Amph P 256 rim	CB1482 Amph P 263 core	CB1482 Amph P 264 rim	CB1482 Amph Q 261 core	CB1482 Amph Q 262 rim	CB1482 Amph Q 269 core	SP0003 Amph D 56 core
43.66	43.03	44.77	45.91	44.11	43.96	43.63	44.62
1.88	1.87	1.77	1.75	1.64	1.65	1.53	0.86
12.72	12.26	11.33	11.73	11.82	12.91	11.69	11.13
0.00	0.02	0.03	0.01	0.00	0.08	0.03	0.05
13.96	13.56	13.05	12.78	13.00	13.81	14.67	16.92
0.01	0.00	0.05	0.02	0.08	0.04	0.04	0.26
0.04	0.01	0.00	0.02	0.00	0.00	0.04	0.04
11.11	11.37	11.71	11.75	11.63	11.24	10.78	9.33
11.59	11.55	11.34	11.56	11.43	11.51	11.11	11.38
1.55	1.53	1.43	1.41	1.43	1.52	1.42	1.29
1.36	1.29	1.05	0.98	1.11	1.29	1.17	0.38
97.88	96.49	96.53	97.92	96.25	98.01	96.11	96.26
6.450	6.446	6.649	6.692	6.580	6.470	6.573	6.740
0.209	0.211	0.198	0.192	0.184	0.183	0.173	0.098
2.215	2.165	1.983	2.015	2.078	2.239	2.075	1.982
0.000	0.002	0.004	0.001	0.000	0.009	0.004	0.006
1.725	1.699	1.621	1.558	1.622	1.700	1.848	2.138
0.000	0.000	0.000	0.000	0.000	0.000	0.000	0.000
0.001	0.000	0.006	0.002	0.010	0.005	0.005	0.033
0.005	0.001	0.000	0.002	0.000	0.000	0.005	0.005
2.444	2.537	2.590	2.551	2.584	2.464	2.419	2.099
1.835	1.854	1.804	1.805	1.827	1.815	1.793	1.842
0.444	0.444	0.412	0.398	0.414	0.434	0.415	0.378
0.256	0.247	0.199	0.182	0.211	0.242	0.225	0.073
15.584	15.605	15.465	15.399	15.509	15.561	15.534	15.394
				93	105		
				8030	8773		
				675	612		
				119	138		
				55	52		
				37	77		
				7.7	4.1		
				32	33		
				4.9	5.1		

24	25
17	10.0
0.198	
104	52
22	24
66	74
9.7	18
52	60
12	14
3.6	2.31
6.6	7.3
0.617	0.649
2.06	2.55
0.201	0.289
0.276	0.445
0.027	0.031
0.078	0.207
0.006	0.017
1.47	1.53
0.753	0.400
4.7	5.9
0.073	1.181
0.021	0.020

SP0003 Amph D 57 rim	SP0003 Amph G 71 core	SP0003 Amph G 72 rim	SP0003 Amph L 82 core	SP0003 Amph L 83 rim	SP0003 Amph M 84 core	SP0003 Amph M 85 rim	SP0003 Amph O 87 core	SP0003 Amph O 88 rim
44.26	45.05	44.78	44.66	45.40	44.38	44.45	44.68	44.85
0.57	0.67	0.57	0.71	0.58	1.18	1.18	0.75	0.57
12.63	11.57	11.78	11.54	11.55	11.16	11.46	10.99	12.13
0.09	0.11	0.14	0.13	0.14	0.08	0.04	0.04	0.00
16.84	17.18	16.75	16.65	16.33	17.44	17.61	16.81	16.79
0.29	0.31	0.24	0.24	0.29	0.26	0.24	0.21	0.27
0.03	0.03	0.02	0.03	0.02	0.00	0.03	0.00	0.00
8.95	9.62	9.48	9.38	9.85	9.52	9.71	9.92	9.64
11.50	11.55	11.46	11.46	11.67	11.22	11.29	11.25	11.47
1.24	1.34	1.19	1.26	1.22	1.58	1.59	1.34	1.29
0.36	0.38	0.34	0.37	0.31	0.35	0.39	0.37	0.38
96.76	97.81	96.75	96.43	97.36	97.17	97.99	96.36	97.39
6.643	6.703	6.714	6.722	6.749	6.666	6.626	6.736	6.681
0.064	0.075	0.064	0.080	0.065	0.133	0.132	0.085	0.064
2.234	2.029	2.082	2.047	2.023	1.976	2.013	1.953	2.129
0.011	0.013	0.017	0.015	0.016	0.010	0.005	0.005	0.000
2.114	2.138	2.100	2.096	2.030	2.191	2.195	2.119	2.091
0.000	0.000	0.000	0.000	0.000	0.000	0.000	0.000	0.000
0.037	0.039	0.030	0.031	0.037	0.033	0.030	0.027	0.034
0.004	0.004	0.002	0.004	0.002	0.000	0.004	0.000	0.000
2.001	2.132	2.117	2.103	2.181	2.130	2.156	2.227	2.138
1.849	1.841	1.841	1.848	1.859	1.806	1.803	1.817	1.831
0.361	0.387	0.346	0.368	0.352	0.460	0.460	0.392	0.373
0.069	0.072	0.065	0.071	0.059	0.067	0.074	0.071	0.072
15.385	15.431	15.378	15.385	15.372	15.471	15.499	15.432	15.413

62	61
5269	5251
449	450
194	204
55	56
51	51
2.51	2.94
30	25
13	13

23	22
0.842	1.10
0.018	
36	36
1.74	2.22
4.1	5.1
0.587	0.752
3.9	4.3
1.33	1.43
0.410	0.500
1.80	1.88
0.330	0.328
2.17	2.35
0.527	0.547
1.57	1.62
0.230	0.253
1.73	1.73
0.262	0.262
1.33	1.28
0.015	0.050
0.843	0.760
0.006	0.035
	0.019

SP0003 Amph P 91 core	SP0003 Amph P 92 rim	SP0003 Amph Q 95 core	SP0003 Amph Q 96 rim	SP0003 Amph R 97 core	SP0003 Amph R 98 rim
44.83	44.99	44.11	45.25	43.89	44.56
1.00	0.79	1.24	0.72	1.18	0.57
11.12	11.87	11.33	11.93	11.40	11.76
0.00	0.03	0.06	0.06	0.03	0.09
16.81	16.55	17.00	16.86	17.01	16.41
0.27	0.23	0.25	0.24	0.26	0.27
0.02	0.03	0.00	0.00	0.03	0.00
9.91	9.52	9.35	9.55	9.56	9.58
11.53	11.55	11.21	11.62	11.36	11.34
1.41	1.33	1.61	1.23	1.41	1.25
0.39	0.34	0.35	0.38	0.38	0.33
97.29	97.23	96.51	97.84	96.51	96.16
6.702	6.706	6.660	6.708	6.631	6.713
0.112	0.089	0.141	0.080	0.134	0.065
1.959	2.085	2.016	2.084	2.030	2.088
0.000	0.004	0.007	0.007	0.004	0.011
2.102	2.063	2.147	2.090	2.149	2.068
0.000	0.000	0.000	0.000	0.000	0.000
0.034	0.029	0.032	0.030	0.033	0.034
0.002	0.004	0.000	0.000	0.004	0.000
2.206	2.113	2.102	2.108	2.151	2.149
1.847	1.845	1.813	1.846	1.839	1.831
0.409	0.384	0.471	0.354	0.413	0.365
0.074	0.065	0.067	0.072	0.073	0.063
15.448	15.386	15.457	15.379	15.461	15.387
				66	65
				4934	5198
				477	457
				240	224
				55	55
				55	57
				2.75	3.2
				26	26
				13	13

19	20
0.730	0.731
0.012	0.022
30	33
1.43	1.36
3.5	3.4
0.479	0.526
3.2	3.3
1.10	1.16
0.366	0.360
1.60	1.72
0.275	0.303
2.07	2.19
0.471	0.500
1.56	1.55
0.187	0.206
1.54	1.59
0.231	0.245
1.09	1.26
0.005	0.015
0.823	0.862
0.007	0.001
0.023	0.001

Online Resource C Compositions of Clinopyroxene in terms of major (EPMA results, in wt%) and trace (

Sample	CB1042	CB1042	CB1042	CB1042	CB1042	CB1042	CB1042	CB1042
Phase	Cpx	Cpx	Cpx	Cpx	Cpx	Cpx	Cpx	Cpx
Site	A	A	D	D	F	F	H	H
Analysis #	123	124	131	132	137	138	141	142
Position	core	rim	core	rim	core	rim	core	rim
SiO_2	51.89	51.98	52.32	52.69	52.26	52.86	52.45	52.42
TiO_2	0.49	0.57	0.50	0.55	0.50	0.34	0.45	0.42
Al_2O_3	4.86	4.57	4.34	4.23	4.66	3.58	4.59	4.07
Cr_2O_3	1.13	1.11	1.03	1.00	1.05	1.19	1.11	1.03
FeO_T	2.38	2.31	2.47	2.00	2.28	1.96	2.39	2.26
MnO	0.07	0.11	0.06	0.10	0.10	0.10	0.09	0.08
NiO	0.06	0.03	0.05	0.00	0.06	0.09	0.06	0.02
MgO	15.63	15.29	15.81	15.93	15.89	16.18	15.58	15.84
CaO	22.33	23.10	22.31	23.19	22.76	22.79	22.88	22.72
Na_2O	0.76	0.72	0.79	0.70	0.65	0.72	0.77	0.72
K_2O	0.00	0.00	0.00	0.00	0.00	0.00	0.00	0.00
Total	99.60	99.79	99.68	100.39	100.21	99.81	100.37	99.58
C.p.f.u.								
Si	1.892	1.896	1.906	1.906	1.895	1.922	1.900	1.912
Ti	0.013	0.016	0.014	0.015	0.014	0.009	0.012	0.012
Al	0.209	0.196	0.186	0.180	0.199	0.153	0.196	0.175
Cr	0.033	0.032	0.030	0.029	0.030	0.034	0.032	0.030
Fe^{2+}	0.072	0.070	0.075	0.060	0.069	0.059	0.070	0.069
Fe^{3+}	0.000	0.000	0.000	0.000	0.000	0.000	0.002	0.000
Mn	0.002	0.003	0.002	0.003	0.003	0.003	0.003	0.002
Ni	0.002	0.001	0.001	0.000	0.002	0.003	0.002	0.001
Mg	0.850	0.831	0.859	0.859	0.859	0.877	0.841	0.861
Ca	0.873	0.903	0.871	0.899	0.884	0.888	0.888	0.888
Na	0.054	0.051	0.056	0.049	0.046	0.051	0.054	0.051
K	0.000	0.000	0.000	0.000	0.000	0.000	0.000	0.000
Cations	4.000	4.000	4.000	4.000	4.000	4.000	4.000	4.000
ppm								
Sc	91	92	98	93	93	97		
Ti	2770	2679	2856	2185	2447	3004		
V	306	297	258	303	287	319		
Cr	7155	7333	7358	7598	6670	7266		
Co	20	22	23	23	22	22		
Ni	288	321	321	311	290	331		

Rb	0.020	0.035	0.228	0.044	0.040	0.204
Sr	7.3	7.6	9.1	7.5	8.0	13
Y	13	14	14	12	12	15
Zr	14	13	13	11	12	13
Nb	0.004	0.002	0.010	0.001	0.010	0.022
Cs	0.020	0.003	0.022	0.023	0.003	0.025
Ba	0.417	0.087		0.374	0.158	
La	0.422	0.429	0.464	0.392	0.449	0.451
Ce	1.63	1.55	1.73	1.34	1.63	1.77
Pr	0.303	0.286	0.296	0.233	0.29	0.291
Nd	2.04	1.80	2.07	1.53	1.94	2.11
Sm	0.841	0.785	0.971	0.708	0.894	0.976
Eu	0.342	0.328	0.368	0.271	0.338	0.344
Gd	1.29	1.42	1.35	1.20	1.36	1.43
Tb	0.271	0.288	0.298	0.280	0.262	0.271
Dy	2.20	2.31	2.36	2.01	2.09	2.38
Ho	0.486	0.569	0.551	0.443	0.509	0.538
Er	1.72	1.60	1.85	1.59	1.51	1.79
Tm	0.257	0.235	0.287	0.233	0.209	0.261
Yb	1.76	1.70	1.78	1.61	1.59	1.97
Lu	0.205	0.231	0.267	0.219	0.202	0.249
Hf	0.617	0.647	0.618	0.540	0.536	0.606
Ta			0.002		0.001	0.001
Pb	0.264	0.276	0.353	0.274	0.310	0.346
Th	0.001	0.001	0.002	0.001	0.002	0.004
U	0.001	0.001	0.001	0.001		0.002

LA-ICP-MS results, in ppm) elements originating from core and rim regions of each rock sample, respect

CB1042 Cpx M 146 core	CB1042 Cpx M 147 rim	CB1042 Cpx S 162 core	CB1042 Cpx S 163 rim	CB1434 Cpx C 160 core	CB1434 Cpx C 161 rim	CB1434 Cpx C 162 core	CB1434 Cpx C 163 rim
52.50	52.18	52.34	52.38	53.11	54.37	53.37	53.48
0.51	0.52	0.45	0.51	0.22	0.10	0.15	0.16
4.66	4.52	4.31	4.34	2.07	1.62	2.41	2.42
0.97	1.07	0.98	1.02	0.14	0.03	0.15	0.11
2.19	2.13	2.46	2.25	8.50	5.55	6.34	5.68
0.06	0.06	0.05	0.14	0.14	0.08	0.18	0.19
0.00	0.00	0.03	0.05	0.05	0.02	0.08	0.00
15.53	15.48	15.39	15.27	16.28	16.15	15.14	15.77
23.12	23.14	23.02	23.33	18.53	21.73	21.37	21.78
0.78	0.75	0.76	0.75	0.49	0.59	0.62	0.47
0.00	0.00	0.01	0.01	0.00	0.02	0.04	0.01
100.32	99.85	99.80	100.05	99.53	100.26	99.85	100.07
1.901	1.899	1.908	1.905	1.964	1.984	1.964	1.959
0.014	0.014	0.012	0.014	0.006	0.003	0.004	0.004
0.199	0.194	0.185	0.186	0.090	0.070	0.105	0.104
0.028	0.031	0.028	0.029	0.004	0.001	0.004	0.003
0.066	0.063	0.074	0.068	0.262	0.169	0.195	0.174
0.000	0.001	0.001	0.000	0.001	0.000	0.000	0.000
0.002	0.002	0.002	0.004	0.004	0.002	0.006	0.006
0.000	0.000	0.001	0.001	0.001	0.001	0.002	0.000
0.838	0.840	0.836	0.828	0.897	0.878	0.831	0.861
0.897	0.902	0.899	0.909	0.734	0.849	0.843	0.855
0.055	0.053	0.054	0.053	0.035	0.042	0.044	0.033
0.000	0.000	0.000	0.000	0.000	0.001	0.002	0.000
3.999	4.000	4.000	4.000	4.000	4.000	4.000	4.000

ively

CB1434 Cpx G 171 core	CB1434 Cpx G 172 rim	CB1434 Cpx L 177 core	CB1434 Cpx P 191 core	CB1434 Cpx P 192 rim	CB1434 Cpx R 197 core	CB1434 Cpx R 198 rim	CB1464 Cpx A 5 core
53.04	53.65	53.46	53.60	53.63	53.63	54.24	53.14
0.22	0.18	0.33	0.26	0.23	0.26	0.18	0.19
2.37	2.12	2.74	2.38	2.18	2.41	2.07	2.12
0.10	0.07	0.04	0.11	0.13	0.16	0.06	0.19
8.34	5.75	6.39	5.99	5.75	5.28	5.04	6.38
0.14	0.15	0.16	0.16	0.09	0.11	0.18	0.16
0.00	0.04	0.05	0.00	0.02	0.00	0.04	0.03
15.78	16.14	15.02	15.61	15.57	16.55	16.68	14.33
18.94	21.02	21.61	21.39	21.87	20.85	21.25	23.11
0.59	0.58	0.67	0.63	0.57	0.59	0.57	0.43
0.00	0.00	0.01	0.01	0.01	0.00	0.02	0.01
99.52	99.70	100.48	100.14	100.05	99.84	100.33	100.09
1.962	1.969	1.956	1.962	1.965	1.960	1.971	1.961
0.006	0.005	0.009	0.007	0.006	0.007	0.005	0.005
0.103	0.092	0.118	0.103	0.094	0.104	0.089	0.092
0.003	0.002	0.001	0.003	0.004	0.005	0.002	0.006
0.258	0.176	0.195	0.183	0.176	0.161	0.153	0.196
0.000	0.001	0.000	0.000	0.000	0.000	0.000	0.001
0.004	0.005	0.005	0.005	0.003	0.003	0.006	0.005
0.000	0.001	0.001	0.000	0.001	0.000	0.001	0.001
0.870	0.883	0.819	0.852	0.851	0.902	0.904	0.788
0.751	0.826	0.847	0.839	0.859	0.816	0.828	0.914
0.042	0.041	0.048	0.045	0.041	0.042	0.040	0.031
0.000	0.000	0.000	0.000	0.000	0.000	0.001	0.000
4.000	4.000	4.000	4.000	4.000	4.000	3.999	4.000

CB1464	CB1464	CB1464	CB1464	CB1464	CB1464	CB1464	CB1464	CB1464
Cpx	Cpx	Cpx	Cpx	Cpx	Cpx	Cpx	Cpx	Cpx
F	F	H	L	L	M	M	M	Q
17	18	23	29	30	31	32	33	41
core	rim	inc in Opx	core	rim	core	core	rim	core
53.11	52.92	52.73	53.16	53.04	53.16	52.72	53.22	53.30
0.22	0.21	0.27	0.22	0.21	0.19	0.34	0.20	0.24
1.99	2.30	1.91	2.16	2.10	2.11	2.48	2.12	2.19
0.15	0.21	0.21	0.24	0.26	0.12	0.16	0.16	0.12
7.24	6.97	7.57	7.13	7.15	7.58	7.17	6.89	6.84
0.19	0.16	0.20	0.24	0.22	0.27	0.21	0.20	0.21
0.00	0.02	0.01	0.05	0.03	0.01	0.01	0.00	0.06
13.94	13.81	13.88	13.77	13.74	13.88	13.69	13.89	13.85
22.78	22.86	22.36	22.80	22.75	22.51	22.78	23.05	22.98
0.46	0.52	0.45	0.54	0.54	0.47	0.51	0.52	0.57
0.00	0.00	0.01	0.00	0.01	0.00	0.00	0.00	0.01
100.08	99.98	99.60	100.31	100.05	100.30	100.07	100.25	100.37
1.966	1.960	1.964	1.964	1.965	1.965	1.952	1.965	1.965
0.006	0.006	0.008	0.006	0.006	0.005	0.009	0.006	0.007
0.087	0.100	0.084	0.094	0.092	0.092	0.108	0.092	0.095
0.004	0.006	0.006	0.007	0.008	0.004	0.005	0.005	0.003
0.224	0.216	0.236	0.220	0.221	0.234	0.222	0.213	0.211
0.000	0.000	0.000	0.000	0.000	0.000	0.000	0.000	0.000
0.006	0.005	0.006	0.008	0.007	0.008	0.007	0.006	0.007
0.000	0.001	0.000	0.001	0.001	0.000	0.000	0.000	0.002
0.769	0.762	0.771	0.758	0.759	0.765	0.756	0.764	0.761
0.903	0.907	0.892	0.902	0.903	0.892	0.904	0.912	0.908
0.033	0.037	0.032	0.039	0.039	0.034	0.037	0.037	0.041
0.000	0.000	0.000	0.000	0.000	0.000	0.000	0.000	0.000
3.999	4.000	4.000	3.999	4.000	3.999	4.000	4.000	4.000
129	129		136	135	133		134	139
1924	1366		1418	1602	1264		1191	1309
609	585		633	650	653		650	649
1054	1056		1095	1108	1162		1163	1092
39	39		39	40	38		39	39
68	66		69	70	67		70	65

0.047	0.044	0.003	0.044	0.007	0.033	0.040
6.2	6.1	6.2	6.3	6.3	6.5	6.0
36	34	33	33	30	30	33
26	23	23	23	22	22	24
0.009	0.006		0.005	0.004		0.003
0.013	0.012		0.016	0.041		0.009
0.101	0.047	0.128	0.057	0.097	0.099	0.105
1.95	1.90	1.75	1.77	1.69	1.65	1.77
8.6	8.4	8.0	8.0	7.6	7.6	7.9
1.64	1.66	1.49	1.62	1.46	1.49	1.56
12	12	11	11	11	11	11
4.6	4.4	4.2	4.3	4.0	4.2	4.4
0.895	0.848	0.857	0.921	0.847	0.847	0.915
5.6	5.3	5.2	5.2	4.9	4.7	5.3
1.03	0.990	0.887	0.992	0.852	0.889	0.959
6.8	6.5	6.4	6.6	5.9	6.1	6.6
1.48	1.40	1.39	1.40	1.31	1.27	1.45
4.2	4.0	4.0	4.1	3.7	3.8	4.2
0.612	0.600	0.538	0.589	0.535	0.511	0.544
4.0	3.8	3.8	3.7	3.5	3.6	3.9
0.516	0.488	0.512	0.485	0.485	0.511	0.535
1.36	1.31	1.30	1.38	1.26	1.39	1.45
0.001	0.001		0.001		0.001	
0.111	0.116	0.121	0.121	0.104	0.111	0.118
0.044	0.016	0.054	0.049	0.063	0.052	0.087
0.011	0.005	0.006	0.014	0.010	0.009	0.013

CB1464	CB1424	CB1424	CB1424	CB1424	CB1424	CB1424	CB1424
Cpx	Cpx	Cpx	Cpx	Cpx	Cpx	Cpx	Cpx
Q	D	D	Q	Q	R	R	S
42	111	112	133	134	138	139	142
rim	core	rim	core	rim	core	rim	core
53.05	52.00	51.58	51.94	52.18	51.71	51.99	51.82
0.20	0.23	0.16	0.19	0.09	0.16	0.17	0.17
2.05	1.88	2.33	1.94	1.97	2.10	2.19	1.86
0.23	0.01	0.00	0.00	0.01	0.01	0.05	0.00
7.62	12.19	11.61	11.77	11.03	11.47	11.48	11.75
0.24	0.38	0.28	0.39	0.25	0.32	0.31	0.32
0.00	0.03	0.04	0.00	0.00	0.00	0.00	0.00
13.77	11.70	11.66	11.54	12.07	11.52	11.42	11.44
22.59	21.24	21.70	21.78	22.15	22.15	21.89	21.78
0.49	0.37	0.40	0.33	0.43	0.44	0.44	0.42
0.02	0.00	0.00	0.00	0.00	0.00	0.00	0.01
100.26	100.03	99.76	99.88	100.18	99.88	99.94	99.57
1.963	1.965	1.949	1.965	1.958	1.953	1.963	1.966
0.006	0.007	0.005	0.005	0.003	0.005	0.005	0.005
0.089	0.084	0.104	0.086	0.087	0.093	0.097	0.083
0.007	0.000	0.000	0.000	0.000	0.000	0.001	0.000
0.234	0.385	0.349	0.372	0.324	0.338	0.362	0.365
0.002	0.000	0.017	0.000	0.022	0.024	0.000	0.007
0.008	0.012	0.009	0.012	0.008	0.010	0.010	0.010
0.000	0.001	0.001	0.000	0.000	0.000	0.000	0.000
0.760	0.659	0.657	0.651	0.675	0.648	0.643	0.647
0.896	0.860	0.879	0.883	0.891	0.896	0.885	0.885
0.035	0.027	0.029	0.024	0.031	0.032	0.032	0.031
0.001	0.000	0.000	0.000	0.000	0.000	0.000	0.000
4.000	4.000	4.000	3.999	4.000	4.000	3.999	4.000
137			101	94	115	109	
1092			888	972	1124	943	
628			476	398	497	459	
1065			104	94	128	127	
35			45	42	48	47	
58			11	10	12	11	

		0.173		0.001
5.4	12	11	13	13
29	5.0	4.1	5.1	4.9
23	23	27	29	25
0.003	0.010	0.058	0.007	0.012
		0.002		
0.161	0.087		0.002	0.03
1.80	2.16	1.98	2.67	2.54
7.3	7.2	6.2	8.1	7.5
1.43	0.982	0.858	1.05	1.06
9.9	4.9	4.2	5.1	4.8
3.7	0.998	0.919	1.10	1.08
0.846	0.663	0.633	0.677	0.646
4.7	0.886	0.768	0.988	0.824
0.822	0.149	0.120	0.163	0.110
5.6	0.989	0.871	0.920	0.944
1.15	0.207	0.194	0.203	0.182
3.6	0.604	0.561	0.739	0.656
0.530	0.109	0.100	0.123	0.127
3.2	0.937	0.810	1.09	1.07
0.484	0.158	0.133	0.169	0.169
1.38	0.758	0.884	1.01	0.838
0.001	0.003	0.006	0.005	0.004
0.108	0.282	0.306	0.300	0.312
0.118	0.053	0.124	0.055	0.060
0.019	0.008	0.013	0.009	0.011

CB1424		CB1414	CB1414	CB1414	CB1414	CB1414	CB1414	CB1414
Cpx		Cpx	Cpx	Cpx	Cpx	Cpx	Cpx	Cpx
S		B	C	C	D	D	F	N
143		78	81	82	85	86	91	108
rim		core	core	rim	core	rim	rim	core
52.03		53.56	53.83	53.68	53.63	53.76	53.31	53.22
0.15		0.04	0.12	0.14	0.22	0.17	0.12	0.21
2.43		1.42	1.44	1.61	1.57	1.52	1.59	1.72
0.06		0.27	0.35	0.33	0.35	0.28	0.30	0.35
11.14		6.76	7.13	6.20	6.27	5.90	6.19	6.54
0.30		0.25	0.22	0.19	0.17	0.16	0.18	0.16
0.00		0.00	0.00	0.05	0.00	0.01	0.00	0.03
11.57		15.20	15.44	15.14	15.16	15.21	15.08	15.29
22.07		22.40	21.50	22.65	22.56	23.13	22.69	21.81
0.50		0.26	0.45	0.39	0.41	0.36	0.32	0.38
0.00		0.00	0.01	0.01	0.00	0.00	0.00	0.01
100.25	0.00	100.16	100.49	100.39	100.34	100.50	99.78	99.72
1.954		1.974	1.976	1.971	1.970	1.970	1.970	1.967
0.004		0.001	0.003	0.004	0.006	0.005	0.003	0.006
0.108		0.062	0.062	0.070	0.068	0.066	0.069	0.075
0.002		0.008	0.010	0.010	0.010	0.008	0.009	0.010
0.340		0.208	0.217	0.190	0.193	0.179	0.191	0.202
0.010		0.000	0.002	0.000	0.000	0.002	0.000	0.000
0.010		0.008	0.007	0.006	0.005	0.005	0.006	0.005
0.000		0.000	0.000	0.001	0.000	0.000	0.000	0.001
0.648		0.835	0.845	0.829	0.830	0.831	0.831	0.842
0.888		0.885	0.846	0.891	0.888	0.908	0.898	0.863
0.036		0.019	0.032	0.028	0.029	0.026	0.023	0.027
0.000		0.000	0.000	0.000	0.000	0.000	0.000	0.000
4.000		3.999	4.000	4.000	3.999	4.000	4.000	3.999
							119	114
							3039	1681
							761	666
							2230	2064
							42	32
							68	57

0.003	0.005
6.7	6.5
16	15
27	33
0.433	0.225
0.001	0.025
0.132	0.069
2.33	2.34
9.1	8.9
1.48	1.52
8.9	8.3
2.62	2.42
0.315	0.333
2.93	2.68
0.472	0.488
3.2	3.1
0.66	0.634
1.95	1.95
0.254	0.297
1.95	2.07
0.263	0.268
1.39	1.51
0.018	0.014
0.335	0.333
0.316	0.194
0.031	0.032

CB1414	CB1414	CB1414	CB1475	CB1475	CB1475	CB1475	CB1475
Cpx	Cpx	Cpx	Cpx	Cpx	Cpx	Cpx	Cpx
N	O	O	B	B	B	B	C
109	110	111	58	59	60	61	62
rim	core	rim	core	rim	core	rim	core
53.30	53.44	53.33	52.70	53.29	52.74	53.18	53.04
0.16	0.17	0.20	0.11	0.13	0.23	0.25	0.13
1.83	1.74	1.50	1.46	1.36	1.52	1.39	1.49
0.31	0.41	0.30	0.03	0.05	0.00	0.02	0.07
5.77	6.01	6.31	9.27	7.93	7.75	8.77	7.90
0.14	0.21	0.17	0.25	0.21	0.26	0.25	0.24
0.02	0.00	0.00	0.06	0.02	0.04	0.00	0.07
15.14	15.09	15.23	14.21	13.75	13.62	14.04	13.88
22.60	22.68	22.38	21.21	23.21	23.08	22.05	22.99
0.44	0.39	0.34	0.27	0.31	0.35	0.40	0.39
0.00	0.00	0.01	0.02	0.00	0.00	0.00	0.00
99.71	100.14	99.77	99.59	100.26	99.59	100.35	100.20
1.966	1.966	1.970	1.970	1.977	1.969	1.971	1.966
0.004	0.005	0.006	0.003	0.004	0.006	0.007	0.004
0.080	0.075	0.065	0.064	0.059	0.067	0.061	0.065
0.009	0.012	0.009	0.001	0.001	0.000	0.001	0.002
0.177	0.185	0.195	0.281	0.246	0.234	0.261	0.224
0.001	0.000	0.000	0.009	0.000	0.008	0.011	0.021
0.004	0.007	0.005	0.008	0.007	0.008	0.008	0.008
0.001	0.000	0.000	0.002	0.001	0.001	0.000	0.002
0.833	0.828	0.839	0.792	0.760	0.758	0.776	0.767
0.893	0.894	0.886	0.850	0.923	0.923	0.876	0.913
0.031	0.028	0.024	0.020	0.022	0.025	0.029	0.028
0.000	0.000	0.000	0.001	0.000	0.000	0.000	0.000
4.000	3.999	4.000	4.000	4.000	4.000	4.000	4.000
116	112	117	146	150	149	147	
1163	783	1024	821	894	836	766	
651	624	642	649	691	674	658	
2057	2680	2559	223	237	217	232	
33	33	33	42	42	40	41	
58	56	56	34	35	33	33	

0.026	0.019		0.006	0.005	0.014	0.020
6.8	6.4	6.7	7.5	8.3	7.6	7.8
16	12	16	54	55	51	49
30	23	29	25	26	23	24
0.003	0.001	0.011	0.014	0.007	0.013	0.010
			0.012			
0.061	0.122	0.053	0.044	0.024	0.041	0.244
2.34	2.10	2.45	3.8	4.4	4.2	3.9
9.2	7.6	9.5	18	20	19	18
1.52	1.21	1.52	3.9	4.1	3.7	3.5
8.6	7.2	8.3	27	27	26	24
2.70	2.20	2.76	9.2	9.9	9.0	8.6
0.315	0.265	0.368	0.730	0.728	0.772	0.687
3.0	2.14	2.77	10	10	9.6	8.8
0.545	0.412	0.542	1.76	1.72	1.54	1.50
3.3	2.52	3.2	11	11	11	10
0.662	0.581	0.691	2.23	2.12	2.01	2.01
2.04	1.54	1.95	6.3	6.6	6.4	5.9
0.297	0.225	0.292	0.894	0.871	0.836	0.766
1.94	1.69	2.17	6.0	6.2	5.9	5.5
0.271	0.228	0.282	0.73	0.798	0.783	0.723
1.48	1.19	1.49	1.38	1.54	1.56	1.37
		0.001	0.002	0.002	0.003	0.003
0.339	0.329	0.322	0.359	0.380	0.310	0.334
0.061	0.226	0.081	0.070	0.062	0.079	0.094
0.009	0.017	0.011	0.022	0.008	0.009	0.012

CB1475 Cpx C 63 rim	CB1475 Cpx D 64 core	CB1475 Cpx D 65 rim	CB1475 Cpx E 68 core	CB1475 Cpx E 69 rim	CB1475 Cpx G 76 core	CB1475 Cpx G 77 rim	CB1475 Cpx G 79 core	CB1475 Cpx G 80 rim
53.04	53.19	53.70	53.18	53.20	53.20	53.19	53.11	53.06
0.17	0.10	0.04	0.06	0.13	0.08	0.07	0.16	0.16
1.49	1.32	1.25	1.14	1.18	0.99	1.05	1.45	1.50
0.00	0.03	0.02	0.05	0.03	0.00	0.06	0.06	0.02
7.87	7.30	7.33	8.00	7.50	8.96	7.81	8.72	7.67
0.22	0.25	0.24	0.26	0.18	0.20	0.26	0.31	0.20
0.02	0.00	0.00	0.00	0.00	0.07	0.00	0.00	0.01
13.82	13.98	14.13	13.93	14.03	14.12	14.07	13.86	13.68
22.95	23.12	23.14	22.56	22.96	22.05	22.89	22.07	23.06
0.34	0.35	0.41	0.35	0.35	0.33	0.29	0.42	0.39
0.00	0.00	0.00	0.00	0.00	0.00	0.00	0.00	0.01
99.92	99.64	100.26	99.53	99.56	100.00	99.69	100.16	99.76
1.972	1.980	1.985	1.985	1.983	1.980	1.982	1.973	1.976
0.005	0.003	0.001	0.002	0.004	0.002	0.002	0.004	0.004
0.065	0.058	0.054	0.050	0.052	0.043	0.046	0.063	0.066
0.000	0.001	0.001	0.001	0.001	0.000	0.002	0.002	0.001
0.240	0.226	0.225	0.250	0.234	0.264	0.238	0.261	0.237
0.005	0.001	0.002	0.000	0.000	0.015	0.005	0.010	0.002
0.007	0.008	0.008	0.008	0.006	0.006	0.008	0.010	0.006
0.001	0.000	0.000	0.000	0.000	0.002	0.000	0.000	0.000
0.766	0.776	0.779	0.775	0.779	0.784	0.782	0.768	0.759
0.914	0.922	0.917	0.902	0.917	0.879	0.914	0.879	0.920
0.025	0.025	0.029	0.025	0.025	0.024	0.021	0.030	0.028
0.000	0.000	0.000	0.000	0.000	0.000	0.000	0.000	0.000
4.000	4.000	4.000	4.000	4.000	4.000	4.000	4.000	4.000

145
797
632
216
39
30

0.037
11
44
23
0.034
0.011
2.96
4.3
18
3.4
23
7.8
0.788
8.1
1.35
9.0
1.77
5.5
0.757
5.5
0.731
1.37
0.001
0.510
0.162
0.019

CB1475 Cpx G 81 core	CB1475 Cpx G 82 rim	CB1475 Cpx I 85 core	CB1475 Cpx I 86 rim	SP0003 Cpx A 45 core	SP0003 Cpx A 46 rim	SP0003 Cpx B 49 core	SP0003 Cpx B 50 rim
53.06	53.60	53.13	53.31	52.07	52.31	52.23	52.18
0.17	0.10	0.12	0.14	0.22	0.10	0.16	0.11
1.08	1.29	1.31	1.36	1.44	1.26	1.50	1.39
0.00	0.02	0.03	0.04	0.06	0.02	0.00	0.02
8.08	7.13	8.60	7.66	12.11	11.81	12.11	11.64
0.20	0.17	0.25	0.23	0.33	0.40	0.35	0.34
0.00	0.04	0.00	0.00	0.06	0.00	0.03	0.02
13.89	14.55	14.16	14.20	10.77	11.11	10.85	10.89
22.97	23.15	21.93	23.07	22.72	22.95	22.81	23.17
0.25	0.27	0.37	0.39	0.33	0.29	0.33	0.29
0.00	0.00	0.02	0.01	0.00	0.00	0.00	0.00
99.70	100.32	99.92	100.41	100.11	100.25	100.37	100.05
1.980	1.978	1.976	1.969	1.974	1.977	1.974	1.977
0.005	0.003	0.003	0.004	0.006	0.003	0.005	0.003
0.047	0.056	0.057	0.059	0.064	0.056	0.067	0.062
0.000	0.001	0.001	0.001	0.002	0.001	0.000	0.001
0.251	0.220	0.257	0.214	0.384	0.369	0.383	0.369
0.001	0.000	0.010	0.023	0.000	0.004	0.000	0.000
0.006	0.005	0.008	0.007	0.011	0.013	0.011	0.011
0.000	0.001	0.000	0.000	0.002	0.000	0.001	0.001
0.773	0.801	0.785	0.782	0.609	0.626	0.611	0.615
0.918	0.916	0.874	0.913	0.923	0.930	0.924	0.940
0.018	0.019	0.027	0.028	0.024	0.021	0.024	0.021
0.000	0.000	0.001	0.000	0.000	0.000	0.000	0.000
4.000	4.000	4.000	4.000	3.999	4.000	4.000	3.999
						60	64
						761	954
						227	248
						222	295
						43	48
						61	68

4.8	11
14	15
1.63	2.30
10	15
0.006	0.007
0.005	0.117
0.202	0.206
0.379	0.491
0.808	1.08
0.117	0.151
0.620	0.854
0.123	0.234
0.071	0.088
0.240	0.350
0.040	0.062
0.250	0.412
0.055	0.087
0.198	0.251
0.017	0.040
0.186	0.372
0.051	0.069
0.519	0.703
0.002	0.005
0.427	0.279
	0.003

SP0003 Cpx F 63 core	SP0003 Cpx F 64 rim	SP0003 Cpx F 65 core	SP0003 Cpx F 66 rim	SP0003 Cpx I 76 core	SP0003 Cpx I 77 rim	SP0003 Cpx L 80 core	SP0003 Cpx L 81 rim
52.23	51.83	52.38	52.37	51.81	52.45	52.01	52.02
0.14	0.15	0.06	0.09	0.22	0.08	0.19	0.10
1.58	1.77	1.55	1.19	1.71	1.13	1.71	1.31
0.00	0.05	0.01	0.02	0.01	0.00	0.00	0.03
11.97	11.71	11.99	11.60	11.84	11.15	12.00	11.76
0.35	0.35	0.38	0.40	0.36	0.41	0.46	0.47
0.08	0.02	0.03	0.00	0.00	0.00	0.00	0.03
10.80	10.81	10.76	11.17	10.82	11.25	10.89	10.94
22.74	22.85	22.94	23.17	22.64	23.17	22.96	22.80
0.40	0.33	0.36	0.27	0.37	0.31	0.27	0.32
0.00	0.00	0.00	0.00	0.00	0.00	0.01	0.00
100.29	99.87	100.46	100.28	99.78	99.95	100.50	99.78
1.974	1.967	1.977	1.978	1.968	1.984	1.963	1.976
0.004	0.004	0.002	0.003	0.006	0.002	0.005	0.003
0.070	0.079	0.069	0.053	0.077	0.050	0.076	0.059
0.000	0.002	0.000	0.001	0.000	0.000	0.000	0.001
0.376	0.370	0.379	0.362	0.374	0.353	0.372	0.368
0.002	0.002	0.000	0.005	0.002	0.000	0.007	0.005
0.011	0.011	0.012	0.013	0.012	0.013	0.015	0.015
0.002	0.001	0.001	0.000	0.000	0.000	0.000	0.001
0.609	0.612	0.606	0.629	0.613	0.635	0.613	0.620
0.921	0.929	0.928	0.938	0.921	0.939	0.929	0.928
0.029	0.024	0.026	0.020	0.027	0.023	0.020	0.024
0.000	0.000	0.000	0.000	0.000	0.000	0.000	0.000
4.000	4.000	4.000	4.000	4.000	4.000	4.000	4.000

Online Resource C Compositions of Garnet in terms of major (EPMA results, in wt%) and trace (LA-ICP-M

Sample	CB1060	CB1060	CB1060	CB1060	CB1060	CB1060	CB1482
Phase	Grt	Grt	Grt	Grt	Grt	Grt	Grt
Site	A	N	N	P	P	Q	B
Analysis #	165	195	196	206	207	208	214
Position	rim	core	rim	core	rim	core	core
SiO_2	38.05	38.23	38.34	38.06	38.33	38.19	38.24
TiO_2	0.00	0.02	0.02	0.00	0.09	0.07	0.13
Al_2O_3	21.52	21.61	21.65	20.80	21.14	21.42	21.67
Cr_2O_3	0.04	0.02	0.00	0.00	0.03	0.00	0.00
FeO_T	28.81	28.68	28.87	29.08	28.42	28.78	27.53
MnO	1.06	0.98	0.94	1.24	1.22	1.25	0.98
NiO	0.00	0.06	0.00	0.06	0.00	0.00	0.00
MgO	5.37	5.50	5.13	5.58	5.53	5.51	4.79
CaO	4.69	4.92	5.39	4.83	5.57	4.68	6.84
Total	99.54	100.02	100.34	99.65	100.33	99.90	100.18
C.p.f.u.							
Si	3.000	2.997	3.000	3.000	2.996	3.000	2.993
Ti	0.000	0.001	0.001	0.000	0.005	0.004	0.008
Al	2.000	1.996	1.997	1.932	1.947	1.983	1.999
Cr	0.002	0.001	0.000	0.000	0.002	0.000	0.000
Fe^{3+}	0.000	0.007	0.001	0.067	0.048	0.009	0.000
Fe^{2+}	1.899	1.873	1.889	1.850	1.810	1.882	1.802
Mn	0.071	0.065	0.062	0.083	0.081	0.083	0.065
Ni	0.000	0.004	0.000	0.004	0.000	0.000	0.000
Mg	0.631	0.643	0.598	0.656	0.644	0.645	0.559
Ca	0.396	0.413	0.452	0.408	0.466	0.394	0.574
Cations	7.999	8.000	8.000	8.000	8.000	8.000	8.000
ppm							
Sc	61	51	66			48	73
Ti	592	152	40			168	1075
V	58	59	89			81	146
Cr	140	117	145			138	39
Co	33	33	33			31	30
Ni	0.484	0.165	0.490			0.096	0.508
Rb			0.125			0.051	0.336
Sr	0.027	0.014	1.08			0.021	0.135
Y	25	33	15			27	28
Zr	2.13	3.5	1.66			4.6	17
Nb	0.047	0.003	0.003			0.028	0.083
Cs							0.003
Ba	0.011	0.008	0.398			0.091	0.942
La	0.003	0.094	0.294			0.005	0.328

Ce	0.012	0.087	0.236	0.028	0.493
Pr	0.004	0.016	0.076	0.018	0.076
Nd	0.101	0.228	0.330	0.342	0.795
Sm	0.358	0.624	0.257	0.877	1.06
Eu	0.360	0.618	0.242	0.720	1.15
Gd	1.74	2.46	1.30	2.94	2.26
Tb	0.411	0.627	0.337	0.587	0.513
Dy	3.9	5.2	2.77	3.8	4.7
Ho	0.914	1.29	0.620	0.837	1.17
Er	2.92	4.4	1.86	2.59	4.0
Tm	0.396	0.638	0.250	0.328	0.692
Yb	2.88	4.4	1.96	2.77	5.9
Lu	0.386	0.628	0.253	0.375	0.855
Hf	0.035	0.040	0.036	0.096	0.251
Ta	0.001	0.001	0.001	0.001	0.006
Pb	0.024	0.023	0.060	0.100	0.058
Th		0.001		0.059	0.035
U	0.002	0.003	0.006	0.003	0.022

ʃS results, in ppm) elements originating from core and rim regions of each rock sample, respectively

CB1482 Grt B 215 rim	CB1482 Grt C 211 core	CB1482 Grt C 212 rim	CB1482 Grt C 218 core	CB1482 Grt C 219 rim	CB1482 Grt F 222 core	CB1482 Grt F 223 rim	CB1482 Grt F 228 core	CB1482 Grt F 229 rim
38.12	38.24	38.26	38.02	38.10	38.48	38.13	38.08	38.33
0.10	0.05	0.07	0.09	0.05	0.00	0.01	0.07	0.08
21.67	21.52	21.64	21.43	21.57	21.64	21.58	21.58	21.75
0.00	0.04	0.01	0.00	0.00	0.06	0.00	0.02	0.00
27.66	27.74	27.40	27.63	27.60	27.57	28.06	28.25	27.64
0.82	0.86	0.85	0.74	0.77	0.74	0.66	0.86	0.79
0.00	0.00	0.00	0.05	0.00	0.00	0.02	0.00	0.00
4.76	4.70	4.89	4.62	4.68	5.07	4.39	4.75	5.04
6.87	6.87	6.89	6.88	6.91	6.85	7.00	6.53	6.55
100.00	100.02	100.01	99.46	99.68	100.41	99.85	100.14	100.18
2.989	3.000	2.997	3.000	2.998	3.000	3.000	2.986	2.996
0.006	0.003	0.004	0.005	0.003	0.000	0.001	0.004	0.005
2.003	1.990	1.998	1.993	2.000	1.988	2.001	1.995	2.003
0.000	0.002	0.001	0.000	0.000	0.004	0.000	0.001	0.000
0.007	0.001	0.000	0.000	0.000	0.008	0.000	0.023	0.000
1.807	1.819	1.795	1.823	1.816	1.790	1.846	1.829	1.806
0.054	0.057	0.056	0.049	0.051	0.049	0.044	0.057	0.052
0.000	0.000	0.000	0.003	0.000	0.000	0.001	0.000	0.000
0.556	0.550	0.571	0.543	0.549	0.589	0.515	0.555	0.587
0.577	0.577	0.578	0.582	0.582	0.572	0.590	0.549	0.548
8.000	8.000	8.000	7.999	7.999	8.000	7.999	8.000	7.998
84			54	84	102	85	97	94
1071			578	315	197	224	252	220
261			135	113	139	124	127	82
64			60	50	179	132	66	88
26			29	28	29	29	29	28
0.062			0.215	0.587	0.568	0.485	0.537	0.719
0.008			0.213		0.164	0.051		1.048
0.151			0.124	0.028	0.122	0.017	0.009	0.03
54			49	46	33	24	52	51
18			9.9	3.9	2.65	3.4	3.6	3.1
0.343			0.147	0.002	0.014	0.003	0.005	0.004
			0.104		0.024		0.004	0.014
0.232			1.39	0.105	0.352	0.060	0.222	2.01
0.011			0.094	0.035	0.043	0.018	0.010	0.004

0.138	0.240	0.127	0.179	0.140	0.095	0.098
0.154	0.078	0.050	0.052	0.064	0.050	0.052
1.80	1.02	0.795	0.935	1.20	0.818	0.736
3.5	1.92	1.18	1.75	1.71	1.38	1.10
1.39	1.21	0.996	0.837	1.07	0.784	0.759
6.4	5.2	2.92	5.5	4.9	3.3	3.3
1.33	1.14	0.781	1.47	1.03	0.874	0.871
10.0	8.6	6.8	12	5.8	7.5	7.9
2.02	1.88	1.86	3.2	0.960	2.18	2.08
6.2	5.5	6.8	9.2	1.94	7.6	7.3
0.898	0.781	1.21	1.14	0.202	1.21	1.06
6.6	5.7	6.2	7.5	1.07	10	8.2
0.833	0.749	1.44	1.05	0.103	1.62	1.22
0.385	0.167	0.058	0.052	0.068	0.055	0.054
0.018	0.007		0.002			
0.443	0.040	0.005	0.031	0.015	0.014	0.032
0.398	0.002	0.008		0.007		0.001
0.203	0.006	0.003	0.005	0.004	0.002	

CB1482 Grt G 224 core	CB1482 Grt G 225 rim	CB1482 Grt G 232 core	CB1482 Grt G 233 rim	CB1482 Grt L 242 core	CB1482 Grt L 243 rim	CB1482 Grt M 241 core	CB1482 Grt M 242 rim	CB1482 Grt O 254 core
38.25	38.16	38.30	38.28	38.29	38.31	38.23	37.95	38.38
0.04	0.07	0.06	0.02	0.03	0.01	0.00	0.00	0.18
21.61	21.54	21.62	21.71	21.53	21.59	21.67	21.50	21.45
0.00	0.04	0.05	0.00	0.02	0.03	0.00	0.03	0.11
27.92	27.43	27.54	28.17	27.93	27.84	27.61	28.19	27.76
0.84	0.83	0.93	0.92	0.85	0.84	0.79	0.71	0.90
0.01	0.00	0.00	0.00	0.01	0.10	0.00	0.03	0.00
4.67	4.75	4.99	4.56	4.75	4.74	4.63	4.33	4.71
6.80	6.98	6.61	6.70	6.83	6.93	6.97	6.89	6.96
100.14	99.80	100.10	100.36	100.24	100.39	99.90	99.63	100.45
2.998	2.998	2.998	2.997	2.998	2.994	3.000	2.996	3.000
0.002	0.004	0.004	0.001	0.002	0.001	0.000	0.000	0.011
1.996	1.994	1.994	2.003	1.987	1.989	2.004	2.000	1.976
0.000	0.002	0.003	0.000	0.001	0.002	0.000	0.002	0.007
0.003	0.000	0.000	0.001	0.013	0.019	0.000	0.007	0.000
1.827	1.802	1.803	1.843	1.815	1.800	1.812	1.854	1.814
0.056	0.055	0.062	0.061	0.056	0.056	0.053	0.047	0.060
0.001	0.000	0.000	0.000	0.001	0.006	0.000	0.002	0.000
0.546	0.556	0.582	0.532	0.554	0.552	0.542	0.510	0.549
0.571	0.587	0.554	0.562	0.573	0.580	0.586	0.583	0.583
8.000	8.000	8.000	8.000	8.000	8.000	7.997	8.000	7.998

93	87
244	212
112	100
89	71
28	28
0.335	0.245
0.603	0.035
0.066	0.058
71	41
4.1	2.90
0.008	0.002
0.017	0.004
0.012	0.028
0.050	0.021

0.203	0.124
0.076	0.064
1.000	0.804
1.53	1.35
1.02	1.01
3.6	3.2
1.07	0.864
9.8	7.0
2.77	1.61
11	5.2
1.90	0.783
16	5.3
2.37	0.674
0.087	0.050
0.001	
0.034	0.025
0.001	0.003
0.004	0.003

CB1482 Grt O 255 rim	CB1482 Grt O 258 core	CB1482 Grt O 259 rim	CB1482 Grt P 251 core	CB1482 Grt P 252 rim
38.15	37.88	38.27	38.06	38.24
0.15	0.01	0.17	0.01	0.01
21.66	21.73	21.42	21.61	21.66
0.00	0.00	0.05	0.03	0.00
27.65	27.63	27.40	27.38	28.01
0.88	0.89	0.99	0.81	0.72
0.00	0.00	0.00	0.04	0.06
4.84	4.27	4.69	4.75	4.43
6.77	7.08	7.10	6.91	7.10
100.10	99.49	100.09	99.60	100.23
2.988	2.990	3.000	2.995	2.997
0.009	0.001	0.010	0.001	0.001
2.000	2.022	1.979	2.004	2.001
0.000	0.000	0.003	0.002	0.000
0.006	0.000	0.000	0.003	0.004
1.805	1.824	1.796	1.799	1.832
0.058	0.060	0.066	0.054	0.048
0.000	0.000	0.000	0.003	0.004
0.565	0.503	0.548	0.557	0.518
0.568	0.599	0.596	0.583	0.596
8.000	7.998	7.999	8.000	8.000

Online Resource C Compositions of Ilmenite in terms of major (EPMA results, in wt%) elements origina

Sample	CB1434	CB1434	CB1434	CB1434	CB1464	CB1464	CB1464
Phase	Ilm	Ilm	Ilm	Ilm	Ilm	Ilm	Ilm
Site	B	E	I	I	C	C	H
Analysis #	159	168	175	176	8	9	26
Position	core	core	core	rim	core	rim	core
SiO_2	0.00	0.04	0.03	0.03	0.01	0.08	0.12
TiO_2	53.39	53.40	53.23	53.85	53.27	53.50	53.17
Al_2O_3	0.04	0.23	0.02	0.01	0.00	0.00	0.00
Cr_2O_3	0.05	0.11	0.18	0.16	0.23	0.38	0.28
FeO_T	43.23	43.48	43.58	43.43	43.62	43.31	43.94
MnO	0.49	0.46	0.49	0.51	0.55	0.53	0.39
NiO	0.00	0.08	0.07	0.03	0.09	0.07	0.00
MgO	2.25	2.11	2.05	2.32	2.07	2.26	2.03
CaO	0.03	0.00	0.01	0.05	0.04	0.18	0.05
Na_2O	0.04	0.06	0.02	0.05	0.00	0.00	0.00
K_2O	0.00	0.00	0.00	0.01	0.00	0.00	0.00
Total	99.52	99.97	99.68	100.45	99.88	100.31	99.98
C.p.f.u.							
Si	0.000	0.001	0.001	0.001	0.000	0.002	0.003
Ti	1.000	0.996	0.998	0.999	0.997	0.995	0.994
Al	0.001	0.007	0.001	0.000	0.000	0.000	0.000
Fe2+ all fer	0.900	0.902	0.908	0.896	0.908	0.895	0.913
Mn	0.010	0.010	0.010	0.011	0.012	0.011	0.008
Mg	0.084	0.078	0.076	0.085	0.077	0.083	0.075
Ca	0.001	0.000	0.000	0.001	0.001	0.005	0.001
Na	0.002	0.003	0.001	0.002	0.000	0.000	0.000
K	0.000	0.000	0.000	0.000	0.000	0.000	0.000
Cr	0.001	0.002	0.004	0.003	0.005	0.007	0.006
Ni	0.000	0.002	0.001	0.001	0.002	0.001	0.000
Cations	2.000	2.000	2.000	2.000	2.001	2.000	2.000

ting from core and rim regions of each rock sample, respectively

CB1424	CB1424	CB1424	CB1424	CB1424	CB1424	CB1424
Ilm	Ilm	Ilm	Ilm	Ilm	Ilm	Ilm
B	B	T	T	U	U	V
103	104	145	146	149	150	151
core	rim	core	rim	core	rim	core
0.03	0.04	0.00	0.02	0.00	0.00	0.02
53.20	52.90	52.89	52.77	52.95	52.56	53.03
0.00	0.00	0.00	0.00	0.00	0.00	0.00
0.04	0.06	0.00	0.04	0.09	0.13	0.04
45.63	45.58	45.76	45.72	45.85	45.38	45.62
0.63	0.57	0.65	0.63	0.53	0.68	0.65
0.04	0.06	0.09	0.00	0.00	0.05	0.01
0.85	0.67	0.62	0.56	0.65	0.69	0.69
0.04	0.10	0.00	0.14	0.02	0.09	0.03
0.00	0.00	0.00	0.00	0.00	0.00	0.00
0.00	0.00	0.00	0.00	0.00	0.00	0.00
100.46	99.98	100.01	99.88	100.09	99.58	100.09
0.001	0.001	0.000	0.001	0.000	0.000	0.001
0.999	0.999	1.000	0.999	0.999	0.997	1.000
0.000	0.000	0.000	0.000	0.000	0.000	0.000
0.953	0.957	0.962	0.962	0.962	0.957	0.957
0.013	0.012	0.014	0.013	0.011	0.015	0.014
0.032	0.025	0.023	0.021	0.024	0.026	0.026
0.001	0.003	0.000	0.004	0.001	0.002	0.001
0.000	0.000	0.000	0.000	0.000	0.000	0.000
0.000	0.000	0.000	0.000	0.000	0.000	0.000
0.001	0.001	0.000	0.001	0.002	0.003	0.001
0.001	0.001	0.002	0.000	0.000	0.001	0.000
2.000	1.999	2.000	2.000	2.000	2.001	1.999

CB1414	CB1060	CB1475	CB1475	CB1482	CB1482
Ilm	Ilm	Ilm	Ilm	Ilm	Ilm
F	E	G	M	A	A
93	177	78	91	205	206
core	core	core	core	core	rim
0.00	0.01	0.00	0.00	0.02	0.03
53.30	52.78	53.52	53.50	53.06	53.00
0.00	0.03	0.00	0.02	0.01	0.00
0.23	0.00	0.07	0.10	0.00	0.01
43.26	45.49	44.57	44.57	46.72	46.64
0.62	0.28	0.51	0.62	0.28	0.26
0.06	0.00	0.00	0.00	0.00	0.00
2.15	0.94	1.73	1.67	0.39	0.39
0.10	0.04	0.00	0.00	0.00	0.02
0.00	0.00	0.00	0.00	0.00	0.00
0.00	0.00	0.00	0.00	0.00	0.00
99.72	99.57	100.40	100.48	100.48	100.35
0.000	0.000	0.000	0.000	0.001	0.001
0.998	0.999	0.999	0.998	1.000	1.000
0.000	0.001	0.000	0.001	0.000	0.000
0.901	0.957	0.925	0.925	0.979	0.978
0.013	0.006	0.011	0.013	0.006	0.006
0.080	0.035	0.064	0.062	0.015	0.015
0.003	0.001	0.000	0.000	0.000	0.001
0.000	0.000	0.000	0.000	0.000	0.000
0.000	0.000	0.000	0.000	0.000	0.000
0.005	0.000	0.001	0.002	0.000	0.000
0.001	0.000	0.000	0.000	0.000	0.000
2.000	2.000	2.000	2.000	2.000	1.999

CB1482	CB1482	CB1482	CB1482	CB1482	CB1482	SP30003
Ilm	Ilm	Ilm	Ilm	Ilm	Ilm	Ilm
G	G	I	I	P	P	B
226	227	235	236	257	258	53
core	rim	core	rim	core	rim	core
0.00	0.02	0.04	0.03	0.05	0.01	0.04
52.84	52.74	52.47	52.93	52.79	52.83	52.82
0.02	0.01	0.01	0.02	0.00	0.02	0.00
0.05	0.01	0.07	0.02	0.06	0.04	0.01
46.67	46.72	46.35	46.71	46.60	46.65	44.14
0.27	0.20	0.23	0.29	0.25	0.26	1.66
0.00	0.00	0.00	0.00	0.00	0.00	0.02
0.32	0.27	0.38	0.33	0.35	0.33	0.61
0.00	0.03	0.00	0.03	0.02	0.06	0.49
0.00	0.00	0.00	0.00	0.00	0.00	0.00
0.00	0.00	0.00	0.00	0.00	0.00	0.00
100.17	100.00	99.55	100.36	100.12	100.20	99.79
0.000	0.001	0.001	0.001	0.001	0.000	0.001
0.999	0.999	0.998	0.999	0.998	0.999	0.999
0.001	0.000	0.000	0.001	0.000	0.001	0.000
0.981	0.984	0.980	0.980	0.980	0.980	0.928
0.006	0.004	0.005	0.006	0.005	0.006	0.035
0.012	0.010	0.014	0.012	0.013	0.012	0.023
0.000	0.001	0.000	0.001	0.001	0.002	0.013
0.000	0.000	0.000	0.000	0.000	0.000	0.000
0.000	0.000	0.000	0.000	0.000	0.000	0.000
0.001	0.000	0.001	0.000	0.001	0.001	0.000
0.000	0.000	0.000	0.000	0.000	0.000	0.000
2.000	2.000	2.000	2.000	2.000	2.000	2.000

Online Resource C Compositions of Orthopyroxene in terms of major (EPMA results, in wt%) elements

Sample	CB1042	CB1042	CB1042	CB1042	CB1042	CB1042	CB1042	CB1042
Phase	Opx	Opx	Opx	Opx	Opx	Opx	Opx	Opx
Site	B	B	C	C	I	I	M	N
Analysis #	127	128	129	130	144	145	150	151
Position	core	rim	core	rim	core	rim	core	core
SiO_2	54.88	55.24	55.04	54.93	55.24	54.78	55.12	55.56
TiO_2	0.08	0.02	0.06	0.02	0.10	0.04	0.04	0.04
Al_2O_3	3.50	2.81	3.22	3.39	2.96	3.13	3.12	3.02
Cr_2O_3	0.59	0.50	0.54	0.61	0.53	0.57	0.39	0.55
FeO_T	8.63	8.89	8.46	8.68	8.27	8.58	8.79	8.74
MnO	0.20	0.22	0.13	0.15	0.21	0.19	0.22	0.19
NiO	0.05	0.10	0.12	0.09	0.08	0.07	0.02	0.03
MgO	31.70	31.75	31.38	31.72	31.83	31.90	31.69	32.07
CaO	0.19	0.19	0.93	0.23	0.51	0.27	0.20	0.28
Na_2O	0.01	0.00	0.01	0.00	0.05	0.03	0.04	0.00
K_2O	0.00	0.01	0.01	0.00	0.00	0.00	0.01	0.00
Total	99.83	99.73	99.90	99.82	99.78	99.56	99.64	100.48
C.p.f.u.								
Si	1.918	1.935	1.925	1.920	1.930	1.918	1.930	1.929
Ti	0.002	0.001	0.002	0.001	0.003	0.001	0.001	0.001
Al	0.144	0.116	0.133	0.140	0.122	0.129	0.129	0.124
Cr	0.016	0.014	0.015	0.017	0.015	0.016	0.011	0.015
Fe^{2+}	0.252	0.260	0.246	0.252	0.240	0.232	0.256	0.253
Fe^{3+}	0.000	0.000	0.001	0.002	0.001	0.019	0.001	0.000
Mn	0.006	0.007	0.004	0.004	0.006	0.006	0.007	0.006
Ni	0.001	0.003	0.003	0.003	0.002	0.002	0.001	0.001
Mg	1.652	1.658	1.636	1.653	1.658	1.665	1.654	1.660
Ca	0.007	0.007	0.035	0.009	0.019	0.010	0.008	0.010
Na	0.001	0.000	0.001	0.000	0.003	0.002	0.003	0.000
K	0.000	0.000	0.000	0.000	0.000	0.000	0.000	0.000
Cations	4.000	4.000	4.000	4.000	4.000	4.000	4.000	4.000

originating from core and rim regions of each rock sample, respectively

CB1042 Opx N 152 rim	CB1042 Opx P 155 core	CB1042 Opx P 156 rim	CB1042 Opx Q 158 core	CB1042 Opx Q 159 rim	CB1042 Opx G 139 core	CB1042 Opx G 140 rim	CB1434 Opx C 164 core
55.15	54.96	55.11	55.12	55.56	54.92	55.18	53.39
0.07	0.08	0.04	0.08	0.04	0.05	0.06	0.08
2.77	3.04	3.31	3.46	2.64	3.27	3.15	1.58
0.48	0.58	0.50	0.61	0.46	0.54	0.61	0.00
8.74	8.87	8.91	9.08	8.83	8.52	8.56	19.60
0.20	0.13	0.19	0.19	0.16	0.14	0.15	0.40
0.10	0.11	0.07	0.05	0.06	0.00	0.03	0.05
31.74	31.60	31.76	31.60	32.07	31.90	31.87	24.24
0.30	0.21	0.14	0.25	0.17	0.16	0.21	0.57
0.00	0.01	0.00	0.00	0.00	0.01	0.05	0.00
0.00	0.00	0.00	0.02	0.00	0.01	0.01	0.01
99.55	99.59	100.03	100.46	99.99	99.52	99.88	99.92
1.934	1.928	1.924	1.918	1.939	1.923	1.926	1.962
0.002	0.002	0.001	0.002	0.001	0.001	0.002	0.002
0.115	0.126	0.136	0.142	0.109	0.135	0.130	0.068
0.013	0.016	0.014	0.017	0.013	0.015	0.017	0.000
0.256	0.260	0.259	0.263	0.258	0.247	0.249	0.599
0.000	0.000	0.001	0.001	0.000	0.003	0.001	0.003
0.006	0.004	0.006	0.006	0.005	0.004	0.004	0.012
0.003	0.003	0.002	0.001	0.002	0.000	0.001	0.001
1.660	1.652	1.653	1.639	1.668	1.665	1.659	1.328
0.011	0.008	0.005	0.009	0.006	0.006	0.008	0.022
0.000	0.001	0.000	0.000	0.000	0.001	0.003	0.000
0.000	0.000	0.000	0.001	0.000	0.000	0.000	0.000
4.000	4.000	4.000	4.000	4.000	4.000	4.000	4.000

CB1434 Opx C 165 rim	CB1434 Opx F 169 core	CB1434 Opx F 170 rim	CB1434 Opx M 179 core	CB1434 Opx Q 193 core	CB1434 Opx Q 194 rim	CB1434 Opx S 199 core	CB1434 Opx S 200 rim
53.40	53.25	53.31	53.78	54.11	53.63	53.93	54.14
0.04	0.06	0.06	0.00	0.05	0.01	0.11	0.02
1.73	1.73	1.72	1.42	1.71	1.87	1.52	1.57
0.00	0.03	0.08	0.06	0.02	0.03	0.00	0.08
19.22	19.33	19.34	19.43	18.00	17.82	17.02	17.26
0.46	0.40	0.43	0.47	0.34	0.35	0.37	0.39
0.00	0.10	0.00	0.05	0.02	0.03	0.07	0.00
24.41	24.33	24.35	24.78	25.67	25.66	26.21	26.27
0.37	0.38	0.38	0.22	0.30	0.25	0.33	0.29
0.04	0.01	0.02	0.00	0.03	0.00	0.03	0.00
0.01	0.03	0.02	0.00	0.01	0.00	0.00	0.00
99.68	99.65	99.71	100.21	100.26	99.65	99.59	100.02
1.963	1.960	1.961	1.967	1.964	1.957	1.963	1.963
0.001	0.002	0.002	0.000	0.001	0.000	0.003	0.001
0.075	0.075	0.075	0.061	0.073	0.080	0.065	0.067
0.000	0.001	0.002	0.002	0.001	0.001	0.000	0.002
0.591	0.592	0.594	0.591	0.546	0.540	0.513	0.520
0.000	0.003	0.001	0.003	0.000	0.004	0.005	0.003
0.014	0.012	0.013	0.015	0.010	0.011	0.011	0.012
0.000	0.003	0.000	0.001	0.001	0.001	0.002	0.000
1.338	1.335	1.335	1.351	1.389	1.396	1.422	1.420
0.015	0.015	0.015	0.009	0.012	0.010	0.013	0.011
0.003	0.001	0.001	0.000	0.002	0.000	0.002	0.000
0.000	0.001	0.001	0.000	0.000	0.000	0.000	0.000
4.000	4.000	4.000	4.000	3.999	4.000	4.000	4.000

CB1464	CB1464	CB1464	CB1464	CB1464	CB1464	CB1464	CB1464	CB1464
Opx	Opx	Opx	Opx	Opx	Opx	Opx	Opx	Opx
A	A	H	H	H	H	I	I	N
3	4	21	22	24	25	27	28	34
core	rim	core	rim	core	rim	core	rim	core
52.72	52.92	52.67	52.69	52.94	52.98	53.14	52.52	52.96
0.15	0.02	0.08	0.10	0.11	0.09	0.02	0.03	0.04
1.35	1.35	1.44	1.40	1.68	1.59	1.31	1.42	1.51
0.06	0.06	0.12	0.12	0.08	0.00	0.08	0.01	0.10
21.63	21.57	22.20	22.40	22.13	22.46	22.24	22.41	22.02
0.48	0.47	0.45	0.46	0.54	0.46	0.45	0.47	0.43
0.03	0.00	0.02	0.03	0.00	0.01	0.00	0.00	0.00
22.73	23.01	22.51	22.26	22.47	22.42	22.53	22.89	22.57
0.51	0.29	0.65	0.34	0.50	0.26	0.51	0.59	0.48
0.03	0.02	0.02	0.00	0.00	0.01	0.01	0.00	0.04
0.00	0.01	0.01	0.00	0.02	0.01	0.01	0.01	0.00
99.69	99.72	100.17	99.80	100.47	100.29	100.30	100.35	100.15
1.962	1.966	1.955	1.966	1.959	1.965	1.970	1.943	1.964
0.004	0.001	0.002	0.003	0.003	0.003	0.001	0.001	0.001
0.059	0.059	0.063	0.062	0.073	0.069	0.057	0.062	0.066
0.002	0.002	0.004	0.004	0.002	0.000	0.002	0.000	0.003
0.664	0.662	0.667	0.699	0.684	0.697	0.689	0.642	0.679
0.009	0.008	0.022	0.000	0.001	0.000	0.001	0.051	0.004
0.015	0.015	0.014	0.015	0.017	0.014	0.014	0.015	0.014
0.001	0.000	0.001	0.001	0.000	0.000	0.000	0.000	0.000
1.261	1.274	1.245	1.238	1.240	1.239	1.245	1.262	1.248
0.020	0.012	0.026	0.014	0.020	0.010	0.020	0.023	0.019
0.002	0.001	0.001	0.000	0.000	0.001	0.001	0.000	0.003
0.000	0.000	0.000	0.000	0.001	0.000	0.000	0.000	0.000
4.000	4.000	4.000	3.999	4.000	3.999	4.000	4.000	4.000

CB1464	CB1464	CB1464	CB1424	CB1424	CB1424	CB1424	CB1424
Opx	Opx	Opx	Opx	Opx	Opx	Opx	Opx
N	Q	Q	C	C	D	D	G
35	39	40	105	106	109	110	117
rim	core	rim	core	rim	core	rim	core
52.72	52.95	52.63	50.77	50.48	50.53	50.96	50.89
0.13	0.05	0.08	0.05	0.05	0.02	0.02	0.05
1.56	1.40	1.38	1.14	1.27	1.37	1.50	1.17
0.09	0.07	0.07	0.03	0.00	0.00	0.02	0.00
22.03	22.25	22.35	29.99	30.37	30.38	30.14	30.32
0.43	0.42	0.50	0.81	0.75	0.78	0.88	0.85
0.01	0.00	0.03	0.00	0.02	0.01	0.00	0.04
22.50	22.70	22.30	16.75	16.54	16.62	16.29	16.46
0.42	0.48	0.32	0.40	0.44	0.45	0.57	0.39
0.00	0.00	0.00	0.00	0.01	0.01	0.03	0.04
0.01	0.02	0.00	0.00	0.01	0.00	0.00	0.00
99.90	100.34	99.66	99.94	99.94	100.17	100.41	100.21
1.961	1.960	1.966	1.965	1.956	1.953	1.966	1.968
0.004	0.001	0.002	0.001	0.001	0.001	0.001	0.001
0.068	0.061	0.061	0.052	0.058	0.062	0.068	0.053
0.003	0.002	0.002	0.001	0.000	0.000	0.001	0.000
0.685	0.675	0.697	0.957	0.956	0.950	0.973	0.969
0.000	0.014	0.001	0.014	0.028	0.032	0.000	0.011
0.014	0.013	0.016	0.027	0.025	0.026	0.029	0.028
0.000	0.000	0.001	0.000	0.001	0.000	0.000	0.001
1.248	1.253	1.242	0.967	0.955	0.957	0.937	0.949
0.017	0.019	0.013	0.017	0.018	0.019	0.024	0.016
0.000	0.000	0.000	0.000	0.001	0.001	0.002	0.003
0.000	0.001	0.000	0.000	0.000	0.000	0.000	0.000
4.000	4.000	4.000	4.000	4.000	4.000	4.000	4.000

CB1424 Opx G 118 rim	CB1424 Opx N 127 core	CB1424 Opx N 128 rim	CB1424 Opx O 129 core	CB1424 Opx O 130 rim	CB1424 Opx R 135 core	CB1424 Opx R 136 rim	CB1424 Opx S 140 core	CB1424 Opx S 141 rim
50.84	50.95	50.61	50.83	50.72	50.40	50.83	50.94	50.68
0.12	0.07	0.08	0.04	0.05	0.07	0.01	0.06	0.08
1.22	1.30	1.50	1.27	1.30	1.43	1.59	1.31	1.41
0.00	0.06	0.00	0.03	0.02	0.05	0.02	0.00	0.03
29.97	30.41	29.97	30.29	29.93	29.73	30.13	30.33	30.13
0.83	0.78	0.81	0.85	0.76	0.83	0.80	0.82	0.78
0.02	0.00	0.13	0.03	0.00	0.00	0.03	0.04	0.00
16.47	16.44	16.23	16.44	16.51	16.24	16.49	16.35	16.35
0.39	0.41	0.43	0.40	0.36	0.83	0.39	0.47	0.39
0.04	0.00	0.04	0.01	0.01	0.04	0.00	0.00	0.02
0.00	0.00	0.00	0.00	0.00	0.00	0.01	0.01	0.00
99.90	100.42	99.80	100.19	99.66	99.62	100.30	100.33	99.87
1.970	1.967	1.965	1.966	1.969	1.959	1.962	1.968	1.966
0.003	0.002	0.002	0.001	0.001	0.002	0.000	0.002	0.002
0.056	0.059	0.069	0.058	0.059	0.066	0.072	0.060	0.064
0.000	0.002	0.000	0.001	0.001	0.002	0.001	0.000	0.001
0.971	0.980	0.973	0.972	0.972	0.952	0.969	0.980	0.977
0.000	0.001	0.000	0.007	0.000	0.014	0.003	0.000	0.000
0.027	0.026	0.027	0.028	0.025	0.027	0.026	0.027	0.026
0.001	0.000	0.004	0.001	0.000	0.000	0.001	0.001	0.000
0.952	0.946	0.939	0.948	0.956	0.941	0.949	0.942	0.945
0.016	0.017	0.018	0.017	0.015	0.035	0.016	0.019	0.016
0.003	0.000	0.003	0.001	0.001	0.003	0.000	0.000	0.002
0.000	0.000	0.000	0.000	0.000	0.000	0.000	0.000	0.000
4.000	4.000	4.000	4.000	3.999	4.000	4.000	4.000	4.000

CB1424	CB1424	CB1424	CB1424	CB1414	CB1414	CB1414	CB1414
Opx	Opx	Opx	Opx	Opx	Opx	Opx	Opx
Z	Z	Z1	Z1	B	B	D	E
152	153	154	155	79	80	87	88
core	rim	core	rim	core	core	core	core
50.60	51.01	50.52	50.56	53.27	53.29	53.54	53.79
0.08	0.05	0.11	0.12	0.03	0.06	0.08	0.08
1.31	1.57	1.17	1.25	1.20	0.99	1.27	1.04
0.03	0.02	0.02	0.04	0.14	0.07	0.14	0.14
30.06	29.87	30.13	30.14	20.38	20.62	20.61	20.05
0.91	0.79	0.90	0.82	0.49	0.50	0.44	0.43
0.06	0.00	0.00	0.04	0.00	0.00	0.05	0.03
16.51	16.64	16.65	16.60	23.70	23.55	23.76	24.23
0.40	0.37	0.43	0.41	0.41	0.47	0.38	0.46
0.02	0.02	0.07	0.02	0.02	0.00	0.03	0.03
0.00	0.01	0.01	0.01	0.00	0.00	0.00	0.00
99.98	100.35	100.01	100.01	99.64	99.55	100.30	100.28
1.960	1.965	1.955	1.957	1.971	1.976	1.969	1.974
0.002	0.001	0.003	0.003	0.001	0.002	0.002	0.002
0.060	0.071	0.053	0.057	0.052	0.043	0.055	0.045
0.001	0.001	0.001	0.001	0.004	0.002	0.004	0.004
0.958	0.962	0.939	0.954	0.630	0.640	0.634	0.614
0.016	0.000	0.036	0.022	0.001	0.000	0.000	0.001
0.030	0.026	0.029	0.027	0.015	0.016	0.014	0.013
0.002	0.000	0.000	0.001	0.000	0.000	0.001	0.001
0.953	0.955	0.960	0.958	1.308	1.302	1.303	1.325
0.017	0.015	0.018	0.017	0.016	0.019	0.015	0.018
0.002	0.001	0.005	0.002	0.001	0.000	0.002	0.002
0.000	0.000	0.000	0.000	0.000	0.000	0.000	0.000
4.000	3.999	4.000	4.000	4.000	3.999	4.000	4.000

CB1414 Opx E 89 rim	CB1414 Opx L 104 core	CB1414 Opx L 105 rim	CB1414 Opx P 112 core	CB1414 Opx P 113 core	CB1414 Opx Q 114 core	CB1414 Opx Q 115 rim	CB1475 Opx E 70 core
53.31	53.60	53.82	53.44	53.93	53.70	53.56	52.14
0.05	0.06	0.04	0.06	0.05	0.00	0.03	0.06
1.19	1.19	1.15	1.03	1.11	1.05	1.33	0.99
0.09	0.25	0.13	0.15	0.14	0.23	0.14	0.04
20.33	19.37	19.83	19.47	19.74	19.83	19.98	24.72
0.49	0.40	0.40	0.50	0.42	0.43	0.45	0.48
0.03	0.00	0.01	0.09	0.00	0.00	0.00	0.01
23.71	24.66	24.49	24.23	24.44	24.31	24.35	20.76
0.43	0.34	0.34	0.57	0.51	0.45	0.26	0.31
0.03	0.00	0.01	0.06	0.02	0.00	0.02	0.00
0.00	0.00	0.00	0.00	0.01	0.01	0.00	0.01
99.66	99.87	100.22	99.60	100.37	100.01	100.12	99.52
1.972	1.969	1.973	1.971	1.974	1.974	1.966	1.972
0.001	0.002	0.001	0.002	0.001	0.000	0.001	0.002
0.052	0.052	0.050	0.045	0.048	0.045	0.058	0.044
0.003	0.007	0.004	0.004	0.004	0.007	0.004	0.001
0.628	0.594	0.608	0.591	0.604	0.610	0.607	0.774
0.001	0.001	0.000	0.010	0.000	0.000	0.006	0.008
0.015	0.012	0.012	0.016	0.013	0.013	0.014	0.015
0.001	0.000	0.000	0.003	0.000	0.000	0.000	0.000
1.308	1.350	1.338	1.332	1.333	1.332	1.332	1.170
0.017	0.013	0.013	0.023	0.020	0.018	0.010	0.013
0.002	0.000	0.001	0.004	0.001	0.000	0.001	0.000
0.000	0.000	0.000	0.000	0.000	0.000	0.000	0.000
4.000	4.000	4.000	4.000	4.000	4.000	4.000	4.000

CB1475	CB1475	CB1475	CB1475	CB1475	CB1475	CB1475	CB1475	CB1475
Opx	Opx	Opx	Opx	Opx	Opx	Opx	Opx	Opx
E	F	F	M	M	O	O	P	P
71	72	73	89	90	94	95	96	97
rim	core	rim	core	rim	core	rim	core	rim
52.76	52.13	52.07	52.30	52.30	52.59	52.41	52.51	52.78
0.01	0.08	0.06	0.00	0.06	0.07	0.08	0.12	0.01
0.95	1.13	1.11	0.89	0.97	1.01	0.82	0.97	0.96
0.00	0.00	0.06	0.01	0.01	0.05	0.04	0.03	0.00
25.02	25.04	24.69	24.54	24.95	24.14	24.57	24.56	24.77
0.54	0.55	0.51	0.54	0.58	0.52	0.52	0.61	0.56
0.00	0.00	0.00	0.02	0.00	0.00	0.00	0.00	0.03
20.73	21.11	20.55	20.94	21.06	21.12	20.74	20.86	20.85
0.36	0.35	0.61	0.35	0.45	0.56	0.54	0.39	0.35
0.04	0.02	0.00	0.00	0.02	0.03	0.01	0.01	0.02
0.00	0.00	0.01	0.01	0.01	0.00	0.00	0.00	0.00
100.41	100.41	99.67	99.60	100.41	100.09	99.73	100.06	100.33
1.979	1.952	1.968	1.974	1.959	1.973	1.978	1.975	1.980
0.000	0.002	0.002	0.000	0.002	0.002	0.002	0.003	0.000
0.042	0.050	0.049	0.040	0.043	0.045	0.036	0.043	0.042
0.000	0.000	0.002	0.000	0.000	0.001	0.001	0.001	0.000
0.783	0.742	0.770	0.763	0.744	0.750	0.774	0.772	0.777
0.002	0.043	0.011	0.012	0.037	0.007	0.002	0.000	0.000
0.017	0.017	0.016	0.017	0.018	0.017	0.017	0.019	0.018
0.000	0.000	0.000	0.001	0.000	0.000	0.000	0.000	0.001
1.159	1.179	1.158	1.178	1.176	1.181	1.167	1.170	1.166
0.014	0.014	0.025	0.014	0.018	0.023	0.022	0.016	0.014
0.003	0.001	0.000	0.000	0.001	0.002	0.001	0.001	0.001
0.000	0.000	0.000	0.000	0.000	0.000	0.000	0.000	0.000
4.000	4.000	4.000	4.000	4.000	4.000	4.000	4.000	4.000

CB1482 Opx D 216 core	CB1482 Opx D 217 rim	CB1482 Opx M 246 core	CB1482 Opx M 247 rim	CB1482 Opx O 250 core	CB1482 Opx O 251 rim	CB1482 Opx Q 267 core	CB1482 Opx Q 268 rim
51.49	51.67	51.18	51.44	51.74	51.56	51.43	51.57
0.04	0.11	0.14	0.05	0.17	0.09	0.05	0.06
0.90	1.02	0.96	0.79	0.88	0.90	0.86	1.01
0.00	0.02	0.00	0.01	0.00	0.02	0.02	0.00
28.64	28.51	28.45	28.57	28.44	28.20	29.03	29.15
0.27	0.31	0.33	0.32	0.36	0.24	0.26	0.26
0.00	0.00	0.02	0.03	0.03	0.00	0.00	0.04
18.32	17.90	17.66	17.89	18.15	18.39	17.61	17.43
0.68	0.67	0.79	0.58	0.59	0.59	0.50	0.77
0.03	0.04	0.02	0.00	0.02	0.03	0.02	0.01
0.00	0.00	0.00	0.00	0.01	0.01	0.01	0.00
100.37	100.25	99.55	99.68	100.39	100.03	99.79	100.30
1.964	1.976	1.974	1.980	1.976	1.972	1.981	1.978
0.001	0.003	0.004	0.001	0.005	0.003	0.001	0.002
0.040	0.046	0.044	0.036	0.040	0.041	0.039	0.046
0.000	0.001	0.000	0.000	0.000	0.001	0.001	0.000
0.883	0.912	0.916	0.920	0.907	0.888	0.935	0.935
0.031	0.000	0.002	0.000	0.001	0.013	0.000	0.000
0.009	0.010	0.011	0.010	0.012	0.008	0.008	0.008
0.000	0.000	0.001	0.001	0.001	0.000	0.000	0.001
1.042	1.021	1.015	1.027	1.033	1.048	1.011	0.996
0.028	0.027	0.033	0.024	0.024	0.024	0.021	0.032
0.002	0.003	0.001	0.000	0.001	0.002	0.001	0.001
0.000	0.000	0.000	0.000	0.000	0.000	0.000	0.000
4.000	3.999	4.000	4.000	4.000	4.000	3.999	3.998

Online Resource C Compositions of Biotite n terms of major (EPMA results, in wt%) and trace (LA-ICP-M

Sample	CB1482	CB1482	CB1482	CB1482	CB1482	CB1482	CB1482	CB1482
Phase	Bt	Bt	Bt	Bt	Bt	Bt	Bt	Bt
Site	A	A	A	A	C	C	C	C
Analysis #	207	208	212	213	214	215	220	221
Position	core	rim	core	rim	core	rim	core	rim
SiO_2	36.73	36.19	36.45	36.85	36.02	36.63	36.37	36.17
TiO_2	4.65	4.77	4.62	4.63	4.18	4.51	4.93	4.77
Al_2O_3	15.78	15.28	15.31	15.45	16.14	15.48	15.13	15.81
Cr_2O_3	0.00	0.02	0.03	0.04	0.00	0.09	0.01	0.00
FeO_T	15.68	15.61	15.92	16.17	15.55	16.03	16.46	16.65
MnO	0.00	0.03	0.00	0.02	0.01	0.02	0.00	0.02
NiO	0.00	0.00	0.00	0.00	0.00	0.02	0.02	0.00
MgO	12.75	12.37	12.37	12.41	12.69	12.41	11.52	12.00
CaO	0.03	0.01	0.01	0.00	0.03	0.00	0.01	0.04
Na_2O	0.15	0.10	0.12	0.12	0.12	0.12	0.15	0.12
K_2O	9.48	9.48	9.44	9.41	9.29	9.49	9.25	9.36
Total	95.25	93.86	94.27	95.10	94.03	94.80	93.85	94.94
C.p.f.u.								
Si	5.509	5.519	5.537	5.546	5.471	5.535	5.561	5.472
Ti	0.525	0.547	0.528	0.524	0.478	0.513	0.567	0.543
Al	2.789	2.747	2.741	2.741	2.889	2.757	2.726	2.819
Cr	0.000	0.002	0.004	0.005	0.000	0.011	0.001	0.000
Fe^{2+}	1.967	1.991	2.022	2.035	1.975	2.026	2.105	2.107
Fe^{3+}	0.000	0.000	0.000	0.000	0.000	0.000	0.000	0.000
Mn	0.000	0.004	0.000	0.003	0.001	0.003	0.000	0.003
Mg	2.848	2.810	2.798	2.782	2.870	2.793	2.623	2.704
Ca	0.005	0.002	0.002	0.000	0.005	0.000	0.002	0.006
Na	0.044	0.030	0.035	0.035	0.035	0.035	0.044	0.035
K	1.814	1.844	1.829	1.807	1.800	1.829	1.804	1.807
Cations	15.500	15.496	15.496	15.478	15.525	15.501	15.433	15.496
ppm								
Ca	163	116	50	36			2458	1566
Sc	10	10	9.6	9.5			11	9.4
Ti	27110	27160	27160	27890			29370	29740
V	350	343	373	365			318	322
Cr	100	99	105	105			92	96
Co	75	74	75	76			74	75
Ni	59	55	59	59			55	57

Rb	466	455	482	476	479	479
Sr	3.3	3.2	4.1	4.1	4.3	3.9
Y	0.055	0.034	0.023	0.025	0.183	0.086
Zr	1.34	1.40	0.629	0.800	1.88	1.26
Nb	26	25	27	23	21	21
Cs	11	12	12	12	12	11
Ba	3664	3530	3579	3589	3960	3903
La	0.041	0.051	0.006	0.012	0.301	0.427
Ce	0.040	0.052	0.001	0.014	0.585	0.766
Pr	0.003	0.005	0.001	0.003	0.075	0.095
Nd	0.011	0.008		0.008	0.308	0.409
Sm	0.003			0.002	0.065	0.072
Eu	0.017	0.017	0.021	0.028	0.048	0.036
Gd	0.010	0.003			0.056	0.029
Tb	0.002			0.001	0.006	0.007
Dy	0.003		0.003		0.039	0.019
Ho	0.001				0.010	0.003
Er	0.002		0.001	0.002	0.016	0.015
Tm					0.006	
Yb			0.002	0.002	0.005	0.004
Lu					0.005	0.001
Hf	0.051	0.038	0.030	0.040	0.065	0.052
Ta	1.22	1.14	1.07	0.953	0.743	0.727
Pb	4.0	4.1	4.7	5.1	4.5	4.8
Th	0.001		0.001		0.002	0.001
U			0.001	0.001	0.002	0.001

MS results, in ppm) elements originating from core and rim regions of each rock sample, respectively

CB1482 Bt D 223 core	CB1482 Bt E 226 core	CB1482 Bt E 227 rim	CB1482 Bt H 236 core	CB1482 Bt H 237 rim	CB1482 Bt I 233 core	CB1482 Bt I 234 rim	CB1482 Bt L 239 core	CB1482 Bt L 240 rim
37.22	36.40	36.97	36.79	37.31	36.86	35.97	36.91	36.26
3.74	5.02	4.97	4.57	4.54	4.54	4.85	4.36	4.49
16.28	15.52	15.22	15.31	15.00	15.87	15.30	15.94	15.66
0.09	0.07	0.03	0.05	0.01	0.00	0.06	0.05	0.00
16.78	16.14	16.54	15.99	16.19	15.58	15.78	15.71	15.27
0.00	0.00	0.03	0.00	0.00	0.00	0.00	0.08	0.05
0.00	0.08	0.00	0.07	0.00	0.02	0.00	0.03	0.00
11.25	11.77	11.75	12.20	11.78	13.03	12.14	12.55	12.40
0.02	0.00	0.01	0.03	0.04	0.01	0.03	0.02	0.04
0.13	0.09	0.10	0.11	0.11	0.11	0.11	0.11	0.09
9.46	9.51	9.46	9.34	9.22	9.36	9.26	9.42	9.49
94.97	94.60	95.08	94.46	94.20	95.38	93.50	95.18	93.75
5.611	5.521	5.576	5.574	5.657	5.512	5.508	5.537	5.524
0.424	0.573	0.564	0.521	0.518	0.511	0.559	0.492	0.514
2.893	2.774	2.706	2.734	2.681	2.797	2.761	2.818	2.811
0.011	0.008	0.004	0.006	0.001	0.000	0.007	0.006	0.000
2.116	2.047	2.086	2.026	2.053	1.948	2.021	1.971	1.945
0.000	0.000	0.000	0.000	0.000	0.000	0.000	0.000	0.000
0.000	0.000	0.004	0.000	0.000	0.000	0.000	0.010	0.006
2.526	2.659	2.639	2.753	2.660	2.902	2.768	2.804	2.813
0.003	0.000	0.002	0.005	0.006	0.002	0.005	0.003	0.007
0.038	0.026	0.029	0.032	0.032	0.032	0.033	0.032	0.027
1.819	1.840	1.820	1.805	1.783	1.786	1.809	1.803	1.844
15.441	15.448	15.430	15.455	15.392	15.488	15.470	15.476	15.492
							87	61
							11	10
							27410	26580
							403	390
							134	129
							81	78
							61	60

481	460
2.87	2.64
0.039	0.040
1.72	1.54
34	32
12	12
3451	3238
0.110	0.021
0.133	0.015
0.017	0.002
0.082	
0.018	
0.022	0.015
0.003	0.004
0.001	
0.003	0.003
0.003	
0.003	
0.004	
	0.011
0.048	0.043
1.52	1.47
4.0	3.9
0.005	0.002

CB1482	CB1482	CB1482	CB1482	CB1482	CB1482
Bt	Bt	Bt	Bt	Bt	Bt
O	P	P	P	P	P
260	250	253	254	261	262
core inc Grt	inc in Grt	core	rim	core	rim
36.32	35.73	36.14	36.43	36.91	36.75
4.69	4.55	4.57	4.42	4.50	4.69
15.58	15.43	15.23	15.13	15.21	15.59
0.00	0.00	0.00	0.00	0.03	0.02
16.04	15.75	15.22	15.81	15.15	15.20
0.01	0.01	0.01	0.01	0.00	0.00
0.03	0.02	0.00	0.00	0.08	0.00
12.04	12.95	12.88	12.85	12.96	13.01
0.05	0.02	0.04	0.09	0.00	0.00
0.19	0.13	0.11	0.07	0.06	0.03
9.10	9.33	9.41	8.98	9.50	9.60
94.05	93.92	93.61	93.79	94.40	94.89
5.525	5.453	5.516	5.546	5.577	5.523
0.537	0.522	0.525	0.506	0.511	0.530
2.793	2.775	2.739	2.715	2.709	2.761
0.000	0.000	0.000	0.000	0.004	0.002
2.040	2.010	1.943	2.013	1.914	1.910
0.000	0.000	0.000	0.000	0.000	0.000
0.001	0.001	0.001	0.001	0.000	0.000
2.727	2.944	2.928	2.913	2.916	2.912
0.008	0.003	0.007	0.015	0.000	0.000
0.056	0.038	0.033	0.021	0.018	0.009
1.766	1.817	1.832	1.744	1.831	1.841
15.453	15.564	15.522	15.473	15.480	15.489

Online Resource C Compositions of Quartz in terms of trace (LA-ICP-MS results, in ppm) elements origi

Sample	CB1425	CB1425	CB1425	CB1425	CB1425	CB1425	CB1425	CB1425
Phase	Qtz	Qtz	Qtz	Qtz	Qtz	Qtz	Qtz	Qtz
Site	E	E	E	E	E	E	E	E
Analysis #	1	2	3	4	5	6	7	8
ppm								
Sc	3.1	2.25	2.65	2.48	2.59	3.1	2.53	2.43
Ti	43	15	70	15	15	15	17	13
V	0.579	0.106	0.144		0.306	0.358		0.356
Cr		0.130	0.899	0.565	5.8		2.54	0.148
Co	0.009	0.083		0.165	0.146			
Ni	0.634	2.13	1.16		2.79	1.92		0.996
Rb		0.011	0.018	0.045	0.025	0.030	0.040	0.019
Sr	0.109	0.132	0.017	2.30	0.02	0.025	1.08	0.055
Y	0.029	0.015	0.018	0.011	0.044	0.047	0.066	0.052
Zr	0.027	0.006	0.028			0.011	0.046	
Nb		0.016		0.068	0.005	0.017		0.009
Cs		0.006	0.016	0.020	0.005			0.046
Ba	0.132	0.120	0.105	0.013	0.065	0.016	3.8	0.025
La	0.016	0.015	0.012	0.020	0.060	0.019	0.018	0.045
Ce	0.249	0.042	0.031	0.068	0.029	0.063	0.093	0.170
Pr	0.086		0.370	0.111	0.062	0.009	0.779	0.527
Nd	7.8	1.61	22	16	7.8	25	21	41
Sm	0.048	0.076	0.175	0.041	0.310	0.091	0.241	0.278
Eu		0.002					0.009	0.006
Gd	0.074	0.010	0.029	0.138	0.019	0.054	0.050	0.057
Tb		0.002				0.009	0.019	0.006
Dy	0.009	0.002		0.003		0.002	0.002	0.003
Ho				0.002			0.157	
Er	0.006			0.004		0.008		
Tm				0.002				
Yb	0.003	0.012			0.004			
Lu	0.001					0.002		
Hf	0.003		0.002	0.002	0.004	0.009	0.002	0.003
Ta	0.001	0.001						
Pb	0.156	0.155	0.785	0.021	0.079	0.068	0.157	0.106
Th	0.007	0.005	0.008			0.012	0.004	0.015
U	0.001	0.002	0.001		0.002		0.002	

nating from core and rim regions of each rock sample, respectively

CB1425 Qtz E 9	CB1425 Qtz E 10	CB1425 Qtz E 11	CB1425 Qtz D 1	CB1425 Qtz D 2	CB1425 Qtz D 3	CB1425 Qtz D 4
2.45	2.85	2.79	3.00	2.57	3.4	2.46
11	15	19	406	157	20	730
	0.407		0.683	0.133	0.058	0.042
2.56		0.869		0.701		0.896
0.027		0.132	0.047	0.271		
	1.32	0.131	0.715	0.578	2.20	1.77
0.167	0.003	0.021	0.044	0.055		0.115
0.603	0.109	0.035	0.449	0.072	0.034	0.252
0.017	0.022	0.005	0.061	0.022	0.038	0.016
0.152	0.017	0.009	0.105	0.034		0.175
	0.003		0.011	0.003	0.010	0.017
	0.011	0.018	0.037			0.013
0.035	0.017	0.652	0.811	0.101	0.095	0.290
0.027	0.011	0.023	0.106	0.003	0.020	0.058
0.232	0.199	0.071	0.394	0.017	0.062	0.114
0.589	0.124	0.155	0.292	0.075	0.114	0.073
29	22	16	31	13	27	28
0.051	0.038	0.159	1.14	0.077	0.050	0.298
0.001	0.002	0.001	0.013	0.003	0.002	
0.102	0.034	0.026	0.040	0.022	0.136	0.017
0.004		0.001	0.005	0.012	0.011	0.007
	0.011	0.006	0.005			0.006
0.006	0.012		0.022	0.003		
0.027					0.004	0.004
0.061			0.008			
	0.001		0.003			0.002
0.003	0.001	0.002	0.011	0.002	0.003	0.008
	0.002		0.001			
0.165	0.084	0.192	0.355	0.062	0.153	0.161
0.008	0.010	0.001	0.030	0.027	0.005	0.018
0.001	0.002	0.001	0.010	0.002	0.001	0.011

Online Resource C Compositions of Plagioclase in terms of major (EPMA results, in wt%) and trace (LA-

Sample	CB1042	CB1042	CB1042	CB1042	CB1042	CB1042	CB1042	CB1042
Phase	Plg	Plg	Plg	Plg	Plg	Plg	Plg	Plg
Site	D	D	M	M	O	O	R	R
Analysis #	133	134	148	149	153	154	160	161
Position	core	rim	core	rim	core	rim	core	rim
SiO_2	47.82	47.31	48.03	48.20	48.34	48.30	48.17	47.76
TiO_2	0.00	0.00	0.03	0.00	0.03	0.00	0.00	0.00
Al_2O_3	34.08	34.27	33.54	33.79	33.13	33.70	33.24	34.23
Cr_2O_3	0.00	0.01	0.03	0.00	0.00	0.00	0.00	0.09
FeO_T	0.02	0.04	0.03	0.08	0.01	0.05	0.05	0.07
MnO	0.00	0.00	0.00	0.00	0.02	0.01	0.01	0.02
NiO	0.05	0.00	0.03	0.00	0.00	0.05	0.02	0.00
MgO	0.00	0.00	0.00	0.02	0.00	0.01	0.01	0.00
CaO	15.54	15.71	15.58	15.71	15.45	15.59	15.59	16.13
Na_2O	2.34	2.22	2.41	2.39	2.56	2.44	2.47	2.18
K_2O	0.04	0.03	0.04	0.04	0.03	0.02	0.02	0.02
Total	99.89	99.59	99.72	100.23	99.57	100.17	99.58	100.50
C.p.f.u.								
Si	2.187	2.172	2.201	2.199	2.218	2.203	2.211	2.176
Ti	0.000	0.000	0.001	0.000	0.001	0.000	0.000	0.000
Al	1.836	1.854	1.811	1.817	1.791	1.811	1.798	1.838
Cr	0.000	0.000	0.001	0.000	0.000	0.000	0.000	0.003
Fe_T	0.001	0.002	0.001	0.003	0.000	0.002	0.002	0.003
Mn	0.000	0.000	0.000	0.000	0.001	0.000	0.000	0.001
Ni	0.002	0.000	0.001	0.000	0.000	0.002	0.001	0.000
Mg	0.003	0.000	0.002	0.000	0.000	0.003	0.001	0.000
Ca	0.761	0.773	0.765	0.768	0.759	0.762	0.767	0.787
Na	0.207	0.198	0.214	0.211	0.228	0.216	0.220	0.193
K	0.002	0.002	0.002	0.002	0.002	0.001	0.001	0.001
Cations	5.000	5.000	5.000	5.000	5.000	5.000	5.001	5.001
ppm								
Sc	1.04	1.13			0.954	0.844		
Ti	16	11			29	28		
V					0.760	0.429		
Cr	1.63	0.863				0.954		
Co		0.140			0.037	0.115		
Ni	0.967	0.911			0.067	0.090		
Rb	0.097	0.478				0.044		

Sr	300	347	270	284
Y	0.081	0.059	0.092	0.077
Zr	0.019	0.060		0.004
Nb	0.004		0.009	
Cs	0.029			0.016
Ba	119	134	76	103
La	0.956	0.878	0.908	0.851
Ce	0.994	0.972	1.01	0.937
Pr	0.074	0.062	0.067	0.086
Nd	0.170	0.338	0.222	0.306
Sm		0.027	0.029	0.053
Eu	0.328	0.365	0.256	0.241
Gd	0.025	0.019	0.029	0.005
Tb			0.002	0.001
Dy	0.007	0.004	0.023	0.013
Ho	0.005	0.002	0.008	0.001
Er	0.007		0.016	0.007
Tm		0.001		
Yb	0.011		0.003	0.003
Lu				
Hf		0.006	0.002	0.002
Ta				
Pb	5.6	5.9	5.0	5.1
Th	0.001			
U	0.001		0.001	

ICP-MS results, in ppm) elements originating from core and rim regions of each rock sample, respectivel

CB1434 Plg A 157 core	CB1434 Plg A 158 rim	CB1434 Plg H 173 core	CB1434 Plg H 174 rim	CB1434 Plg M 181 core	CB1434 Plg N 185 core	CB1434 Plg O 187 core	CB1434 Plg O 188 rim
48.84	48.61	50.68	49.85	50.40	49.59	49.99	49.92
0.02	0.04	0.01	0.04	0.05	0.00	0.00	0.00
34.89	34.61	31.63	32.71	33.15	33.95	33.52	33.46
0.00	0.01	0.00	0.00	0.00	0.00	0.00	0.02
0.02	0.28	0.08	0.07	0.02	0.04	0.00	0.03
0.00	0.08	0.00	0.06	0.00	0.05	0.02	0.02
0.00	0.00	0.01	0.02	0.08	0.02	0.00	0.03
0.00	0.00	0.02	0.00	0.00	0.00	0.00	0.01
12.84	12.68	13.63	14.06	11.78	13.09	13.41	13.06
3.32	3.25	3.59	3.24	3.98	3.40	3.42	3.50
0.06	0.08	0.06	0.05	0.06	0.07	0.08	0.06
99.99	99.64	99.71	100.10	99.52	100.21	100.44	100.11
2.215	2.215	2.310	2.266	2.288	2.245	2.260	2.262
0.001	0.001	0.000	0.001	0.002	0.000	0.000	0.000
1.865	1.859	1.699	1.752	1.774	1.812	1.786	1.787
0.000	0.000	0.000	0.000	0.000	0.000	0.000	0.001
0.001	0.011	0.003	0.003	0.001	0.002	0.000	0.001
0.000	0.003	0.000	0.002	0.000	0.002	0.001	0.001
0.000	0.000	0.000	0.001	0.003	0.001	0.000	0.001
0.000	0.000	0.001	0.001	0.005	0.001	0.000	0.002
0.624	0.619	0.666	0.685	0.573	0.635	0.649	0.634
0.292	0.287	0.317	0.286	0.350	0.298	0.300	0.307
0.003	0.005	0.003	0.003	0.003	0.004	0.005	0.003
5.000	5.000	5.000	5.000	5.000	5.000	5.000	5.000

ly

CB1434 Plg O 189 core	CB1434 Plg O 190 rim	CB1464 Plg B 6 core	CB1464 Plg B 7 rim	CB1464 Plg D 10 core	CB1464 Plg D 11 rim	CB1464 Plg G 19 core	CB1464 Plg G 20 rim
49.47	49.15	48.54	48.56	48.98	48.06	49.14	48.30
0.02	0.00	0.02	0.02	0.00	0.05	0.00	0.00
33.87	34.22	33.51	33.06	33.24	33.62	32.77	33.36
0.00	0.00	0.00	0.00	0.00	0.00	0.00	0.01
0.05	0.00	0.12	0.07	0.00	0.11	0.04	0.12
0.01	0.00	0.00	0.00	0.00	0.00	0.00	0.00
0.00	0.03	0.00	0.00	0.00	0.00	0.00	0.00
0.00	0.01	0.00	0.00	0.00	0.00	0.00	0.00
13.18	13.60	15.62	15.29	15.18	15.68	14.76	15.71
3.36	3.18	2.48	2.62	2.74	2.37	2.90	2.39
0.07	0.04	0.07	0.06	0.07	0.06	0.07	0.06
100.03	100.23	100.36	99.68	100.21	99.95	99.68	99.95
2.245	2.227	2.211	2.225	2.230	2.199	2.248	2.210
0.001	0.000	0.001	0.001	0.000	0.002	0.000	0.000
1.811	1.828	1.799	1.785	1.784	1.813	1.766	1.799
0.000	0.000	0.000	0.000	0.000	0.000	0.000	0.000
0.002	0.000	0.005	0.003	0.000	0.004	0.002	0.005
0.000	0.000	0.000	0.000	0.000	0.000	0.000	0.000
0.000	0.001	0.000	0.000	0.000	0.000	0.000	0.000
0.000	0.002	0.000	0.000	0.000	0.000	0.000	0.000
0.641	0.660	0.762	0.751	0.741	0.769	0.723	0.770
0.296	0.279	0.219	0.233	0.242	0.210	0.257	0.212
0.004	0.002	0.004	0.004	0.004	0.004	0.004	0.004
4.999	5.000	5.000	5.000	5.001	5.000	5.000	4.999
		1.83	2.07	2.08	1.94	2.69	2.08
		30	32	27	30	27	27
		0.488	0.372	1.51	0.333	1.01	
		2.29	1.98		1.18	8.5	4.5
		0.259	0.064	0.077	0.080	0.059	0.262
		0.709	0.761			2.07	
		0.171	0.142	0.058	0.066		

291	269	242	264	277	280
0.222	0.183	0.234	0.218	0.382	0.306
	0.008	0.006	0.072	0.029	0.192
0.030	0.018		0.005	0.013	0.009
0.172	0.107	0.062	0.026	0.137	0.220
133	116	114	130	153	149
4.6	4.0	3.9	4.0	4.3	4.6
5.9	5.3	5.4	5.8	6.4	6.2
0.446	0.439	0.405	0.425	0.439	0.593
1.93	1.41	1.51	1.59	1.73	2.29
0.075	0.165	0.167	0.243	0.256	0.352
0.841	0.685	0.790	0.890	1.02	0.908
0.123	0.123	0.100	0.118	0.130	0.174
0.076	0.013	0.014	0.011	0.012	0.015
0.020	0.081	0.037	0.030	0.043	0.046
0.010	0.006	0.009	0.010	0.057	0.018
0.007	0.020	0.008	0.027	0.034	0.012
	0.005	0.002	0.003		0.050
0.041	0.008	0.008	0.018	0.008	0.037
0.006		0.002	0.003	0.010	0.013
0.017			0.014	0.003	0.038
0.007		0.004			
1.89	1.76	1.86	1.97	2.04	2.33
0.028			0.004	0.009	0.015
	0.004		0.001	0.010	0.010

CB1464	CB1464	CB1464	CB1464	CB1424	CB1424	CB1424	CB1424
Plg	Plg	Plg	Plg	Plg	Plg	Plg	Plg
P	P	R	R	E	E	F	F
37	38	43	44	113	114	115	116
core	rim	core	rim	core	rim	core	rim
48.55	47.25	47.98	48.27	45.84	45.08	45.55	45.87
0.02	0.00	0.00	0.03	0.00	0.07	0.01	0.04
33.20	34.56	33.80	33.09	34.97	35.38	35.30	35.39
0.00	0.01	0.01	0.00	0.00	0.00	0.00	0.00
0.04	0.07	0.01	0.20	0.12	0.19	0.07	0.14
0.00	0.00	0.00	0.00	0.00	0.00	0.00	0.00
0.00	0.00	0.00	0.00	0.00	0.00	0.00	0.00
0.00	0.00	0.00	0.00	0.00	0.00	0.00	0.00
15.24	16.61	15.80	15.34	17.23	17.66	17.45	17.43
2.62	1.88	2.31	2.52	1.44	1.14	1.28	1.36
0.07	0.04	0.09	0.07	0.00	0.00	0.04	0.02
99.74	100.42	100.00	99.52	99.60	99.52	99.70	100.25
2.222	2.156	2.194	2.217	2.114	2.085	2.100	2.103
0.001	0.000	0.000	0.001	0.000	0.002	0.000	0.001
1.791	1.859	1.821	1.791	1.901	1.928	1.918	1.912
0.000	0.000	0.000	0.000	0.000	0.000	0.000	0.000
0.002	0.003	0.000	0.008	0.005	0.007	0.003	0.005
0.000	0.000	0.000	0.000	0.000	0.000	0.000	0.000
0.000	0.000	0.000	0.000	0.000	0.000	0.000	0.000
0.000	0.000	0.000	0.000	0.000	0.000	0.000	0.000
0.747	0.812	0.774	0.755	0.851	0.875	0.862	0.856
0.233	0.166	0.205	0.224	0.129	0.102	0.114	0.121
0.004	0.002	0.005	0.004	0.000	0.000	0.002	0.001
5.000	4.999	5.000	5.000	5.000	5.000	4.999	5.000

CB1424 Plg H 119 core	CB1424 Plg H 120 rim	CB1424 Plg P 131 core	CB1424 Plg P 132 rim	CB1424 Plg U 147 core	CB1424 Plg U 148 rim	CB1414 Plg C 83 core	CB1414 Plg C 84 rim
46.09	45.96	45.94	45.72	46.06	45.64	48.32	47.55
0.00	0.00	0.00	0.03	0.01	0.00	0.00	0.00
35.45	35.54	35.27	35.39	35.00	35.09	33.96	34.14
0.00	0.00	0.00	0.00	0.02	0.01	0.04	0.00
0.02	0.03	0.02	0.25	0.12	0.22	0.02	0.03
0.00	0.00	0.00	0.00	0.00	0.00	0.00	0.00
0.00	0.00	0.00	0.00	0.00	0.00	0.00	0.00
0.00	0.00	0.00	0.00	0.00	0.00	0.00	0.00
17.29	17.58	17.44	17.37	17.41	17.35	15.53	16.11
1.45	1.35	1.40	1.32	1.42	1.33	2.48	2.14
0.02	0.01	0.02	0.01	0.01	0.02	0.03	0.02
100.32	100.47	100.09	100.09	100.05	99.66	100.38	99.99
2.109	2.102	2.109	2.100	2.116	2.106	2.199	2.176
0.000	0.000	0.000	0.001	0.000	0.000	0.000	0.000
1.912	1.916	1.908	1.916	1.895	1.908	1.821	1.841
0.000	0.000	0.000	0.000	0.001	0.000	0.001	0.000
0.001	0.001	0.001	0.010	0.005	0.008	0.001	0.001
0.000	0.000	0.000	0.000	0.000	0.000	0.000	0.000
0.000	0.000	0.000	0.000	0.000	0.000	0.000	0.000
0.000	0.000	0.000	0.000	0.000	0.000	0.000	0.000
0.848	0.861	0.858	0.855	0.857	0.858	0.757	0.790
0.129	0.120	0.125	0.118	0.126	0.119	0.219	0.190
0.001	0.001	0.001	0.001	0.001	0.001	0.002	0.001
5.000	5.000	5.000	5.000	5.000	5.000	5.000	4.999
0.959	1.08	1.12	0.983				
4.2	3.8	6.3	9.0				
	0.332	1.27	0.308				
		4.6	3.2				
0.044	0.062	0.099	0.054				
	0.110		0.426				
0.674	0.052	0.061	0.024				

465	490	475	458
0.020	0.018	0.022	0.036
0.009	0.015		
0.004	0.005		
0.016	0.055		
107	111	116	112
4.3	4.3	4.1	4.0
4.0	3.9	4.0	3.9
0.217	0.224	0.239	0.229
0.643	0.568	0.565	0.505
0.022	0.038	0.049	0.051
0.683	0.747	0.702	0.786
0.032	0.016	0.017	0.008
	0.003	0.002	0.002
0.006	0.002	0.013	0.007
0.001		0.003	
	0.002	0.005	0.006
			0.001
		0.006	
0.001			
			0.001
4.2	4.4	4.2	4.0
	0.003		0.001
		0.001	

CB1414 Plg I 102 core	CB1414 Plg I 103 rim	CB1414 Plg M 106 core	CB1414 Plg M 107 rim	CB1414 Plg T 120 core	CB1414 Plg T 121 rim	CB1475 Plg A 54 core	CB1475 Plg A 55 rim
47.95	47.64	47.61	47.05	47.44	47.44	48.93	48.79
0.00	0.02	0.03	0.05	0.00	0.01	0.00	0.02
33.86	34.46	34.27	34.27	34.47	34.39	32.90	33.37
0.01	0.00	0.00	0.00	0.00	0.00	0.02	0.00
0.03	0.00	0.00	0.08	0.03	0.03	0.00	0.04
0.00	0.00	0.00	0.00	0.00	0.00	0.02	0.01
0.00	0.00	0.00	0.00	0.00	0.00	0.00	0.05
0.00	0.00	0.00	0.00	0.00	0.00	0.00	0.00
15.32	15.38	16.11	16.41	16.48	16.51	15.51	15.49
2.47	2.38	2.16	1.95	2.01	2.01	2.65	2.56
0.04	0.03	0.03	0.04	0.01	0.00	0.05	0.07
99.68	99.91	100.21	99.85	100.44	100.39	100.08	100.40
2.197	2.177	2.174	2.159	2.163	2.164	2.233	2.219
0.000	0.001	0.001	0.002	0.000	0.000	0.000	0.001
1.828	1.856	1.844	1.853	1.852	1.849	1.770	1.789
0.000	0.000	0.000	0.000	0.000	0.000	0.001	0.000
0.001	0.000	0.000	0.003	0.001	0.001	0.000	0.002
0.000	0.000	0.000	0.000	0.000	0.000	0.001	0.000
0.000	0.000	0.000	0.000	0.000	0.000	0.000	0.002
0.000	0.000	0.000	0.000	0.000	0.000	0.000	0.003
0.752	0.753	0.788	0.807	0.805	0.807	0.758	0.755
0.219	0.211	0.191	0.173	0.178	0.178	0.234	0.226
0.002	0.002	0.002	0.002	0.001	0.000	0.003	0.004
5.000	5.000	5.000	5.000	5.000	5.000	5.000	5.001
1.73	1.61	1.49				1.01	1.20
20	18	19				12	9.9
	1.33	0.667				0.263	0.157
1.92	0.169	0.47					
0.034	0.075	0.033				0.008	0.033
1.11	1.18	1.27					
0.214	0.078	0.118				0.023	

316	300	322	313	317
0.112	0.124	0.149	0.477	0.399
	0.008	0.035	0.016	0.012
0.018	0.015	0.029	0.002	0.002
0.342		0.002		0.029
173	171	180	143	150
7.3	7.4	8.1	12	12
8.2	9.3	10	17	17
0.547	0.737	0.677	1.39	1.40
1.47	2.05	2.15	5.0	4.7
0.038	0.099	0.233	0.520	0.482
1.07	1.22	1.26	1.75	1.68
0.106	0.084	0.100	0.233	0.294
0.001	0.006		0.034	0.01
0.037	0.030	0.020	0.100	0.123
	0.022	0.014	0.012	0.008
0.057	0.023	0.03	0.025	0.036
0.007			0.006	0.003
0.116		0.015	0.013	0.014
0.027		0.004	0.002	0.001
0.008		0.004		
	0.002	0.002	0.001	
6.6	6.2	6.2	5.6	5.7
	0.004	0.003	0.003	
	0.005	0.002	0.016	

CB1475 Plg A 56 core	CB1475 Plg A 57 rim	CB1475 Plg D 66 core	CB1475 Plg D 67 rim	CB1475 Plg G 83 core	CB1475 Plg G 84 rim	CB1475 Plg L 87 core	CB1475 Plg L 88 rim	CB1475 Plg N 92 core
49.21	48.61	48.65	48.36	48.72	48.46	48.16	48.31	48.49
0.00	0.03	0.03	0.00	0.00	0.00	0.03	0.00	0.05
32.66	32.82	32.80	33.31	32.93	32.99	33.92	33.40	33.26
0.06	0.06	0.01	0.00	0.00	0.00	0.00	0.00	0.00
0.04	0.04	0.02	0.18	0.17	0.18	0.02	0.05	0.00
0.00	0.01	0.00	0.01	0.04	0.00	0.00	0.00	0.00
0.09	0.00	0.01	0.02	0.00	0.00	0.01	0.00	0.11
0.01	0.03	0.00	0.00	0.01	0.00	0.00	0.00	0.00
15.18	15.26	15.52	15.79	15.28	15.30	15.93	15.85	15.91
2.73	2.67	2.59	2.38	2.62	2.58	2.31	2.39	2.38
0.08	0.03	0.06	0.05	0.06	0.04	0.06	0.05	0.03
100.06	99.56	99.69	100.10	99.83	99.55	100.44	100.05	100.23
2.244	2.230	2.230	2.210	2.230	2.224	2.193	2.208	2.211
0.000	0.001	0.001	0.000	0.000	0.000	0.001	0.000	0.002
1.755	1.775	1.772	1.794	1.776	1.784	1.820	1.799	1.787
0.002	0.002	0.000	0.000	0.000	0.000	0.000	0.000	0.000
0.002	0.002	0.001	0.007	0.007	0.007	0.001	0.002	0.000
0.000	0.000	0.000	0.000	0.002	0.000	0.000	0.000	0.000
0.003	0.000	0.000	0.001	0.000	0.000	0.000	0.000	0.004
0.006	0.000	0.001	0.001	0.000	0.000	0.001	0.000	0.007
0.742	0.750	0.762	0.773	0.749	0.752	0.777	0.776	0.777
0.241	0.238	0.230	0.211	0.232	0.230	0.204	0.212	0.210
0.005	0.002	0.004	0.003	0.004	0.002	0.003	0.003	0.002
5.000	5.000	5.000	5.000	5.000	5.000	5.000	5.000	5.000
0.877	0.989							
15	12							
0.386	0.170							
1.31								
0.001	0.023							
	0.656							
	0.018							

297	286
0.408	0.355
0.003	0.010
	0.004
0.027	0.005
128	127
11	11
16	16
1.32	1.23
4.8	3.8
0.548	0.372
1.64	1.55
0.264	0.183
0.033	0.024
0.083	0.100
0.012	0.011
0.039	0.028
0.004	0.005
0.029	0.006
0.003	0.003

5.2	5.1
0.001	0.001
0.001	

CB1475	CB1060	CB1060	CB1060	CB1060	CB1060	CB1060	CB1060
Plg	Plg	Plg	Plg	Plg	Plg	Plg	Plg
N	B	B	B	B	H	H	I
93	168	169	170	171	186	187	188
rim	core	rim	core	rim	core	rim	core
48.19	48.41	47.11	46.73	46.99	46.51	47.46	47.20
0.02	0.00	0.01	0.00	0.00	0.00	0.01	0.00
33.44	33.47	33.82	34.33	34.24	34.44	33.79	34.36
0.00	0.00	0.00	0.04	0.00	0.00	0.02	0.00
0.04	0.02	0.05	0.02	0.15	0.00	0.00	0.00
0.02	0.00	0.06	0.00	0.06	0.00	0.01	0.01
0.03	0.03	0.01	0.00	0.08	0.00	0.00	0.00
0.00	0.00	0.00	0.00	0.00	0.01	0.03	0.00
15.94	16.05	16.94	16.91	16.76	17.00	16.49	16.75
2.33	2.34	1.82	1.76	1.76	1.67	2.05	1.91
0.04	0.02	0.02	0.00	0.02	0.03	0.01	0.00
100.05	100.34	99.84	99.79	100.06	99.66	99.87	100.23
2.203	2.206	2.165	2.148	2.154	2.141	2.178	2.158
0.001	0.000	0.000	0.000	0.000	0.000	0.000	0.000
1.802	1.798	1.832	1.860	1.849	1.869	1.827	1.852
0.000	0.000	0.000	0.001	0.000	0.000	0.001	0.000
0.002	0.001	0.002	0.001	0.006	0.000	0.000	0.000
0.001	0.000	0.002	0.000	0.002	0.000	0.000	0.000
0.001	0.001	0.000	0.000	0.003	0.000	0.000	0.000
0.002	0.002	0.001	0.000	0.005	0.000	0.000	0.000
0.781	0.784	0.834	0.833	0.823	0.839	0.811	0.821
0.206	0.207	0.162	0.157	0.156	0.149	0.182	0.169
0.002	0.001	0.001	0.000	0.001	0.002	0.001	0.000
5.000	4.999	5.000	5.000	5.000	5.000	5.000	5.000
					1.19		1.12
					2.82		2.89
							0.805
					0.564		0.30
					0.067		0.059
					0.266		0.467
					0.343		0.342

1194	1144
0.003	0.017
0.005	
0.002	0.006
0.017	0.061
83	89
0.143	0.739
0.256	0.769
0.033	0.071
0.120	0.275
0.032	0.044
0.380	0.526
0.010	0.011
0.002	0.002
0.002	
	0.002
	0.003
	0.011
	0.006
	0.004
14	14
0.008	0.001

CB1060 Plg I 189 rim	CB1060 Plg M 193 core	CB1060 Plg M 194 rim	CB1060 Plg P 201 core	CB1060 Plg P 202 rim	CB1060 Plg P 203 rim (2)	CB1060 Plg P 204 rim (3)	CB1060 Plg P 205 rim (4)
46.79	46.80	47.31	49.67	46.71	62.04	57.67	46.72
0.00	0.00	0.00	0.00	0.04	0.04	0.02	0.00
34.56	34.20	34.23	32.46	34.69	23.39	26.89	34.22
0.00	0.00	0.00	0.00	0.00	0.04	0.00	0.00
0.17	0.00	0.05	0.00	0.03	0.08	0.24	0.13
0.00	0.00	0.00	0.00	0.01	0.00	0.00	0.00
0.00	0.00	0.06	0.00	0.00	0.00	0.04	0.00
0.00	0.02	0.02	0.00	0.01	0.00	0.00	0.00
17.05	16.70	16.73	14.78	16.72	5.13	8.68	16.67
1.67	1.84	1.88	3.07	1.80	8.75	6.62	1.82
0.03	0.03	0.01	0.02	0.01	0.04	0.03	0.01
100.27	99.59	100.29	100.00	100.02	99.51	100.19	99.57
2.142	2.155	2.162	2.264	2.141	2.763	2.578	2.152
0.000	0.000	0.000	0.000	0.001	0.001	0.001	0.000
1.865	1.856	1.843	1.743	1.874	1.228	1.417	1.858
0.000	0.000	0.000	0.000	0.000	0.001	0.000	0.000
0.007	0.000	0.002	0.000	0.001	0.003	0.009	0.005
0.000	0.000	0.000	0.000	0.000	0.000	0.000	0.000
0.000	0.000	0.002	0.000	0.000	0.000	0.001	0.000
0.000	0.000	0.004	0.000	0.000	0.000	0.003	0.000
0.836	0.824	0.819	0.722	0.821	0.245	0.416	0.823
0.148	0.164	0.167	0.271	0.160	0.756	0.574	0.163
0.002	0.002	0.001	0.001	0.001	0.002	0.002	0.001
5.000	5.000	5.000	5.001	5.000	5.000	5.000	5.001
1.17	1.11	1.23					
2.41	20	3.2					
0.411	0.842						
0.031	0.064	0.050					
0.395	0.251	0.083					
0.288	1.10	0.225					

1151	1233	1119
0.008	0.010	0.008
0.006	0.178	0.008
	0.010	0.001
0.046	0.207	0.018
82	81	83
0.710	2.47	0.779
0.802	2.54	0.859
0.064	0.186	0.076
0.234	0.336	0.324
0.023	0.014	0.020
0.484	0.769	0.545
0.016	0.012	0.011
	0.002	
	0.005	0.010
0.008		
	0.003	
0.003	0.001	0.002
0.001	0.003	
13	16	13
	0.001	
0.002	0.021	

CB1482 Plg E 220 core	CB1482 Plg E 221 rim	CB1482 Plg N 245 core	CB1482 Plg N 246 rim	CB1482 Plg N 247 rim (2)	CB1482 Plg O 248 core	CB1482 Plg O 249 rim	CB1482 Plg Q 259 core	CB1482 Plg Q 260 rim
46.36	46.76	48.12	47.73	55.07	47.30	48.83	47.28	47.43
0.01	0.02	0.00	0.03	0.00	0.01	0.00	0.00	0.03
34.93	34.53	33.98	33.26	28.95	34.38	33.28	34.00	33.78
0.03	0.00	0.00	0.00	0.00	0.00	0.02	0.00	0.00
0.02	0.14	0.06	0.18	0.28	0.00	0.02	0.00	0.06
0.00	0.00	0.00	0.00	0.00	0.00	0.00	0.00	0.00
0.00	0.00	0.00	0.00	0.00	0.00	0.00	0.00	0.00
0.00	0.00	0.00	0.00	0.00	0.00	0.00	0.00	0.00
16.93	16.71	15.94	16.14	10.74	16.60	15.53	16.35	16.22
1.63	1.78	2.33	2.21	5.36	1.95	2.60	2.04	2.11
0.02	0.02	0.01	0.01	0.10	0.02	0.05	0.04	0.03
99.93	99.96	100.44	99.56	100.50	100.26	100.33	99.71	99.66
2.128	2.146	2.191	2.196	2.471	2.161	2.223	2.172	2.179
0.000	0.001	0.000	0.001	0.000	0.000	0.000	0.000	0.001
1.890	1.867	1.823	1.803	1.531	1.851	1.786	1.840	1.829
0.001	0.000	0.000	0.000	0.000	0.000	0.001	0.000	0.000
0.001	0.005	0.002	0.007	0.011	0.000	0.001	0.000	0.002
0.000	0.000	0.000	0.000	0.000	0.000	0.000	0.000	0.000
0.000	0.000	0.000	0.000	0.000	0.000	0.000	0.000	0.000
0.000	0.000	0.000	0.000	0.000	0.000	0.000	0.000	0.000
0.833	0.821	0.778	0.795	0.516	0.813	0.757	0.804	0.798
0.145	0.158	0.206	0.197	0.466	0.173	0.229	0.182	0.188
0.001	0.001	0.001	0.001	0.006	0.001	0.003	0.002	0.002
4.999	5.000	5.000	5.000	5.000	5.000	5.000	5.000	5.000
1.56	1.51						1.40	1.43
14	8.7						8.6	16
0.279	0.879						0.292	0.235
1.51	1.59						0.351	0.245
0.096							0.033	0.005
0.660	0.719							0.236
0.239	0.056						0.514	0.212

512	513	522	618
0.027	0.037	0.088	0.022
0.012	0.010	0.005	0.003
0.025	0.012	0.001	
	0.027	0.102	0.048
39	38	53	54
9.1	9.1	9.9	9.2
9.5	9.2	11	9.4
0.624	0.695	0.689	0.617
1.70	2.08	2.41	1.83
0.308	0.094	0.163	0.130
2.31	2.17	2.09	2.35
0.049	0.086	0.097	0.054
0.011	0.004	0.007	0.002
0.007	0.007	0.020	0.002
	0.004	0.002	0.008
0.007		0.004	
			0.002
	0.012	0.003	
0.003	0.003	0.001	
0.003	0.001		
26	25	27	31
0.001	0.006	0.001	0.001
0.001		0.002	

CB1482 Plg R 263 core	CB1482 Plg R 264 rim	CB1482 Plg R 265 rim (2)	CB1482 Plg B 216 core inc Grt	CB1482 Plg B 217 rim inc Grt	CB1482 Plg F 230 core	CB1482 Plg F 231 rim	CB1482 Plg I 238 core	CB1482 Plg I 239 rim
47.23	47.20	54.42	48.03	56.24	49.25	51.64	46.54	47.06
0.00	0.01	0.00	0.00	0.00	0.00	0.00	0.02	0.00
34.34	34.39	29.57	33.52	28.06	32.71	30.80	34.24	34.45
0.00	0.00	0.04	0.00	0.00	0.01	0.00	0.00	0.02
0.00	0.12	0.03	0.07	0.04	0.02	0.10	0.00	0.11
0.00	0.00	0.00	0.00	0.01	0.00	0.00	0.02	0.03
0.00	0.00	0.00	0.00	0.02	0.00	0.01	0.04	0.01
0.00	0.00	0.00	0.00	0.01	0.00	0.01	0.01	0.00
16.50	16.61	11.02	16.27	9.42	15.14	13.00	17.00	16.73
1.96	1.91	5.17	2.23	6.10	2.81	4.00	1.68	1.82
0.05	0.01	0.10	0.01	0.05	0.07	0.05	0.03	0.03
100.08	100.25	100.35	100.13	99.95	100.01	99.61	99.58	100.26
2.162	2.158	2.445	2.196	2.525	2.247	2.352	2.145	2.153
0.000	0.000	0.000	0.000	0.000	0.000	0.000	0.001	0.000
1.852	1.853	1.566	1.806	1.485	1.759	1.653	1.859	1.857
0.000	0.000	0.001	0.000	0.000	0.000	0.000	0.000	0.001
0.000	0.005	0.001	0.003	0.002	0.001	0.004	0.000	0.004
0.000	0.000	0.000	0.000	0.000	0.000	0.000	0.001	0.001
0.000	0.000	0.000	0.000	0.001	0.000	0.000	0.001	0.000
0.000	0.000	0.000	0.000	0.001	0.000	0.001	0.003	0.001
0.809	0.814	0.530	0.797	0.453	0.740	0.634	0.839	0.820
0.174	0.169	0.450	0.198	0.531	0.249	0.353	0.150	0.161
0.003	0.001	0.006	0.001	0.003	0.004	0.003	0.002	0.002
5.000	5.000	5.000	5.000	5.000	5.000	5.000	5.001	5.000
					1.33	1.06	1.31	1.18
					12	9.7	13	10
					0.156	0.377	0.209	0.632
						0.203	0.907	0.528
					0.032	0.030		0.058
					0.246	0.074	0.155	0.020
					0.133	0.063	0.052	0.041

567	489	503	439
0.018	0.020	0.041	0.031
0.018	0.002	0.004	0.005
0.002	0.002		0.007
0.009	0.012	0.016	0.022
46	44	46	46
7.6	6.3	10	9.0
7.6	5.9	12	10
0.473	0.392	0.846	0.728
1.48	1.03	3.3	2.64
0.114	0.066	0.320	0.188
1.61	1.34	2.03	2.02
0.030	0.023	0.152	0.105
0.004	0.003	0.014	0.003
0.005	0.006	0.011	0.009
	0.001	0.002	0.003
	0.011	0.002	0.008
	0.001		
0.002	0.003	0.003	
0.002	0.001		0.001
0.001			0.002
	0.001		
22	19	20	19
	0.001	0.002	0.004

CB1482 Plg L 240 core	CB1482 Plg L 241 rim	CB1482 Plg N 248 core	CB1482 Plg N 249 rim	CB1482 Plg O 256 core	CB1482 Plg O 257 rim	CB1482 Plg Q 265 core	CB1482 Plg Q 266 rim
48.01	47.68	46.93	47.56	47.43	47.47	50.54	53.08
0.00	0.00	0.03	0.07	0.00	0.02	0.00	0.00
33.67	33.49	34.15	34.10	34.08	34.22	31.53	29.72
0.06	0.06	0.00	0.03	0.00	0.00	0.02	0.02
0.03	0.27	0.04	0.00	0.01	0.10	0.00	0.28
0.00	0.05	0.00	0.00	0.04	0.00	0.00	0.04
0.00	0.00	0.01	0.00	0.01	0.00	0.00	0.02
0.00	0.00	0.00	0.00	0.00	0.01	0.00	0.02
16.40	16.34	16.46	16.51	16.62	16.69	13.98	12.37
2.17	2.06	1.93	2.06	1.95	1.94	3.48	4.45
0.03	0.04	0.03	0.01	0.04	0.02	0.07	0.07
100.37	99.99	99.58	100.34	100.18	100.47	99.62	100.07
2.191	2.187	2.160	2.171	2.170	2.166	2.307	2.404
0.000	0.000	0.001	0.002	0.000	0.001	0.000	0.000
1.811	1.810	1.852	1.835	1.837	1.840	1.696	1.586
0.002	0.002	0.000	0.001	0.000	0.000	0.001	0.001
0.001	0.010	0.002	0.000	0.000	0.004	0.000	0.011
0.000	0.002	0.000	0.000	0.002	0.000	0.000	0.002
0.000	0.000	0.000	0.000	0.000	0.000	0.000	0.001
0.000	0.000	0.001	0.000	0.001	0.000	0.000	0.001
0.802	0.803	0.811	0.808	0.814	0.816	0.684	0.600
0.192	0.183	0.172	0.182	0.173	0.172	0.308	0.391
0.002	0.002	0.002	0.001	0.002	0.001	0.004	0.004
5.000	5.000	5.000	5.000	4.999	5.000	5.000	5.000

SP0003	SP0003	SP0003	SP0003	SP0003	SP0003	SP0003	SP0003	SP0003
Plg	Plg	Plg	Plg	Plg	Plg	Plg	Plg	Plg
E	E	F	F	G	G	I	I	O
61	62	67	68	74	75	78	79	89
core	rim	core	rim	core	rim	core	rim	core
46.74	45.95	46.71	46.16	47.09	47.55	46.72	46.73	49.12
0.00	0.00	0.03	0.01	0.00	0.00	0.00	0.03	0.00
34.81	34.93	34.51	35.12	34.56	34.05	34.51	34.48	33.34
0.00	0.00	0.00	0.01	0.00	0.00	0.01	0.00	0.00
0.05	0.06	0.08	0.22	0.11	0.13	0.11	0.06	0.12
0.00	0.00	0.00	0.00	0.00	0.00	0.00	0.00	0.00
0.00	0.00	0.00	0.00	0.00	0.00	0.00	0.00	0.00
0.00	0.00	0.00	0.00	0.00	0.00	0.00	0.00	0.00
17.08	17.09	16.58	17.23	16.47	16.12	16.69	16.53	15.10
1.67	1.51	1.84	1.47	1.92	2.15	1.80	1.86	2.78
0.00	0.02	0.01	0.00	0.01	0.00	0.00	0.00	0.02
100.35	99.56	99.76	100.22	100.16	100.00	99.84	99.69	100.48
2.137	2.119	2.146	2.116	2.154	2.177	2.146	2.148	2.231
0.000	0.000	0.001	0.000	0.000	0.000	0.000	0.001	0.000
1.876	1.898	1.869	1.898	1.863	1.837	1.868	1.868	1.784
0.000	0.000	0.000	0.000	0.000	0.000	0.000	0.000	0.000
0.002	0.002	0.003	0.008	0.004	0.005	0.004	0.002	0.005
0.000	0.000	0.000	0.000	0.000	0.000	0.000	0.000	0.000
0.000	0.000	0.000	0.000	0.000	0.000	0.000	0.000	0.000
0.000	0.000	0.000	0.000	0.000	0.000	0.000	0.000	0.000
0.837	0.844	0.816	0.846	0.807	0.791	0.821	0.814	0.735
0.148	0.135	0.164	0.131	0.170	0.191	0.160	0.166	0.245
0.000	0.001	0.001	0.000	0.001	0.000	0.000	0.000	0.001
4.999	5.000	5.000	5.000	5.000	5.000	5.000	5.000	5.000
1.76	1.69							
3.6	2.87							
0.126	0.495							
0.667	0.382							
0.049	0.442							
0.452	0.145							
0.125	0.065							

485	532
0.053	0.004
181	0.002
0.002	0.003
	0.011
24	26
0.442	0.336
0.288	0.261
0.018	0.016
0.077	0.145
0.007	0.098
0.099	0.069
0.005	0.145
	0.007
	0.087
0.002	0.036
0.016	0.063
0.002	0.013
0.045	0.062
0.009	0.007
3.2	0.002
3.5	3.2
0.003	
0.002	

SP0003 Plg O 90 rim	SP0003 Plg P 93 core	SP0003 Plg P 94 rim
46.50	50.99	47.07
0.06	0.00	0.01
34.67	31.49	34.18
0.03	0.00	0.02
0.24	0.10	0.23
0.00	0.00	0.00
0.00	0.00	0.00
0.00	0.00	0.00
16.39	13.42	16.24
1.80	3.74	1.97
0.01	0.04	0.02
99.70	99.78	99.74
2.139	2.321	2.163
0.002	0.000	0.000
1.879	1.689	1.851
0.001	0.000	0.001
0.009	0.004	0.009
0.000	0.000	0.000
0.000	0.000	0.000
0.000	0.000	0.000
0.808	0.654	0.799
0.161	0.330	0.175
0.001	0.002	0.001
4.999	5.001	4.999
	1.87	1.99
	27	8.6
	3.6	0.028
	2.58	
	0.469	0.111
	0.381	0.312
	2.95	2.51

441	639
0.159	0.088
0.027	0.002
0.002	0.001
0.008	
27	45
0.475	0.522
0.302	0.333
0.003	0.013
0.069	0.041
0.006	0.015
0.085	0.116
0.002	0.004
0.020	0.002
0.004	0.012
0.014	0.006
0.003	0.002
0.005	
	0.001
0.002	
	0.003
3.6	5.3
	0.004

Online Resource C Compositions of Titanite in terms of major (EPMA results, in wt%) elements originati

Sample	SP0003	SP0003	SP0003	SP0003	SP0003	SP0003	SP0003	SP0003
Phase	Tnt	Tnt	Tnt	Tnt	Tnt	Tnt	Tnt	Tnt
Site	A	A	B	B	C	C	D	D
Analysis #	47	48	51	52	54	55	58	59
Position	core	rim	core	rim	core	rim	core	rim
SiO_2	33.4	32.8	33.5	33.5	33.5	32.8	32.8	33.8
TiO_2	37.0	37.4	36.6	36.4	37.2	37.4	37.7	36.4
Al_2O_3	1.5	1.1	1.6	1.8	1.3	1.2	1.3	1.8
Cr_2O_3	0.0	0.0	0.0	0.1	0.0	0.0	0.0	0.0
FeO_T	0.4	0.5	0.4	0.3	0.4	0.6	0.4	0.7
MnO	0.1	0.1	0.1	0.1	0.0	0.1	0.0	0.1
NiO	0.0	0.0	0.0	0.0	0.0	0.0	0.0	0.0
MgO	0.0	0.0	0.0	0.0	0.0	0.0	0.0	0.0
CaO	27.8	27.6	27.7	27.5	28.0	27.6	27.8	27.5
Total	100.1	99.6	99.8	99.7	100.5	99.7	100.1	100.4
C.p.f.u.								
Si	1.076	1.065	1.081	1.083	1.076	1.064	1.060	1.086
Ti	0.896	0.914	0.888	0.884	0.899	0.912	0.915	0.879
Al	0.058	0.043	0.062	0.068	0.049	0.046	0.050	0.069
Fe_T	0.010	0.014	0.010	0.008	0.010	0.015	0.011	0.017
Mn	0.001	0.001	0.002	0.002	0.001	0.002	0.001	0.003
Mg	0.000	0.000	0.001	0.001	0.000	0.000	0.000	0.000
Ca	0.958	0.961	0.956	0.950	0.962	0.959	0.963	0.945
Cr	0.000	0.000	0.001	0.002	0.001	0.001	0.000	0.000
Ni	0.000	0.000	0.000	0.001	0.001	0.000	0.000	0.001
Cations	2.999	2.999	3.000	2.998	2.999	3.000	3.000	3.000

ng from core and rim regions of each rock sample, respectively

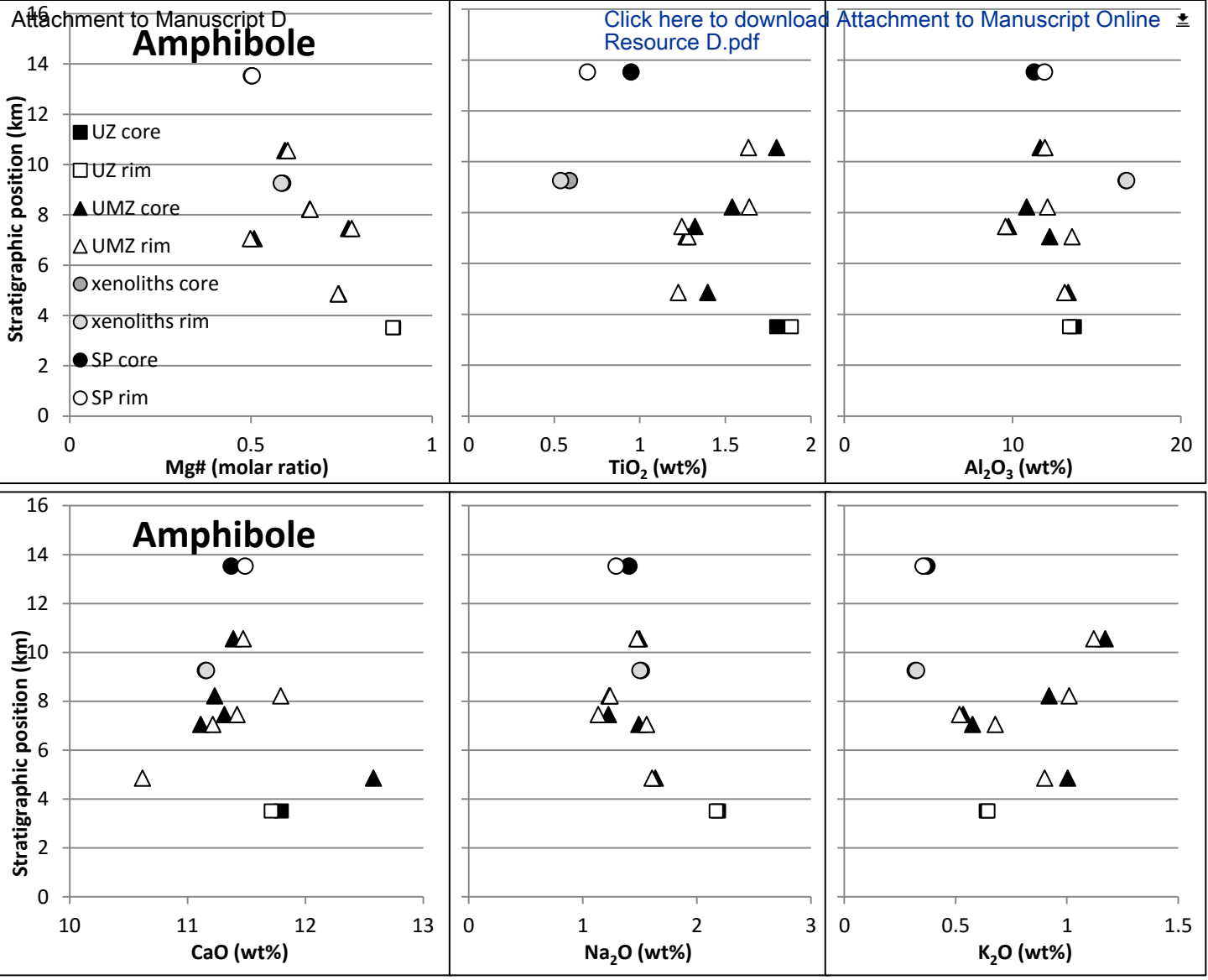

Online Resouce D1: average amphibole Mg# and major elements variations along stratigraphy

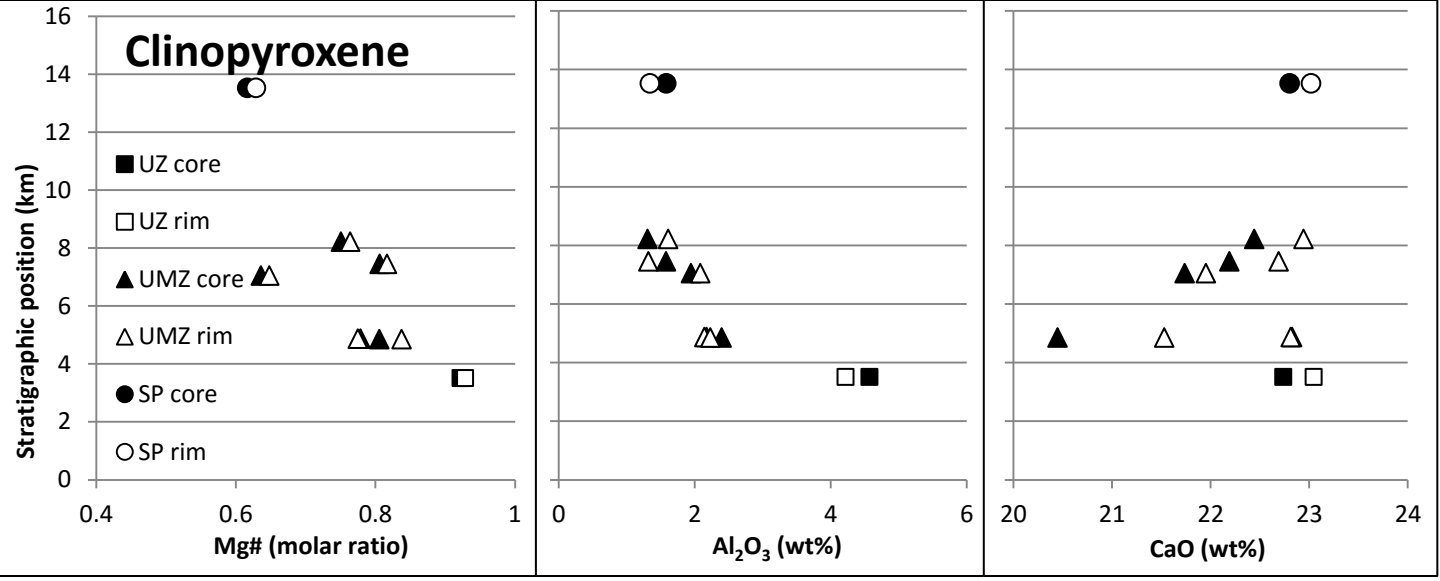

Online Resouce D2: average clinopyroxene Mg# and major elements variations along stratigraphy

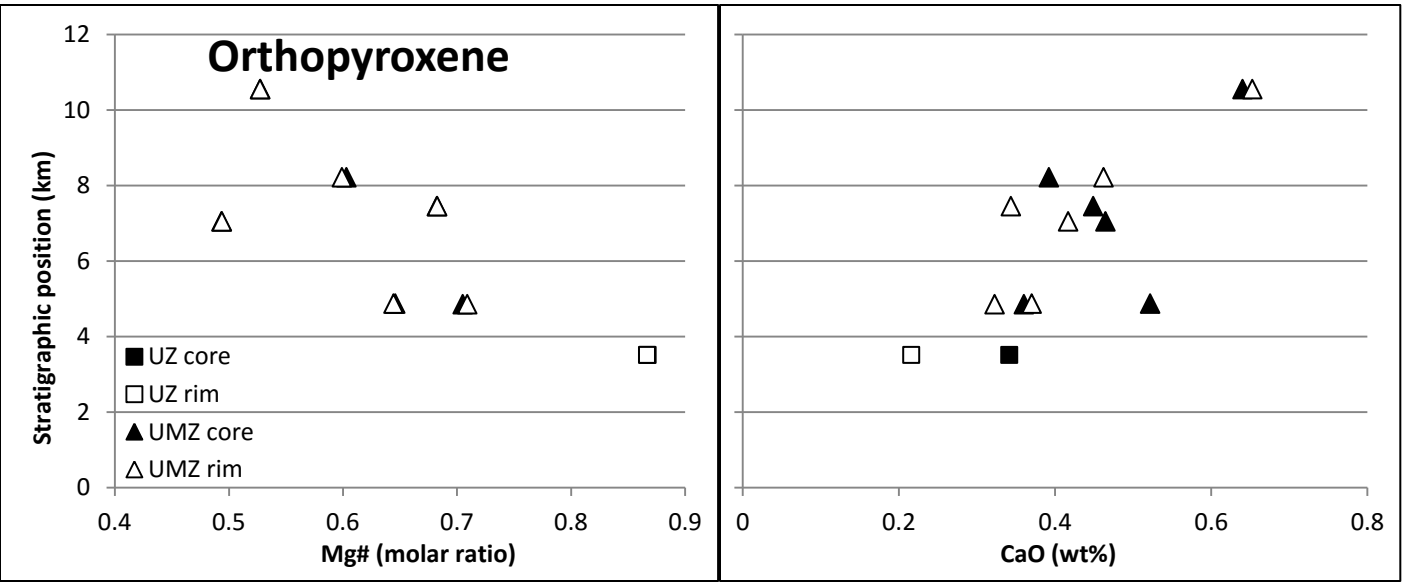

Online Resouce D3: average orthopyroxene Mg# and CaO variations along stratigraphy

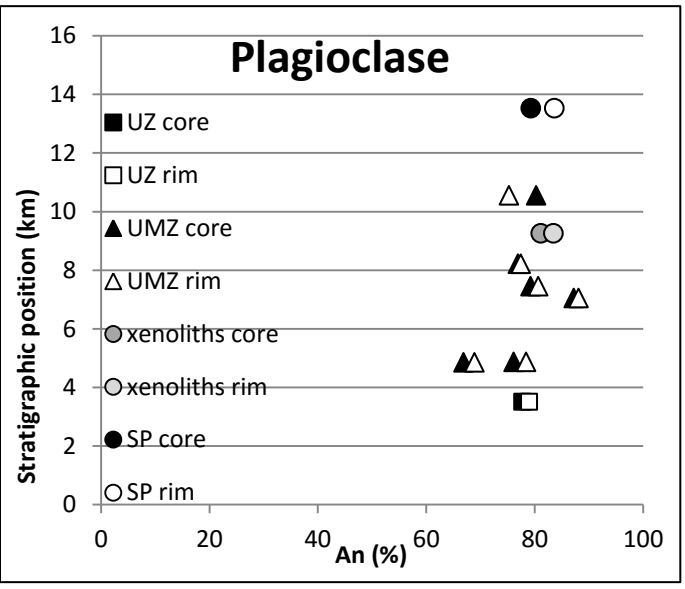

Online Resouce D4: average plagioclase anorthite variations along stratigraphy.